EXPERIMENTAL AND COMPUTATIONAL STUDY OF CATALYTIC COMBUSTION OF METHANE-AIR AND SYNGAS-AIR MIXTURES

By

SAURAV PATHAK

A DISSERTATION PRESENTED TO THE GRADUATE SCHOOL
OF THE UNIVERSITY OF FLORIDA IN PARTIAL FULFILLMENT
OF THE REQUIREMENTS FOR THE DEGREE OF
DOCTOR OF PHILOSOPHY

UNIVERSITY OF FLORIDA

2007

Dedicated to my country (India)

ACKNOWLEDGMENTS

I am thankful to God for having given me an opportunity to fulfill my dreams of higher education. I am thankful to my parents and sister for their continued support and faith in me. I extend my thankfulness to my country India and Birla Institute of Technology, Mesra, India from where I earned my Bachelor of Engineering. At the University of Florida I am thankful to my adviser Dr.C.Segal. Had it not been for the faith and support of Dr C.Segal, Dr Mark Sheplak and Dr. W. Shyy, it would have been impossible for me to pursue my PhD program. I am thankful to all my committee members for their suggestions and support. I also extend my acknowledgments to all my lab mates namely Jonas, Amit, Stepan, Aravind, Kyle, John and Jignesh for helping me out on numerous occasions. I am also thankful to my room mate Rakesh for helping me out whenever I had any problems.

TABLE OF CONTENTS

LIST OF TABLES

Table page

LIST OF FIGURES

Figure page

Abstract of Dissertation Presented to the Graduate School
of the University of Florida in Partial Fulfillment of the
Requirements for the Degree of Doctor of Philosophy

EXPERIMENTAL AND COMPUTATIONAL STUDY OF CATALYTIC COMBUSTION OF METHANE-AIR AND SYNGAS-AIR MIXTURES

By

Saurav Pathak

August 2007

Chair: Corin Segal
Major: Mechanical Engineering

Catalytic combustion and conversion of methane (CH_4) and Syngas (in our case, a gas mixture of H_2, CO, CO_2 and CH_4) is characterized by the complex transport of reacting gases and the chemical reactions on the catalyst surface and in the gas phase. The initiation and the kinetics of reactions on the catalyst surface depend largely on the surface coverage of species. Since the catalyst allows combustion at a low temperature resulting in a lower thermal NO formation, a detailed investigation on the effects of species surface coverage on catalytic combustion becomes an area of concerned research.

In this work, we investigate the dependence of catalytic combustion of two fuel-air mixtures, namely: methane-air and methane + hydrogen-air mixture, based on their surface coverage on Platinum, using a detailed surface reaction mechanism model. We look into the changes brought about in the kinetics and thus on combustion, when different species interact with the platinum surface, individually and in the presence of one another. We further extend our numerical investigation, to understand the kinetics involved in the catalytic combustion of Syngas on platinum. Syngas today can now be made by the gasification of coal and from other fuel sources using detailed technologies, such that the efficient and low energy harnessing of the thermal properties of Syngas is an important area of research. Catalytic combustion of syngas

would meet exactly these goals. Hence the study of a low energy reaction pathway of combustion of syngas on the surface of any catalyst in general has now become an important area of research. Catalytic reactor has been constructed to provide experimental data for comparison with model. Experimentally the ignition process is monitored by thermocouples and mass spectroscopy.

Parameters such as equivalence ratio, temperature and the surface site density of the catalyst surface were varied in the computational works to bring out their influence on the kinetics of combustion.

CHAPTER 1
INTRODUCTION

Catalytic Combustion: Purpose and Application

Catalytic combustion is a process that uses a solid catalyst to promote the combustion reaction by lowering the activation energy of certain reactions. These reactions would take place at lower temperatures relative to homogeneous combustion and at lower equivalence ratios, thus greatly reducing formation of NO_x emissions and eliminating lower flammability limits respectively. The reactors become more compact because the catalytic reactions occur on the surface of the catalyst reducing the required volume but greater surface areas.

Catalytic combustion research currently focuses on reactor design, increase in efficiency, and the search for more efficient catalysts. Thus, there is an urgent need for a better understanding of the physical and chemical processes occurring on the catalytic surface and their coupling with the surrounding flow field. In particular, it is important to understand the ignition and extinction behavior of the oxidation of hydrocarbons. During the last decade, detailed catalytic combustion models have been suggested [1, 2] including multi-step heterogeneous surface-reaction mechanisms which may provide guidelines for a better understanding and for the optimization of catalytic combustion. Since the ignition of methane on Pt occurs at relatively high temperatures at lean conditions [1, 3], there is a major interest to find a way to reduce the light-off temperature. The light off temperature is the temperature at which the first onset of ignition is noticed marked by a sudden rise in temperature and an increase in the conversion of the reactants into products. This is true, in particular for gas turbine applications where the catalytic combustion critically depends on the feasibility of a convenient light-off mechanism of the catalytic combustor.

Catalyzed combustion can be defined as the complete oxidation of a combustible compound on the surface of a catalyst. While conventional combustion occurs in the presence of a flame, catalyzed combustion is a flameless process occurring at lower temperatures and, therefore, emitting less nitrogen oxides. Furthermore, catalyzed combustion offers fewer constraints concerning flammability limits and reactor design. These advantages of catalyzed combustion determine its potential applications. For example, a gaseous mixture of H_2 and O_2 on the platinum is a classical example of heterogeneous catalysis. The sticking probability of H atoms are higher than those of O atoms, hence the exothermic process of adsorption of H_2 on the platinum surface is preferred over O_2. The O atoms are loosely bound on the platinum surface; they combine with H atoms on the platinum surface and form OH species which still remains adsorbed to the surface, this OH species further abstracts O atoms and forms H_2O. This is an exothermic reaction too. The heat released shifts the adsorption/desorption equilibrium towards the desorption side, such that H atoms would leave the platinum surface and become more available to abstract O atoms, thus favoring more OH formation and eventually forming more H_2O.

Using appropriate surface and gas phase reaction mechanisms, the study of catalytic combustion may include Computational Fluid Dynamics (CFD) along with experiments. CFD may thus be a tool to provide early details of different technical design variants. Two main reasons for the application of CFD in combustor studies are- (1) Only CFD is capable of delivering detailed insight into the transport processes encountered. In flow, whereas measurements within the reacting flow of the combustor are physically limited; they can be used successfully to provide data to validate the models and numerical tools applied and, (2) CFD offers a possibility to compare and evaluate different design variants already in the design phase

of a new combustion system. The main objectives of CFD application in the field of gas turbine combustion includes close monitoring of a number of processes including homogeneity at the burner inlet, the velocity profile at the burner inlet, the velocity and concentration profiles at the burner outlet using CFD. Considering the combustor, the thermal wall heat load has to be calculated for the design of the liner cooling. Moreover, for the development of high temperature turbines, a detailed knowledge of the velocity and temperature profile has to be provided by CFD applications. Advantages of employing catalytic combustion extend to reduced combustion instabilities [4, 5] in practical burners, development of micro-power supplier with high power density, reduced emissions from ground based power plants and increased combustion efficiency.

The present research includes both computational and experimental studies of catalytic combustion on model catalysts and is focused on the process of combustion inside a combustor designed for a gas turbine engine motivated by the need to improve efficiency and reduce pollutants.

NO_x Control in Gas Turbine Combustion Chambers

A combustor is a small component or area of a gas turbine, ramjet or pulsejet engine, where combustion takes place [6]. It is also known as a burner or flame can, depending on the design. In a gas turbine engine, the main *combustor* or combustion chamber is located between the high pressure compressor and the high pressure turbine of the gas generator. Combustor design requires that part of the airflow is directed to a region where the fuel and air are mixed and ignited. This area of the combustor is sometimes called a *flame holder* and allows a stable flame front to be established and maintained. The heat addition stage of a gas turbine cycle incurs a slight pressure drop associated with Rayleigh losses with an increasing volume to accommodate the temperature rise. This in turn results in an increase in the velocity of the gas

flow. This is directed over the turbine's blades providing power to the compressor and finally is passed through a nozzle generating thrust.

There are two categories of combustors, annular and can as described by Figure 1-1. Can combustors look like cans and are mounted around the engine core. They can be easily removed for maintenance and provide convenient plumbing for fuel injection. Annular combustors are more compact and lighter. Modern jet engines usually have annular combustors but efficient can combustor arrangements can be used for ground based operations. Double annular combustors are being introduced to reduce emissions.

The combustion efficiency [6] is a measure of the completeness of fuel combustion that takes place in the combustor chamber. If combustion is incomplete not all of the energy potentially available is released and the non-combusted components are released as undesirable pollutants including NO_x, SO_x, Polycyclic Aromatic Hydrocarbons and char. The requirements for complete combustion include sufficient residence to complete mixing and chemical reaction completion to take place. Almost 100% efficiency is achieved in current engines; however as the temperature increases the efficiency tends to diminish. Under these conditions nitrogen oxides are formed. Therefore measures to eliminate NOx emissions are needed.

A range of new and existing technologies can be employed to help gas turbine operators and reduce NO_x. The most common methods involve internal changes to the combustion system of the machine and/or the addition of a selective catalytic reduction (SCR) [7-9] systems to the exhaust [7]. For combustion systems, there are three major modifications available:

- Wet combustor [10]: a process that injects either steam or water into the combustion system and replaces nitrogen with steam diluent to lower the emissions levels, typically from 30–50ppm NOx
- Catalytic combustor: a new technology that employs a catalyst directly in the combustion chamber to lower the emissions, reportedly from 1.5–2ppm NOx

- Dry emissions reduction (DER) combustor [6, 11]: a method that utilizes staged combustion and fuel/air mixing to lower the emission levels as low as 9ppm NOx without the introduction of steam or water during natural gas operation.

An SCR system typically utilizes a heavy metal catalyst injected with anhydrous ammonia to lower the emissions levels. There are two ranges of catalyst: a low-temperature catalyst that can be used in combined-cycle applications and high-temperature catalysts, which are designed for simple-cycle applications. A DER combustor premixes the fuel and air in the combustion chamber to achieve a uniform and lean fuel/air mixture. In these combustors the fuel and air are premixed to avoid stiochiometric fuel air mixtures that yield the highest temperatures hence large quantities of pollutants. The lean mixture results in a cooler flame temperature when compared to a standard diffusion (non-premixed) combustor. Because NOx formation is an exponential function of the flame temperature, NOx levels can be reduced from approximately 150ppm in a standard combustor to less than 9ppm in a DER combustor.

Catalytic Combustion: a Subset of Catalysis

Catalytic combustion includes several essential processes: (1) diffusion of the reactants from the gas phase to the catalytic surface, (2) adsorption of the reactants onto the catalytic surface, (3) movement of adsorbed species, (4) reaction on the surface of the catalyst, (5) desorption of the products from the surface, and (6) diffusion of the products from the catalytic surface to the gas phase. Depending on the conditions, each of these processes can be rate limiting. Since measuring chemical activities near or on a catalyst surface is difficult, experimental data of surface kinetics, temperature, or concentrations of gas phase species near the catalyst surface are scarce. As a result, catalytic combustors have conventionally been modeled as a “black box” that produces a desired amount of fuel conversion. A few basic concepts of catalysis are described below:

Catalysis and Catalysts

The phrase *catalysis* was coined by Jöns Jakob Berzelius [12, 13] in 1835 who was the first to note that certain chemicals speed up a reaction. In chemistry and biology catalysis is the acceleration, i.e. increase in rate of a chemical reaction by means of a substance, called a catalyst and by reducing the activation energy. The catalyst in itself is left unchanged by the reaction. Figure 1-2 shows catalysis taking place at reduced activation energy.

In chemistry a catalyst is a substance that decreases the activation energy of a chemical reaction without itself being changed at the end of the chemical reaction. Catalysts participate in reactions but are neither reactants nor products of the reaction they catalyze. An exception is the process of autocatalysis which is a form of catalysis in which one of the products of a reaction serve as a catalyst for the reaction. Examples of autocatalysis are ozone depletion, binding of oxygen by hemoglobin, reaction of permanganate with oxalic acid. More generally, anything that accelerates a chemical reaction can be defined as a "catalyst". A promoter is an accelerator of catalysis, but not a catalyst by itself. A reaction inhibitor inhibits the working of a catalyst.

Catalysts and Reaction Energetics

Catalysts work by providing an alternative mechanism involving a different transition state and lower activation energy. As a result more molecular collisions have the energy needed to reach the transition state. Hence, catalysts can perform reactions that, albeit thermodynamically feasible, would not run without the presence of a catalyst, or perform them much faster, more specific, or at lower temperatures. This means that catalysts reduce the amount of energy needed to start a chemical reaction.

Catalysts *cannot* make energetically unfavorable reactions possible — they have *no* effect on the chemical equilibrium of a reaction because the rate of both the forward and the reverse

reaction are equally affected. The net free energy change of a reaction is the same whether a catalyst is used or not; the catalyst just makes it easier to activate.

The SI derived unit for measuring the catalytic activity of a catalyst is the katal [14], which is a mole per second. The degree of activity of a catalyst can also be described by the turn over number or TON and the catalytic efficiency by the *turn over frequency,* TOF. TON is defined as the number of moles of substrate that a mole of catalyst can convert before becoming inactivated. An ideal catalyst would have an infinite turnover number in this sense, because it wouldn't ever be consumed, but in actual practice one often sees turnover numbers which go from 100 to a million or more. The term *turn over frequency* is used to refer to the turnover per unit time.

Types of catalysts

It is possible to divide catalytic systems into two distinct categories.

- **Homogeneous catalysis** [15] is when the catalyst is of the same phase as the reactants and no phase boundary exists.
- **Heterogeneous catalysis** [15] is when a phase boundary separates the catalyst from the reactants.

Kinetics of Catalyzed Reactions

The primary effect of a catalyst on a chemical reaction is thus to increase its rate, and this must mean to increase its rate co-efficient. The consequential effects may be analyzed in terms of either the collision theory or the absolute rate theory.

According to the collision theory, the rate coefficient k is given by

$$k = P.Z.\exp(-Ea/RT) \qquad (1\text{-}1)$$

where P is the so-called steric factor which is introduced as a factor into the simple versions of *collision theory* of reactions to take care of the fact that the reaction probability depends on the

certain mutual orientations of the reactant molecules, Z the collision frequency, E_a the activation energy, R the gas constant and T the absolute temperature.

For example a unimolecular transformation (A → B) in which the slow step is the adsorption of the reactant exhibits a collision frequency which is then the number of collisions per unit time between the reactant molecules and the catalytic sites or species. The concentration of the latter will be much smaller, by a factor of some 10^{12} than the number of collisions between reactant molecules alone, which is relevant to the uncatalyzed reaction but irrelevant to the catalyzed reaction. Therefore if the catalyzed reaction is to compete effectively with the uncatalyzed reaction, then its exponential term must be some 10^{12} larger [16], which means that its activation energy must be about 65 kJmol^{-1} less. There may be some relief in the form of a higher steric factor but this is unlikely to contribute more than a factor of 10^2 or 10^3 at most, and the main conclusion is not really altered. Neglecting this effect, activation energy of 65 kJmol^{-1} only makes the rates of the catalyzed and uncatalyzed reaction equal: this scarcely represents efficient catalysis [16], for which activation energy difference must exceed 100 kJmol^{-1}.

In terms of the absolute rate theory, the rate coefficient is given by

$$k = \frac{K.T}{h}\exp(-\Delta G / RT) \qquad (1\text{-}2)$$

where K is the Boltzmann constant, ΔG is the Gibbs free energy of activation and h is the Planck's constant, and so the effect of a catalyst must be to decrease the free energy of activation of the reaction. The entropy of activation in a catalyzed reaction will usually be less than in the corresponding uncatalyzed because the transition state is immobilized on the catalyst surface with the consequent loss of translational freedom. There must therefore be a corresponding decrease in the enthalpy of activation to compensate for this, or more than to compensate if

efficient catalysis is desired. Thus according to either theory, the activation energy for a catalyzed reaction ought to be less than for the same catalyzed reaction.

Mechanism of Catalyzed Reactions: Making and Breaking Bonds

Reactions catalyzed by a heterogeneous catalyst can be represented by a sequence of processes. Reactant molecules are adsorbed at active sites onto the surface of the catalyst. This involves the formation of weak bonds between reactant molecules and the catalyst which causes other bonds in the reactant molecule to be stretched and weakened. The weakened structure is converted to another complex that is essentially the product attached to the catalyst. Finally, this complex breaks down to release the product molecule which moves away to leave the catalyst surface ready to interact with another reactant molecule. Several processes occur during heterogeneous catalysis. They are as follows:

Adsorption [15-17] is a process that occurs when a liquid or gas (called adsorbate) accumulates on the surface of a solid or liquid (adsorbent), forming a molecular or atomic film (adsorbate). It is different from absorption, where a substance diffuses into a liquid or solid to form a "solution". The term *sorption* encompasses both processes, while desorption is the reverse process.

Adsorption is operative in most natural physical, biological, and chemical systems, and is widely used in industrial applications such as activated charcoal, synthetic resins and water purification. Adsorption, ion exchange and chromatography are sorption processes in which certain adsorptives are selectively transferred from the fluid phase to the surface of insoluble, rigid particles suspended in a vessel or packed in a column.

Similar to surface tension, adsorption is a consequence of surface energy. In a bulk material, all the bonding requirements (be they ionic, covalent or metallic) of the constituent atoms of the material are filled. But atoms on the (clean) surface experience a bond deficiency,

because they are not wholly surrounded by other atoms. Thus it is energetically favorable for them to bond with whatever happens to be available. The exact nature of the bonding depends on the details of the species involved, but the adsorbed material is generally classified as exhibiting Pysisorption or Chemisorption.

Pysisorption [15-17] is a type of adsorption in which the adsorbate adheres to the surface only through Van der Waals force (weak intermolecular) interactions. It is characterized by:

- Low temperature, always under the critical temperature of the adsorbate
- Type of interaction: Intermolecular forces (van der Waals forces)
- Low enthalpy: $\Delta H < 20$ kJ mol $^{-1}$
- Adsorption takes place in multilayers
- Low activation energy

Chemisorption [15-17] is a type of adsorption whereby a molecule adheres to a surface through the formation of a chemical bond, as opposed to Pysisorption. It is characterized by:

- High temperatures.
- Type of interaction: strong; covalent bond between adsorbate and surface.
- High enthalpy: $\Delta H \approx 400$ kJ mol $^{-1}$
- Adsorption takes place only in a monolayer.
- High activation energy

Desorption [15-17] is a phenomenon and process opposite of sorption (that is, adsorption or absorption), whereby some of a sorbed substance is released. This occurs in a system being in the state of sorption equilibrium between bulk phase (fluid, i.e. gas or liquid solution) and an adsorbing surface (solid or boundary separating two fluids). When the concentration (or

pressure) of substance in the bulk phase is lowered, some of the sorbed substance changes to the bulk state.

Surface Coverage [14-17] is the number of adsorbed molecules on a surface divided by the number of molecules in a filled monolayer on that surface

Fractional surface coverage [14-17] is the ratio of the amount adsorbed at a given pressure to the maximum amount that the surface can take up.

Sticking Coefficient [14-17] is the ratio of the rate of adsorption to the rate at which the adsorptive strikes the total surface, i.e. covered and uncovered. It is usually a function of the surface coverage, of temperature and of the details of the surface structure of the adsorbent.

Mechanism of Heterogeneous Catalysis

The sequence of steps shown in Figure 1-3 constitutes the mechanism of heterogeneous catalysis. There are a number of theories proposed that capture these steps in sequence. The three most widely known and used in modeling surface chemistry and surface reactions are (1) **Langmuir-Hinshelwood-Hougen-Watson (LHHW)** [14,18,19] shown in Figure 1-4, (2) **Eley-Rideal (E-R)** [18,19] shown in Figure 1-5 and (3) the **Quasi-Homogeneous** [20] mechanism.

Langmuir-Hinshelwood-Hougen-Watson (LHHW) proposes three steps to capture a surface reaction. They are (A) two molecules adsorb onto the surface, (B) they diffuse across the surface and interact when they are close and (C) a molecule is formed which desorbs. The assumed sequence for the LHHW mechanism in an equation would take the following form

$$\text{Step 1: } A + S = (AS)$$
$$\text{Step 2: } B + S = (BS)$$
$$\text{Step 3: } (AS) + (BS) = (CS) + (DS)$$
$$\text{Step 4: } (CS) = C + S$$
$$\text{Step 5: } (DS) = D + S$$

where the letter ‘S’ denotes a surface species. The assumptions made fro the LHHW derivations are:

- The rate determining step is controlled by the surface reaction-step 3.
- Uniformly energetic adsorption sites,
- Monolayer coverage,
- A dual site mechanism is used for the reaction.

Eley-Rideal (E-R) also proposes a three steps mechanism to capture surface reaction, including (A) molecules adsorb on the surface, (B) another atom passes by which interacts with the one on the surface and (C) a molecule is formed which desorbs. The assumed sequence for the E-R mechanism in an equation would take the following form

Step 1: A + S = (AS)
Step 2: (AS) + B = (CS) + (DS)
Step 3: (CS) = C + S
Step 4: (DS) = D + S

where the letter 'S' denotes a surface species. The assumptions made fro the E-R derivations are:

- The rate determining step is controlled by the surface reaction- step 2,
- Uniformly energetic adsorption sites,
- Monolayer coverage,
- A single site mechanism is used for the reaction.

Quasi-Homogeneous catalysis does not allow for any adsorption of the molecules on the catalyst surface, in contrast to the LHHW and E-R mechanisms. The solid catalyst is assumed in the same phase as the reactants.

Catalytic combustion is a chemical process of the oxidation of fuel, initiated at the surface of the catalyst. This heterogeneous catalysis follows one or more of the above mechanisms of reactions. Based on LHHW, methane oxidation on Platinum (Pt) surface was proposed by Deutschmann [1, 21]. It involves a 24 step reaction mechanism and involves 7 species in the gas

phase and 11 species in the adsorbed phase. Table 1-1 shows the equations involved in the mechanism proposed for methane oxidation on Platinum. This surface mechanism is used in this study. Equations 1, 3, 4, 5, 7, 8, 10, 15, 19, 20, 21 and 22 are classical examples of adsorption. Equations 2, 6, 9, 11, 16 and 17 are examples of desorption and Equations 12, 13, 14, 18, 23 and 24 represent complex product formation as a result of surface reactions.

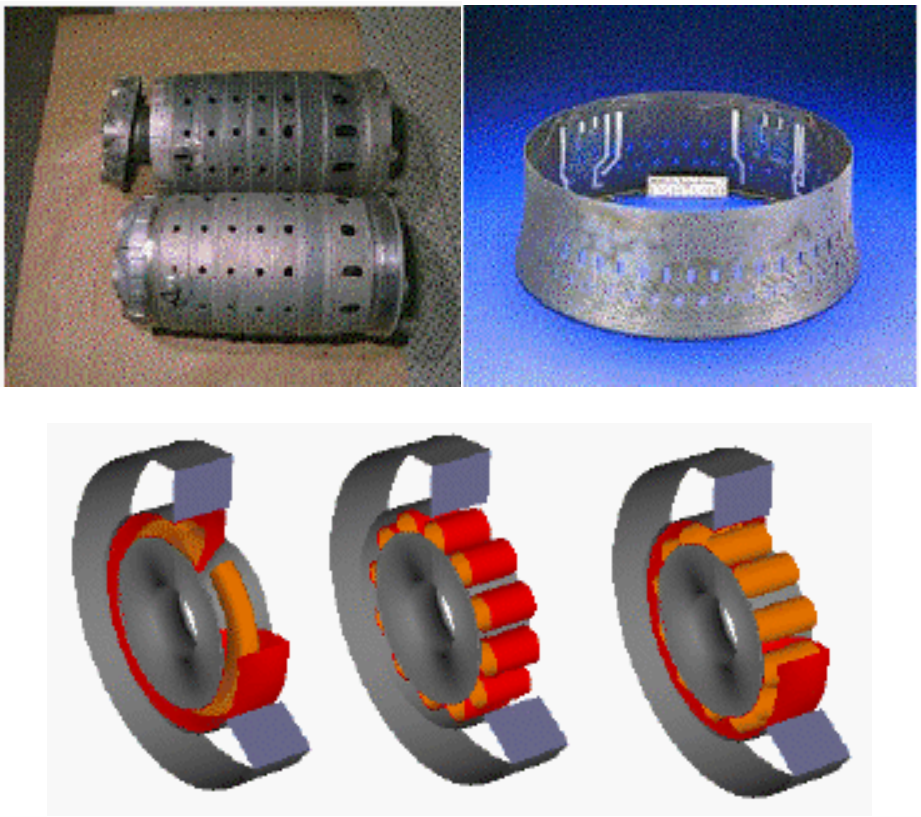

Figure 1-1 Types of combustors

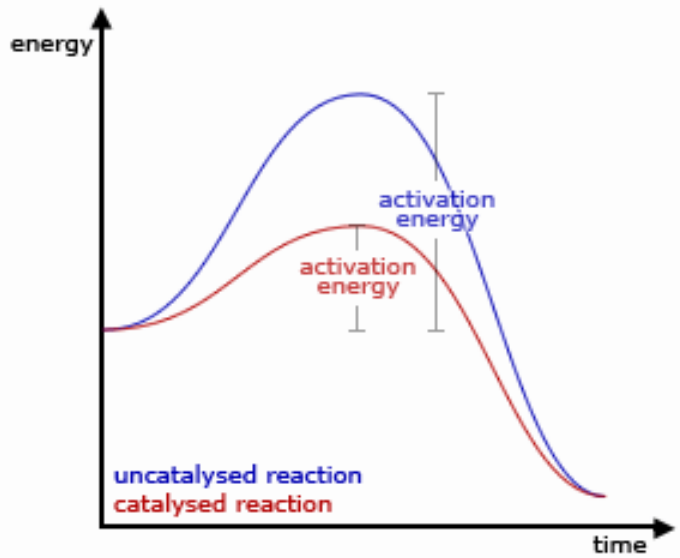

Figure 1-2. Catalysis taking place at reduced activation energy

- Step 1 - Reactants + Catalyst

- Step 2 - Reactants/Catalyst complex

- Step 3 - Products/Catalyst complex

- step 4 - Products + Catalyst

Figure 1-3. Steps involved in heterogeneous catalysis

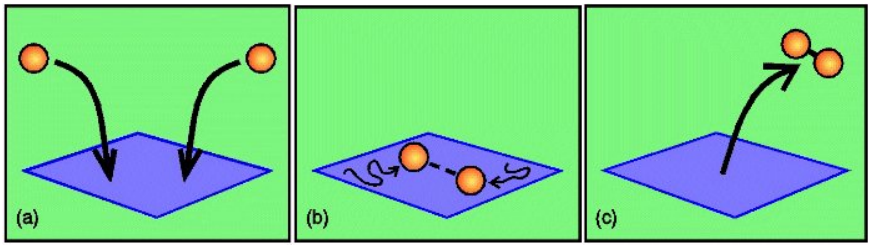

Figure 1-4. Steps involved in Langmuir-Hinshelwood-Hougen-Watson (LHHW) Catalysis

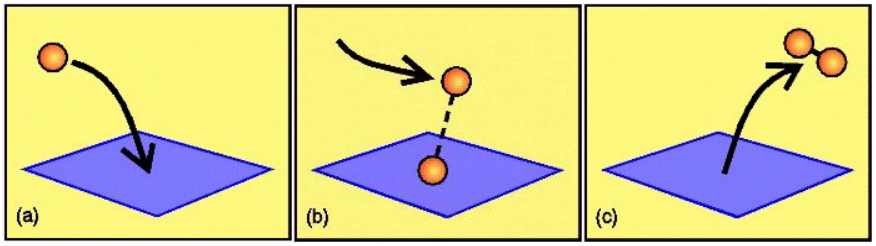

Figure 1-5. Steps involved in Eley-Rideal (E-R) catalysis

Table 1-1. Deutschmann's Surface Reaction Mechanism, A is Pre Exponential Factor (cm.mol.sec), β is Temperature Exponent and Ea (KJ/mol)

No.	Reaction	A (cm.mol.sec)	β	E_a (KJ/mol)
1	H_2+2Pt(s)=>2H(s)	4.60×10^{-2}	0	0
2	2H(s)=> H_2+2Pt(s)	3.70×10^{21}	0	67.4
3	H+Pt(s)=>H(s)	1.00	0	0
4	O_2+2Pt(s)=>2O(s)	1.8×10^{21}	-0.5	0
5	O_2+2Pt(s)=>2O(s)	2.30×10^{-2}	0	0
6	2O(s)=> O_2+2Pt(s)	3.70×10^{21}	0	213.2
7	O+Pt(s)=>O(s)	1.00	0	0
8	H_2O+Pt(s)=>H_2O(s)	0.75	0	0
9	H_2O(s)=>H_2O+Pt(s)	1.00×10^{13}	0	40.3
10	OH+Pt(s)=>OH(s)	1.00	0	0
11	OH(s)=> OH+Pt(s)	1.00×10^{13}	0	192.8
12	O(s)+H(s)<=> OH(s)+Pt(s)	3.70×10^{21}	0	11.5
13	H(s)+OH(s)<=> H_2O(s)+Pt(s)	3.70×10^{21}	0	17.4
14	OH(s)+ OH(s)<=> H_2O(s)+O(s)	3.70×10^{21}	0	48.2
15	CO+Pt(s)=> CO(s)	8.40×10^{-1}	0	0
16	CO(s)=> CO+Pt(s)	1.00×10^{13}	0	125.5
17	CO_2(s)=> CO_2+Pt(s)	1.00×10^{13}	0	20.5
18	CO(s)+O(s)=> CO_2(s)+Pt(s)	3.70×10^{21}	0	105.0
19	CH_4+2Pt(s)=>CH_3(s)+H(s)	1.00×10^{-2}	0	0
20	CH_3(s)+Pt(s)=>CH_2(s)+H(s)	3.70×10^{21}	0	20.0
21	CH_2(s)+Pt(s)=>CH(s)+H(s)	3.70×10^{21}	0	20.0
22	CH(s)+Pt(s)=>C(s)+H(s)	3.70×10^{21}	0	20.0
23	C(s)+O(s)=>CO(s)+Pt(s)	3.70×10^{21}	0	62.8
24	CO(s)+Pt(s)=>C(s)+O(s)	1.00×10^{18}	0	184.0

CHAPTER 2
EXPERIMENTAL STUDIES OF CATALYTIC COMBUSTION

Combustion Diagnostics

The mechanisms of heterogeneous catalysis referred so far models or to say predicts the possible manners in which a combustion process would be initiated. However, the whole purpose of any combustion analysis is rather incomplete without adopting a suitable diagnostics approach. Three most widely diagnostic approaches are (A) Mass Sampling, (B) Optical Diagnostics and (C) Computational Diagnostics.

(A) Mass sampling for species concentration measurement

Two most widespread techniques of mass sampling are mass Spectrometry and gas Chromatography.

Mass sampling techniques using mass spectrometry is during combustion. The technique gives a non intrusive measurement of radicals and reaction products during combustion. Nakra [22] has used mass spectrometry to predict the thermal decomposition of JP-10, Seery [23] probed flame species of JP-10 and Korobeinichev [24] has probed the combustion and the thermal decomposition of GAP. The technique is now widely being used in measuring the concentrations of *in situ* radicals and gas phase reaction products formed during catalytic combustion. Schwiedernoch [50] has investigated the catalytic combustion and hydrogen assisted catalytic partial oxidation of methane on platinum. Horn [34, 57] carried out mass spectra measurements recorded during catalytic partial oxidation of methane at 1500K on a Pt catalyst. The detection of $CH_3\cdot$ radicals was successfully demonstrated the formation of which is the most important step in methane combustion on platinum.Grunwaldt [35] studied the structure of a heterogeneous catalyst inside a catalytic micro-reactor during the partial oxidation of methane and used mass spectrometry to analyze reaction gas products. Yeh [36] used gas

chromatography for the characterization and determination of gas products of methane combustion on hexaluminate catalyst.

(B) Optical Diagnostics-Laser Induced Fluorescence in Combustion

In Laser-Induced Fluorescence (LIF), an atom or molecule gets excited by the absorption of a laser photon. When the atom falls back into the ground state after a certain time (typically 1-100nsec), it undergoes radiative emission, known as fluorescence. Since the fluorescence intensity is dependent on parameters such as ground state population, chemical environment, pressure, and temperature, laser-induced fluorescence measurements have become a vital tool in physical chemistry. For example, some applications include the investigation of elementary chemical reactions and trace analytics down to sub-ppm concentrations. In combustion diagnostics, LIF measurements (also called PLIF in planar illumination) are widely utilized. They allow for the qualitative and quantitative detection of temperatures, flame radicals and combustion intermediates such as OH, C_2, CH, CH_2O, as well as pollutants like NO and CO. Since these radicals are reaction *in situ* products in catalytic combustions LIF is another diagnostics. Dogwiler [34] used PLIF to map the OH concentration field in the streamwise direction while investigating the homogeneous ignition of methane air mixture over platinum catalyst.

(C) Computational Diagnostics

Computational fluid dynamics (CFD) complements experiments with theoretical predictions as a research tool to produce multi-scale information which can not be obtained using any other technique. There are several possible solution techniques in CFD investigation of reacting flows and a choice needs to be made for the proper technique that is to be applied in the present research. Combustion diagnostics is now an investigative technique in catalytic combustion too. Modeling the surface reaction mechanism, chemical kinetics of the reactions on

the surface, predicting the surface coverages of species on the catalyst surface along with modeling the transition from the heterogeneous catalysis to homogeneous are some of the most fundamental areas of catalytic combustion that are studied using CFD techniques. Deutschmann's [1-3, 21] surface chemistry mechanism for the combustion of methane on platinum is among the first using CFD to model catalytic combustion.

Motivation

The motivation behind being able to employ catalytic combustion is to reduce emissions and being able to create a pathway of low activation energy for the reactions to take place. The implementation of a noble-metal catalytic combustor in a natural-gas fired turbine for NO_x (nitrogen oxides) reduction has drawn great attention in recent years (Dalla Betta [37]). Currently NO_x emissions from stationary gas turbine systems are controlled either by lowering the combustion temperature with water injection or by removing NO_x through exhaust gas treatment such as selective catalytic reduction. In a catalytic combustor, a major portion of fuel conversion takes place on the catalyst surface; consequently, the gas phase NO_x production route via the prompt (or Fenimore [38, 39]) pathway is avoided (Schlegel [38, 39]). In addition, the peak gas phase combustion temperature is substantially reduced leading to low thermal (or Zeldovich [38, 39]) NO_x formation rate. However, the use of a solid catalyst then introduces two separate phases, namely, a gas phase wherein the participant reactants flow and a gas-solid (catalyst surface) interface phase, wherein the reactants flow over the surface of the catalyst. Both these phases play a major role in the completion of combustion. Catalytic combustion has a number of potentially important and practical applications like improved flame stability, generation of low-temperature process heat, and reduced pollutant emissions. It is expected that quantitative simulations will play an important role in accelerating the development in this field. Therefore, extensive research has been started to understand the elementary chemical processes occurring at

gas-surface interfaces [40], as well as their coupling to the surrounding flow and the gas phase reaction mechanism. The aim is to get a quantitative understanding of catalytic combustion. Methane is the major constituent of natural gas, and reactions of the methyl radical are among the rate limiting steps in the gas phase combustion of larger hydrocarbons. Thus, understanding of heterogeneous ignition and extinction of methane and the role of intermediate radicals at surfaces is crucial to use heterogeneous combustion processes efficiently and safely. Hence attempts have been made to understand heterogeneous catalysis by way of the kinetic approach. The fuel used is no longer limited to the use of natural gases only. Attempts are made to use mixtures of combustible gases on a catalytic surface to combine the combustion powers of two or more fuels. One such fuel of interest is syngas which is a mixture gaseous H_2 and CO. Both these gases oxidize in the presence of oxidizer usually air to form H_2O and CO_2 respectively and both these oxidation are exothermic process. Hence the reaction kinetics of species in various fuels on a given catalyst is of utmost importance. An attempt to understand the reaction pathway followed by different species on a given catalyst is studied in our research work.

Basically the method of chemical kinetics involves the quantitative determination of reaction products and their dependence on time and temperature, the expression of rates in terms of concentrations and temperature, and the construction of a mechanism to fit the observations[41]. Hence models for such a mechanism for various heterogeneous combustion processes have been tried for methane oxidation on Platinum surface. This thus leads us to understanding various surface chemistry models in details.

Surface Chemistry Models

One-Step Surface Reaction

Due to limited knowledge of the elementary surface reaction kinetics, numerical studies of methane catalytic combustion were often performed with a single step global surface reaction.

Song [42] used a single step surface reaction for predictions of methane catalytic combustion in a stagnation flow. With this simple chemical kinetic model, their calculations showed success in predicting surface ignition/extinction temperatures of lean methane-air mixtures. Since surface ignition temperatures of methane-air catalytic combustion are low, *ca.* 600°C, as predicted by Williams [43], the heterogeneous ignition process is dominated by the surface reaction due to its much lower activation energy compared to those of gas phase reactions. As calculations with a single-step reaction do not involve radicals, the well predicted ignition temperatures of lean methane-air mixture by Song [42] suggest that, under fuel- lean conditions, the interaction between catalytic and gas phase reactions is not important because the heterogeneous ignition is driven by the heat release of surface reaction. However, for high temperature conditions (> 1200 K), the interaction between catalytic and homogeneous reactions via radicals such as hydroxyl (OH) and O atom may potentially affect the ignition process (Pfefferle, Griffin [44]). In order to include the radical interaction between surface and gas phase at high temperatures, Markatou [45] modified the single step surface reaction model by introducing a coefficient to regulate the amount of OH desorbing from surface. The value of this coefficient was determined from experimental data. Their results show that the OH desorbed from the surface enhances the gas phase reactions and, hence, the generation of radicals in the boundary layer for surface temperatures above 1300 K. Markatou suggested the need of detailed surface kinetics and gas-surface energy balance to properly couple phase and surface processes in catalytic combustion calculations.

Multi–Step Surface Reaction Mechanisms

Previous numerical studies of catalytic methane oxidation by using multiple-step surface reactions have been reported by Hickman and Schmidt [46], by Deutschmann and Behredt [40]. These multi-step surface reaction mechanisms were developed with available kinetic and thermal

data along with several assumptions, such as Langmuir- Hinshelwood type surface reaction mechanism, dissociative adsorption of O_2 and CH_4, perfect catalyst surface, no substrate diffusion, and monolayer surface coverage. These resulting mechanisms consist of several basic reactions: adsorption of reactants (O_2 and CH_4) and intermediate species (CO, H_2, and OH), surface reactions of adsorbed species, and desorption of products (CO_2 and H_2O) and intermediate species. Details of these surface reactions are tabulated in Table 1-1. The surface reaction rates are described by an Arrhenius expression or by an initial sticking coefficient for adsorption processes. With the assumption of Langmuir-Hinshelwood surface reaction mechanism, the onset of surface ignition is determined by the competition between O_2 and CH_4 for surface sites. The dominant limiting process changes from oxygen desorption to methane adsorption as the surface temperature increases. When the surface temperature is low, due to the O_2 adsorption process, the catalyst surface is entirely covered by adsorbed O atom. The heat generated by this reaction raises the surface temperature.

As the surface temperature increases, the surface coverage of O atom drops and the methane adsorption reaction starts to increase. When the surface temperature reaches a certain point, the methane adsorption rate exceeds the oxygen adsorption rate such that methane adsorption reaction becomes dominant. Consequently, more heat is generated and ignition soon takes place on the catalyst surface. Similar surface ignition processes have been postulated by Behrendt [40]. Surface ignition temperature is another important feature which should be properly predicted by the surface reaction mechanism. Griffin and Pfefferle [47] measured methane surface ignition temperatures on a platinum wire. Their experimental results show the surface ignition temperature decreases with mixture equivalence ratio.

Moreover, the surface temperature prediction provides useful engineering information, such as the maximum temperature and temperature gradients, for better catalyst designs. Although some groups used Pt foils and N_2 as diluent [48, 49], other groups Pt wires [47], or Pt coated monoliths and Ar dilution (this work), no effect of dilution or shape of catalysts was observed. Hence two cases of methane oxidation, namely catalytic combustion of methane in absence of hydrogen (power heated) and catalytic partial oxidation of methane in presence of hydrogen (hydrogen assisted heating) is being studied on various flow configurations. The discussion beneath is based on platinum honeycomb monolith for both case studies, by Schwiedernoch, although as proven, the shape of the catalyst does not affect the studies.

Catalytic Combustion of Methane on Platinum

Research works based on the catalytic combustion of methane on platinum was conducted by Schwiedernoch [50]. The chemical reactions on the platinum surface were modeled using 27 irreversible elementary chemical reactions among 9 gas phase species and 11 surface species [1, 50]. In order to estimate the potential influence of gas-phase reactions on the methane oxidation, single channel calculations using additional 14 gas-phase species and 168 gas-phase reactions were performed. The homogeneous reaction scheme was based on a reduction of a large set of hydrocarbon oxidation reactions to C1 species. However, for temperatures below 1200 K no significant influence on the conversion was observed. Hence, the presented simulations are performed using only surface reactions. The simulations of this study were carried out by S. Tischer with DETCHEM version 1.4.2. [50, 51]. Our numerical simulation was conducted using FLUENT 6.

Before ignition, the surface is primarily covered with oxygen, because the sticking probability of oxygen is higher than that of methane. With increasing surface temperature a point will be reached where the adsorption/desorption equilibrium of oxygen shifts to desorption. This

results in bare surface sites where CH_4 can be adsorbed, followed by H abstraction, which leads to adsorbed C(s) and H(s) atoms reacting with the surrounding O atoms to form CO(s) and OH(s) immediately. Both molecules quickly form CO_2 and H_2O, which desorb leaving more free surface sites for CH_4-adsorption. For CH_4/O_2-ratios below 0.1 (2 vol.-% CH_4) the reaction is extinguished in a couple of minutes if the external heating is turned off. With the assumption of absence of gas-phase reactions, no CO was formed in the simulation. For CH_4 feeds exceeding 4 vol.-% CH_4/O_2-ratio greater than 0.21), gas-phase reactions become significant due to the high reaction temperature above 1200 K. Thus, simulations for CH_4/O_2-ratios exceeding 0.21, needs to include gas-phase reactions. However, in the study conducted in this research a very fuel rich mixture was used. It was expected that methane combustion on platinum for a rich mixture would also show similar results as when a lean mixture in Schwiedernoch's [50] works were used.

Catalytic Partial Oxidation of Methane on Platinum-Hydrogen Assisted

There are two ways in which the catalyst surface is basically heated. Power heating [50] of the catalyst and hydrogen assisted heating [1, 21, and 40]. The addition of hydrogen to the initial mixture for example may help to reduce the ignition temperature, because the ignition of hydrogen on platinum occurs at room temperature. Deutschmann [21] investigated the dependence of the hydrogen-assisted light-off of methane on platinum and on methane concentrations. They suggested that the light-off was primarily determined by the catalyst temperature that is a result of the heat release due to catalytic oxidation of hydrogen. The addition of H_2 to the feed gas for the catalytic combustion of CH_4 on Pt has a huge impact on the reaction behaviour. H_2 is very likely to contribute more than only heat for the ignition to the oxidation. Since H_2 removes O(s) from the surface by formation of H_2O, it is likely that H_2 has a great impact on the reaction kinetics of CH_4 combustion. Different ignition and maximum

temperatures, conversions, and yields of CO_2 indeed indicate an important role of H_2 on the kinetics causing considerable differences between hydrogen-assisted and thermally initiated reaction .In both cases, the light-off temperature decreases Figure 2-2 with increasing CH_4/O_2 ratio. At 400 K the surface is mainly expected to be covered with O(s) and hardly any Pt vacancies are left. Increasing the wall temperature (500 K) shows that now more CH_4 reaches the surface. This is due to a very small amount of C and CH formed by dissociation of CH_4, which is necessary for the combustion reaction.

At 600 K the first product formation is indicated by increasing amounts of CO and H_2O. However, it can be clearly seen that the addition of H_2 has a positive effect on the ignition temperature, which is more than 100 K lower than in case of common combustion. Here, not only CH_4 and O_2 compete for free vacancies but also H_2, which occupies the surface first. On a Pt catalyst, room temperature is sufficient to start exothermic H_2 combustion, which heats up the monolith. The higher maximum temperature blue symbols in Figure 2-2 (a) of the classical catalytic combustion compared to the H_2-assisted reaction (red) could be due to higher exothermic methane conversion as illustrated in (c). This phenomenon is best explained by surface kinetics. In case of H_2 addition water will be formed immediately by oxidation of H_2. Therefore, a certain amount of the surface area is always occupied by H_2O(s). This can be seen clearly by comparing these results with the surface coverage calculations in Figure 2-3 at 900 K, where with H_2 more surface sites are occupied by OH and H_2O than in absence of H_2. The adsorption of CH_4, dissociation as well as the reaction to CO and CO_2 respectively has to happen on the remaining vacancies downstream of the monolith. The high flow rate and the short length of the catalyst result even for these lean mixtures in a very short contact time of some milliseconds CH_4 breakthrough occurs. The added H_2 occupying the surface first under

dissociation, reacts with the adsorbed O(s). The produced water leaves the surface continuously generating vacancies, which methane can occupy, too. Figure 2-3 (right side) shows that the coverage of the surface is completely different, if H_2 is added. At 400 K already a huge amount of CO is formed, the surface is mostly covered by carbon, and CH and CH_2 can be found on the surface (not shown), too. Compared to the catalytic combustion without H_2, the number of free adsorption sites on Pt is increased by a factor of about 1000. The equilibrium calculations - as depicted in Figure 2-2 (d) dashed lines - show that in case of H_2 addition to the combustion gas more O_2 (in the order of 20%) should be converted; the experimental results support the calculation.

Additionally, the trend of increasing conversion of O_2 with increasing CH4/O2 ratio is observed, too. The reduced yield of CO_2 in case of addition of H_2 to the combustion gas compared to the conventional combustion can be explained with the equilibrium calculations, as well. Due to the higher concentrations of reducing agents CH_4 and H_2 in presence of H_2, more reduced species will be observed as reaction products. In this case more CO is formed. However, not only H_2 is responsible for enhanced formation of CO, but also the higher temperatures. With increasing temperatures, the CO + ½ O2 --> CO_2 equilibrium favor the formation of CO. In both cases gas-phase reactions occurred at a critical CH4/O2 ratio. For pure combustion of methane, they started at a CH_4/O_2 ratio exceeding 0.2 and in case of the H2-assisted combustion at a ratio of 0.35. The gas-phase reactions were indicated by a sudden rise of the concentration of CO and temperature.

Catalytic Combustion of Syngas on Platinum

Syngas is a gaseous mixture of H_2 and CO. From the hydrogen assisted catalytic combustion of methane on platinum performed in the works of Schwiedernoch [50], it is

observed that H_2 is very likely to contribute more than only heat for the ignition to the oxidation. Since H_2 removes O(s) from the surface by formation of H_2O, it is likely that H_2 has a great impact on the reaction kinetics of CH_4 combustion. Due to reducing agent H_2, more reduced species will be observed as reaction products. In this case more CO is formed. In this present study, the syngas reaction mixture comprises of H_2, CO, CH4 and CO_2. Due to the presence of H_2, it is expected that for the given mixture, it would still act as a reducing agent and thus the formation of reduced species such as CO is more likely to be formed than the fully oxidized CO_2. This prompted us to believe that the same surface reaction mechanism as used by Deutschmann's [21] during the hydrogen assisted catalytic combustion of methane would be able to model the catalytic combustion of syngas as well.

Catalytically Stabilized Thermal Combustion (CST)

In Catalytically Stabilized Combustion (CST) [52, 53] partial fuel conversion is accomplished heterogeneously in burners with a large surface-to-volume ratio, such as catalytically-coated honeycomb monoliths. Complete fuel conversion is attained in a post-catalyst homogeneous combustion zone. This process leads to substantial reduction of NOx emissions (typically < 3 ppm) as NOx is produced exclusively from the gaseous (homogeneous) reaction path. Thus the overall predictions of CST combustion take into account both the heterogeneous and the homogeneous phase reaction schemes. The thermal interactions between the two schemes are instrumental in predicting the CST combustion accurately.

Catalytic Activation Index (CAI)

In our present work, combustion experiments were performed on four catalysts of different chemical composition. A basis for comparing the performance of the catalysts is therefore very essential. An overall performance of any catalyst can be judged by the amount of products formed. Since a catalyst actually reduces the activation energy required for any reaction, it means

that a catalyst increases the number density of reactants available for reaction by reducing the activation energy thereby increasing the probability of more reactants participating in a given reaction. However, a new index called the *Catalytic Activation Index* (CAI) [54] conceptualizes the performance of one catalyst over the other. The value of CAI compares different catalysts. This is a non-dimensional number calculated from the delay period (τ_{delay}), combustion duration (τ_{cd}) and the lean misfire limit (Φ_{LLT}). The delay period is defined as the time taken for a 5% heat release. The combustion duration is assumed to be the time period between 5% and 90% heat release[55]. These times would be achieved by running the reacting case in FLUENT and reporting the temperature changes with respect to time. The lean misfire limit was determined experimentally by varying the fuel-air ratio.

$$CAI = [(\tau_{delay})_{base} / (\tau_{delay})_{cat} (\tau_{cd})_{base} / (\tau_{cd})_{cat}]^{0.5} . \chi (\Phi_{LLT})_{base} / (\Phi_{LLT})_{cat}$$

CAI higher than unity indicates catalytic activation. Based on this index, different catalysts can be compared and the apparent surface activation temperatures are obtained from

$$(Ea / Ru)_{surface} = (Ea / Ru)_{global} / CAI$$

The characteristic surface reaction rate is obtained from

$$1 / \tau_{ch} = k(T_W)[Y_{fuel}][Y_{Oxidiser}] \text{ Kmol/s}$$

$$\text{Where } k(T_W) = A(T_W) \exp(-Ea_{surface} / (Ru.T_W))]$$

A characteristic temperature for a catalyst can be defined as the temperature beyond which the catalytic activity increases exponentially. This temperature can be determined by calculating

the Damkohler number (Da), based on the ratio of diffusion rate and the surface reaction rate. The physical meaning of unity Da is that the rate of reaction will be equal to rate of diffusion. For each catalyst, the temperature at which Da becomes unity differs. The surface reaction is expected to increase after the temperature corresponding to unity Da. Hence, we propose that the critical temperature of the catalyst may be the temperature at which Da is unity.

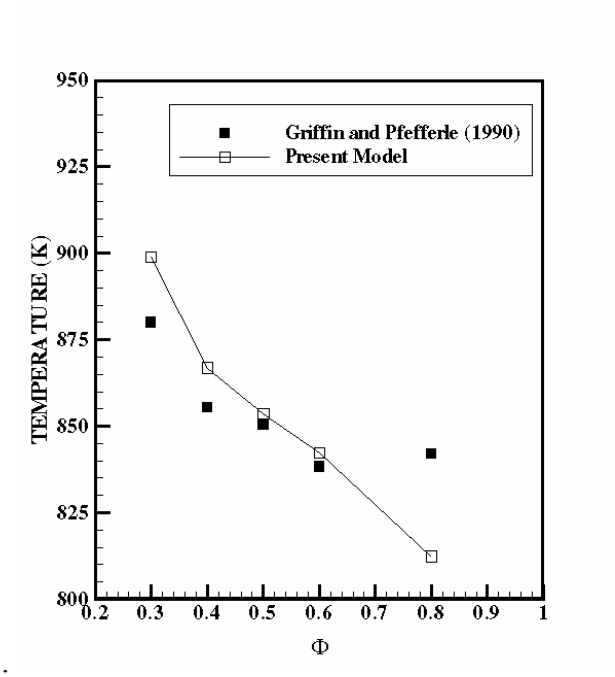

Figure 2-1. Surface Ignition Temperature decreases with increase in methane equivalence ratio

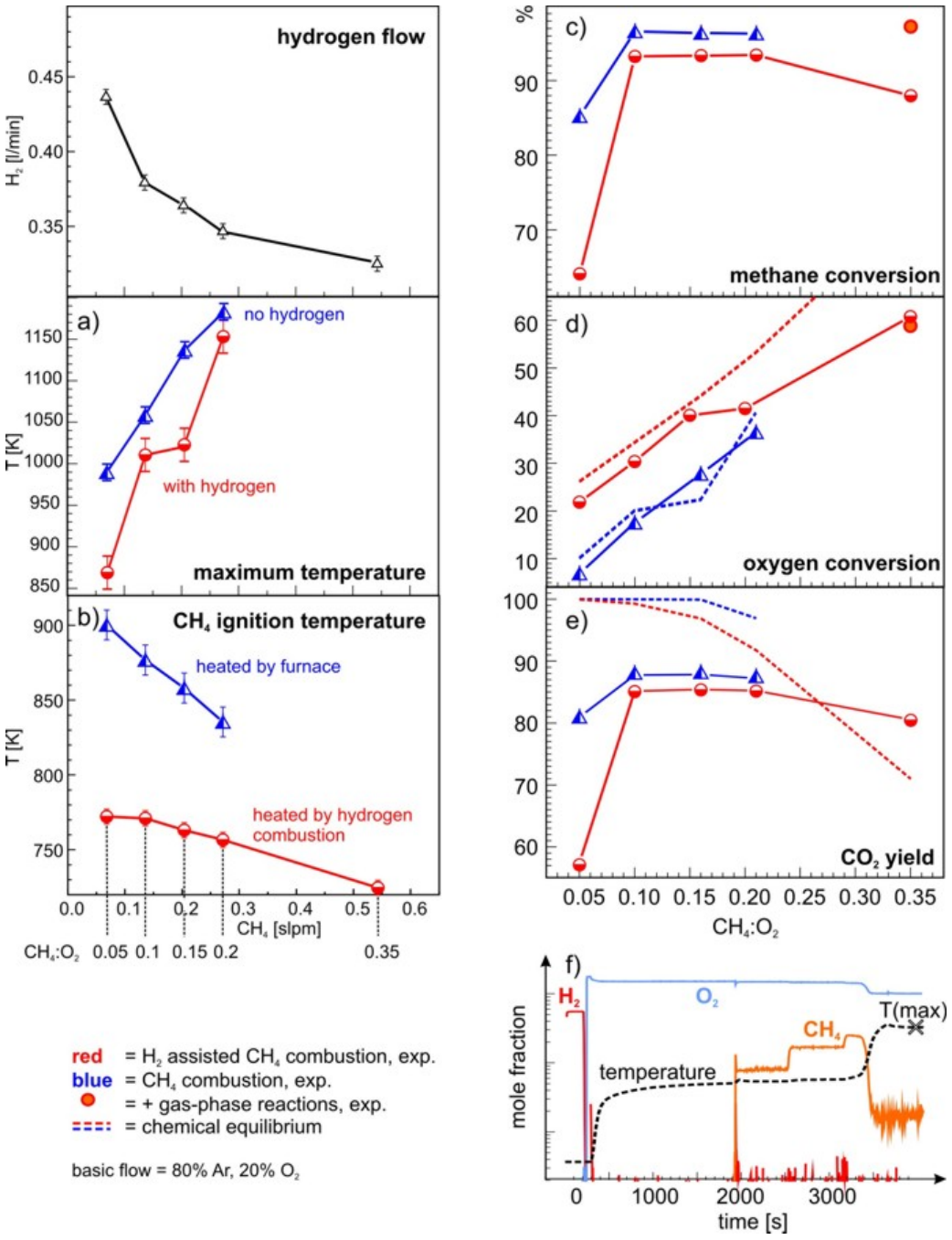

Figure 2-2. Methane Combustion with no H_2 and with H_2 (a) maximum temperature (b) methane ignition temperature (c) methane conversion (d) oxygen conversion and (e) CO_2 yield

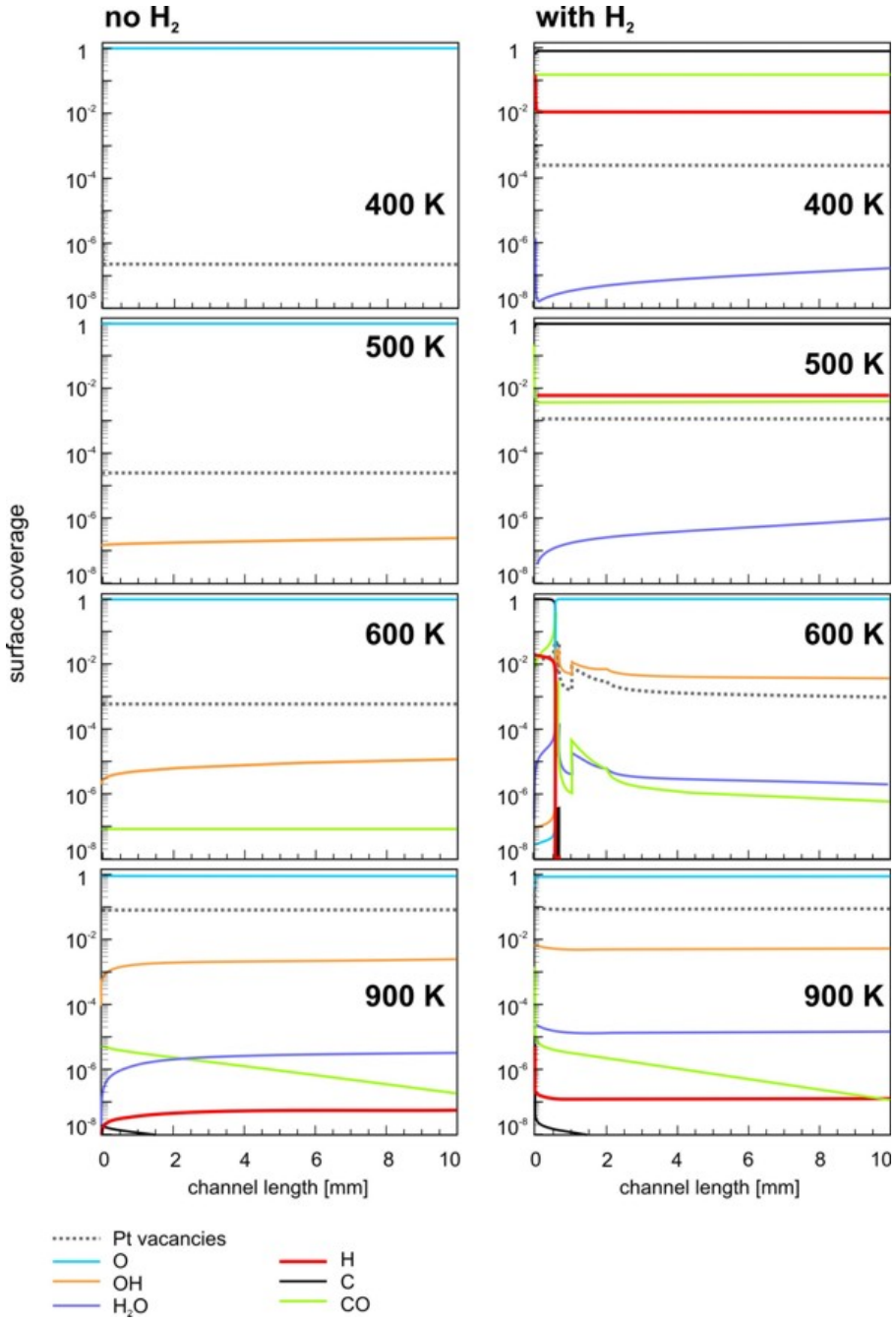

Figure 2-3. Surface coverage of species in methane combustion with no H_2 and with H_2

Table 2-1. Deutschmann's Surface Reaction Mechanism, A is Pre Exponential Factor (cm.mol.sec), β is Temperature Exponent and Ea (KJ/mol)

No.	Reaction	A (cm.mol.sec)	β	E_a (KJ/mol)
1	H_2+2Pt(s)=>2H(s)	4.60×10^{-2}	0	0
2	2H(s)=> H_2+2Pt(s)	3.70×10^{21}	0	67.4
3	H+Pt(s)=>H(s)	1.00	0	0
4	O_2+2Pt(s)=>2O(s)	1.8×10^{21}	-0.5	0
5	O_2+2Pt(s)=>2O(s)	2.30×10^{-2}	0	0
6	2O(s)=> O_2+2Pt(s)	3.70×10^{21}	0	213.2
7	O+Pt(s)=>O(s)	1.00	0	0
8	H_2O+Pt(s)=>H_2O(s)	0.75	0	0
9	H_2O(s)=>H_2O+Pt(s)	1.00×10^{13}	0	40.3
10	OH+Pt(s)=>OH(s)	1.00	0	0
11	OH(s)=> OH+Pt(s)	1.00×10^{13}	0	192.8
12	O(s)+H(s)<=> OH(s)+Pt(s)	3.70×10^{21}	0	11.5
13	H(s)+OH(s)<=> H_2O(s)+Pt(s)	3.70×10^{21}	0	17.4
14	OH(s)+ OH(s)<=> H_2O(s)+O(s)	3.70×10^{21}	0	48.2
15	CO+Pt(s)=> CO(s)	8.40×10^{-1}	0	0
16	CO(s)=> CO+Pt(s)	1.00×10^{13}	0	125.5
17	CO_2(s)=> CO_2+Pt(s)	1.00×10^{13}	0	20.5
18	CO(s)+O(s)=> CO_2(s)+Pt(s)	3.70×10^{21}	0	105.0
19	CH_4+2Pt(s)=>CH_3(s)+H(s)	1.00×10^{-2}	0	0
20	CH_3(s)+Pt(s)=>CH_2(s)+H(s)	3.70×10^{21}	0	20.0
21	CH_2(s)+Pt(s)=>CH(s)+H(s)	3.70×10^{21}	0	20.0
22	CH(s)+Pt(s)=>C(s)+H(s)	3.70×10^{21}	0	20.0
23	C(s)+O(s)=>CO(s)+Pt(s)	3.70×10^{21}	0	62.8
24	CO(s)+Pt(s)=>C(s)+O(s)	1.00×10^{18}	0	184.0

CHAPTER THREE
EXPERIMENTAL AND COMPUTATIONAL SETUPS

Experimental Setup

The test setup is modeling a small part of a catalytic combustor for a stationary gas turbine fuelled by syngas mixtures using a single surface covered with catalyst.

The test setup shown in Figure 3-1 consists of a steel tube coated with catalyst on the outside, which is enclosed in a larger coaxial tube fitted with thermocouples, gas sample ports and optical windows for observation. A rich fuel mixture flows in the annular space between the two tubes while the center of the catalyst tube carries cooling air. Downstream of the catalyst the cooling air is allowed to mix with the rich catalyst exhaust.

The air flowing through the annular portion is called the "mixing air" while the air through the center of the catalyst is called the "cooling air". The fuel is never heated while the "mixing" as well as the "cooling" air are heated as per the experiment specification. The fuel and the hot "mixing air" mixes in a predefined mixing zone, before flowing through the annular portion. Both these streams of air are heated using two Omega® Electric Heaters -AHP-3741 and AHP-7561- and these two air temperatures are read using K-type Omega® thermocouples KMTXL-062E-6. The Omega® heaters are rated as 200W and 750W respectively and their safe working operation is ensured by the use of two Solid State Relays from Omega® SSRL240DC10. The air stream temperatures are controlled using two Proportional-integral-derivative (PID) controllers.

There are four other similar K-type Omega® thermocouples KMTXL-062E-6 that read the catalyst surface temperature, an intermediate downstream temperature, the temperature at the location where the rich catalyst exhaust mixes with the "cooling air" and the temperature of the stainless steel mass sampling tube, respectively. The two thermocouples that register the catalyst surface temperature are located at x/L values of 0.3 and 0.73, where x is the axial distance from

the start of the catalyst tube and L is the length of the catalyst tube. These two thermocouples touch the surface of the catalyst. The thermocouple that registers the gas phase temperature when the combustion exhausts mix with the "cooling air" stream is located at x/L value of 1.2. A 2D-axisymmetry schematic of the combustor section is shown in figure 3-2.

In order to ensure that water vapor formed during combustion does not condense in the stainless steel mass sampling tubes described below a provision of heating this tube up to a set point temperature of 130°C was made using the same principles of PID controllers that was applied to maintain the two air streams at their respective set point temperatures.

Since only the catalyst part of the combustor is studied in this setup, the exhaust is then further diluted with excess air to achieve a non-flammable mixture which is exhausted. The mass flows of the two incoming air streams as well as those of the constituent gases of the syngas, i.e. CO, CO_2, H_2 and CH_4 were controlled by Alicat Scientific 16 series mass flow controllers, allowing full flexibility in the gas composition tested. The operating ranges for these mass flow controllers are shown in Table 3-1, where SLPM and SCCM are Standard Liters Per Minute and Standard Cubic Centimeters per Minute respectively.

Mass Sampling

Hardware

The physical location of mass sampling ports along the axis of the catalytic combustor is shown in Figure 3-2. The axial positions of the two sampling ports are also shown in the figure.

The test section has provisions for two mass sampling ports along the axial direction of the catalytic combustor. Sampling is done from only one of these during a given experiment while the other port is being used to hold a thermocouple for measuring the surface temperature of the catalyst. Thus when the upstream port samples gas species the downstream port records surface temperature of the catalyst at that location and vice versa. This set up allows investigating the

change in temperatures and species concentration at two different locations on the surface of the catalyst. The sampling ports are swapped when running a different experiment. They are located at $x/L = 0.3$ and $x/L = 0.73$, where L is the length of the catalyst, L = 22.8 cm and the x distance is measured from the location where the catalyst starts. These ports are 0.8 mm inner diameter steel tubes and are at right angles to the direction of flow, i.e. they are located radially inside the cylindrical catalytic combustor such that they touch the surface of the catalyst. A schematic diagram of mass sampling from the catalytic combustor and subsequent, real-time analysis by a mass spectrometer is shown in Figure 3-3. The species were analyzed by Stanford Research Systems RGA-300 mass spectrometer, which uses electron ionization to ionize the sampled gas, RF quadrupole filter to sort species according to their mass-to-charge ratio, and Faraday cup to detect ion currents.

The instrument is controlled and operated by software and associated electronics. The ionizer, filter and detector are enclosed in a clean vacuum chamber and require an operating pressure range of 10^{-4} torr (1.3×10^{-7} atm) to ultra high vacuum. Such low pressure is attained in two stages. In first stage, a rotary pump brings the inlet pressure down to about 60 mtorr (7.9×10^{-5} atm). In a second stage, a diffusion pump and a rotary pump operate in series to bring the pressure further down to vacuum conditions. The diffusion pump is surrounded by a water jacket carrying cold water to keep the diffusion pump cool. The water is cooled using a chiller. For the optimum working conditions of the diffusion pump, it is specified to receive water at a temperature between 15°C to 25°C at a flow rate of 0.6 l/s. The spectrometer can detect species up to a mass-to-charge ratio of 300 and has a resolution of 0.5 AMU @ 10% peak height. The sensitivity factor of the instrument, defined as the signal detected per unit partial pressure of a given species (Amp / torr), varies for different gases. Hence calibration of the instrument was

performed for the following gases: helium, nitrogen, oxygen and argon. The sensitivity factor of nitrogen is used as the baseline and sensitivity factors of other gases are normalized with this baseline.

One limitation with the use of compressed air as oxidizer in combustion analysis using Quadruple mass spectrometry is that the peaks of N_2 and CO overlap at an AMU value of 28. Hence concentrations of CO and N_2 in the combustion mixture could not be reported separately. Assuming N_2 inertness, the mass fraction of N_2 after combustion remains the same as known from inlet conditions. The partial pressure of species with AMU 28 was obtained from MS which was then converted into mole fraction and mass fraction. This mass fraction is a result of the contribution made by both N_2 and CO if present. The difference between the mass fractions after and before combustion gives the mass fraction contribution due to CO. However, it was seen in a number of experiments that the calculated value of CO by adopting this method resulted in unrealistic values of CO's mole fraction. A possible solution would be replacement of N_2 in air with a different species. Argon use, attempted here required renewed calibration. Given the higher Ar molecular weight, i.e. 40, the calibration factor for lighter species e.g. H_2 led to large errors and the procedure was discarded. Hence, in what follows compressed air was used as the oxidizer. Over experiments described in chapter 4 the uncertainty of species measurements ranged from 0.9-1.3% for N_2, 0.3-0.7% for O_2, 0.5-0.7% for CH_4, 0.4-0.6% for CO_2 and 0.7-1.1% for H_2O for all methane combustion cases and 0.1-0.4% for N_2, 0.4-3.3% for CO, 0.1-1.6% for O_2, 0.1-0.6% for H_2, 0.3-1.1% for CO_2, 0.2-1.5% for H_2O and 0.1-1.1% for CH_4 for all syngas combustion cases.

Data processing

The composition of gas in the catalytic combustor was analyzed by the mass spectrometer in partial pressure of species vs. time mode. The species scanned were hydrogen (m/z=1 and 2),

methane (m/z=15 and16), oxygen (m/z=16 and 32), (water (m/z=17 and 18), nitrogen (m/z=14 and 28), carbon monoxide (m/z= 28) and carbon monoxide (m/z=28 and 44) for combustion experiments. The local mole fraction of a given species in the sample was determined from the partial pressures of all the component species recorded by the mass spectrometer. The time-averaged fuel mole fraction at a port was obtained by averaging the mole fractions obtained over the sampling time period.

The species mole fractions were corrected using calibration factors for individual gases. The sensitivity or the calibration factor for the mass spectrometer was established using the following the procedure.

The specific inlet composition for the case of methane as well as syngas composition was passed through the test section at room temperature. This represented the non-reacting flow of the gas mixtures through the combustor section. Only one of the sampling ports, located at x/L value of 0.3 was chosen to sample this gas mixture into the mass spectrometer. The mole fractions of the constituent gases in the gas mixture calculated from the partial pressures registered by the mass spectrometer must match the exact inlet mole fractions. Since the mass spectrometer reading was slightly different a factor was formulated for those species for which the mole fraction obtained from the inlet specifications and mass spectrometer did not match. This factor was either less than unity or more than unity depending upon whether the species was over-predicted or under-predicted from the species inlet composition. A gas mixture of each species and nitrogen at room temperature and at 700K was passed through the test section. The calibration factors at both temperatures were the same, thus, indicating the fact that the calibration factor was temperature independent.

Computational Setup

Tools: The computational tools used were GAMBIT 2.2.30 for generating the design of the catalytic combustor as well as generating the mesh over this design, and FLUENT 6.2.16 as the computational solver. The computational setup is therefore divided into two parts, namely (A) the design of the computational domain (catalytic combustor) and grid generation, both using GAMBIT [34] and (B) setting up and running the CASE, using FLUENT [35] solver.

Computational Setup in Gambit

The GAMBIT software package is designed to help analysts and designers build and mesh models for computational fluid dynamics and other scientific applications. GAMBIT receives user input primarily by means of its graphical user interface GUI. The GAMBIT GUI makes the basic steps of building and meshing a model simple and intuitive, yet it is versatile enough to accommodate a wide range of modeling applications. GAMBIT allows creating drawing files, dividing the drawing domain into grids (meshing the model), defining the *boundary condition type* and defining the continuum of the domain, i.e. assigning the domain as either *solid* or *fluid.*

Computational Domain-Creating Drawing Files and Generating Mesh Files

In order to ease the computational expense, the catalytic combustor design is divided into four separate zones. They collectively capture (i) the individual fuel and oxidizer feed line zones, (ii) the premixing zone of the fuel and the oxidizer, (iii) the expansion zone of the fuel-oxidizer mixture over a “CROSS-JOINT” and (iv) the zone where the fuel-oxidizer mixture flows through the annular portion of the catalytic combustor over the surface of the catalyst. The last three zones are collectively shown in Figure 3-1. The first zone is the fuel line and the oxidizer line, each being a quarter inch outer diameter tube. It is long enough to result in a fully developed flow for both the fuel and oxidizer lines. The catalytic combustor has a circular cross section in all the four zones. The meshing model includes boundary layers at all the circular

edges as well as at that portion in the premixing zone , where the fuel comes in contact with the oxidizer for the first time, **"face mesh"** at all the inlet faces of all the four computational zones and finally **"volume mesh"** over the entire volume of all the zones. A brief discussion on the types and procedures of generating the mesh mentioned above is Appendix A.

Computational Setup in FLUENT

Fluent serves as the solver software, general-purpose CFD software for a wide range of industrial applications, along with highly-automated, specifically-focused packages.

FLUENT models fluid flow and heat transfer in complex geometries providing complete mesh flexibility, including the ability to solve flow problems using unstructured meshes that can be generated about complex geometries with relative ease. Supported mesh types include 2D triangular/ quadrilateral, 3D tetrahedral/hexahedral/pyramid/wedge, and mixed (hybrid) meshes. FLUENT also allows us to refine or coarsen our grid based on the flow solution. FLUENT is written in the C computer language and makes full use of the flexibility and power offered by the language.

The commercial CFD software FLUENT is a fully-unstructured finite-volume CFD solver for complex flows ranging from incompressible (subsonic) to mildly compressible (transonic) to highly compressible (supersonic and hypersonic) flows. The cell-based discretization approach used in FLUENT is capable of handling arbitrary convex polyhedral elements. For solution strategy, FLUENT allows a choice of two numerical methods, either segregated or coupled. With either method FLUENT solves the governing integral equations for conservation of mass, momentum, energy and other scalars such as turbulence and chemical species. Both segregated and coupled numerical methods employ a similar finite-volume discretization process but their approach to linearization and solution of the discretized equations is different. A point implicit (Gauss-Seidel) linear equation solver is used in conjunction with an Algebraic Multigrid (AMG)

scheme to solve the resultant linear system for the dependent variables in each cell. In the present study, laminar flame dynamics has been investigated by applying the FLUENT solvers.

Program Capabilites

The FLUENT solver has the following modeling capabilities:

- 2D planar, 2D axisymmetric, 2D axisymmetric with swirl (rotationally symmetric), and 3D flows
- Quadrilateral, triangular, hexahedral (brick), tetrahedral, prism (wedge), pyramid, and mixed element meshes
- Steady-state or transient flows
- Incompressible or compressible flows, including all speed regimes (low subsonic, transonic, supersonic, and hypersonic flows)
- Inviscid, laminar, and turbulent flows
- Newtonian or non-Newtonian flows
- Heat transfer, including forced, natural, and mixed convection, conjugate (solid/fluid) heat transfer, and radiation
- Chemical species mixing and reaction, including homogeneous and heterogeneous combustion models and surface deposition/reaction models.

Numerical Model

A brief description of the numerical model follows. It is a full elliptical two-dimensional axisymmetric model for a steady, laminar two dimensional gaseous reactive flow with the additional presence of surface reactions. For surface chemistry, the reaction mechanism proposed by Deutschmann (Table 1-1) for the catalytic combustion of methane on platinum was used which included 22 irreversible reactions, 8 gaseous and 11 surface species (including Pt). The catalyst site density was taken as 2.7 x 10-8 Kgmol/m2 simulating a polycrystalline platinum surface. The platinum coating on top of a non-porous Al2O3 support closely resembles such a surface. For gaseous chemistry, the five step reaction mechanism is a reasonable simplification

of this study. The mechanism is listed in table. The Chemkin and FLUENT database is used to evaluate gaseous transport and surface species thermodynamic properties.

Mathematical Model

(A) Governing Equations

The governing equations solved are those of continuity, momentum, energy and the species transport. This conservation equation takes the following general form:

Continuity: $$\frac{\partial \rho}{\partial t} + \nabla.(\rho \vec{v}) = 0 \tag{3-1}$$

Momentum:

$$\frac{\partial}{\partial t}(\rho \vec{v}) + \nabla.(\rho \vec{v}\vec{v}) = -\nabla p + \nabla.(\bar{\bar{\tau}}) + \rho \vec{g} + \vec{F} \tag{3-2}$$

where p is the static pressure, $\bar{\bar{\tau}}$ is the stress tensor, $\rho \vec{g}$ and $\vec{F}$ are the gravitational and external body forces respectively, the stress tensor $\bar{\bar{\tau}}$ is given by

$$\bar{\bar{\tau}} = \mu[(\nabla \vec{v} + \nabla \vec{v}^{T}) - \frac{2}{3}\nabla.\vec{v}I] \tag{3-3}$$

where μ is the molecular viscosity, I is the unit tensor and the second term on the right hand side is the effect due to volume dilation.

Energy: $$\frac{\partial}{\partial t}(\rho E) + \nabla.(\vec{v}(\rho E + p)) = \nabla.(k\nabla T - \sum_{j} h_j \vec{J}_j + (\bar{\bar{\tau}}.\vec{v})) + S_h \tag{3-4}$$

where k is the thermal conductivity, $\vec{J}_j$ is the diffusion flux of species j. The first three terms on the right hand side represent energy transfer due to conduction, species diffusion and viscous dissipation respectively. S_h includes the heat of chemical reaction and any other user defined heat source.

When solving conservation equations for chemical species, FLUENT predicts the local mass fraction of each species, Y_i, through the solution of a convection-diffusion equation for the ith species.

$$\frac{\partial}{\partial t}(\rho Y_i) + \nabla.(\rho \vec{v} Y_i) = -\nabla.\vec{J}_i + R_i + S_i \tag{3-5}$$

where R_i is the net rate of production of species i by chemical reaction (described later in this section) and Si is the rate of creation by addition from the dispersed phase plus any user-defined sources. An equation of this form will be solved for N-1 species where N is the total number of fluid phase chemical species present in the system. Since the mass fraction of the species must sum to unity, the N^{th} mass fraction is determined as one minus the sum of the (N-1) solved mass fractions. To minimize numerical error, the N^{th} species should be selected as that species with the overall largest mass fraction, such as N2 when the oxidizer is air.

Mass Diffusion in Laminar Flows

In Equation 3-5, $\vec{J}_i$ is the diffusion flux of species i, which arises due to concentration gradients. By default, FLUENT uses the dilute approximation, under which the diffusion flux can be written as

$$\vec{J}_i = -\rho D_{i,m} \nabla Y_i \tag{3-6}$$

Here $D_{i, m}$ is the diffusion coefficient for species i in the mixture. For certain laminar flows, the dilute approximation may not be acceptable, and full multicomponent diffusion is required. In such cases, the Maxwell-Stefan equations can be solved.

Treatment of Species Transport in the Energy Equation

For many multicomponent mixing flows, the transport of enthalpy due to species diffusion

$$\nabla.\left[\sum_{i=1}^{n} h_i \vec{J}_i\right] \tag{3-7}$$

can have a significant effect on the enthalpy field and should not be neglected. In particular, when the Lewis number

$$Le_i = \frac{k}{\rho c_p D_{i,m}} \tag{3-8}$$

for any species is far from unity, neglecting this term can lead to significant errors. FLUENT will include this term by default and where *k* is the thermal conductivity, for any species is far from unity, neglecting this term can lead to significant errors. FLUENT will include this term by default.

The Generalized Finite-Rate Formulation for Reaction Modeling

The reaction rates that are computed in FLUENT by one of three models:

- Laminar finite-rate model: The effect of turbulent fluctuations are ignored, and reaction rates are determined by Arrhenius expressions.
- Eddy-dissipation model: Reaction rates are assumed to be controlled by the turbulence, so expensive Arrhenius chemical kinetic calculations can be avoided. The model is computationally cheap, but, for realistic results, only one or two step heat-release mechanisms should be used.
- Eddy-dissipation-concept (EDC) model: Detailed Arrhenius chemical kinetics can be incorporated in turbulent flames. Note that detailed chemical kinetic calculations are computationally expensive.

The generalized finite-rate formulation is suitable for a wide range of applications including laminar or turbulent reaction systems, and combustion systems with premixed, non-premixed, or partially-premixed flames. We have adopted the finite rate formulation for setting up our combustion model.

The Laminar Finite-Rate Model

The laminar finite-rate model computes the chemical source terms using Arrhenius expressions, and ignores the effects of turbulent fluctuations. The model is exact for laminar flames, but is generally inaccurate for turbulent flames due to highly non-linear Arrhenius chemical kinetics. The laminar model may, however, be acceptable for combustion with relatively slow chemistry and small turbulent fluctuations, such as supersonic flames. The net source of chemical species i due to reaction R_i is computed as the sum of the Arrhenius reaction sources over the NR reactions that the species participate in:

$$R_i = M_{w,i} \sum_{r=1}^{N_R} \hat{R}_{i,r} \tag{3-9}$$

where $M_{w,i}$ is the molecular weight of species i and $\hat{R}_{i,r}$ is the Arrhenius molar rate of creation/destruction of species i in reaction r. Reaction may occur in the continuous phase between continuous-phase species only, or at wall surfaces resulting in the surface deposition or evolution of a continuous-phase species.

If we consider the rth reaction written in general form as follows:

$$\sum_{i=1}^{N} \nu'_{i,r} \aleph_i \underset{K_{b,r}}{\overset{K_{f,r}}{\rightleftharpoons}} \sum_{i=1}^{N} \nu''_{i,r} \aleph_i \tag{3-10}$$

N = number of chemical species in the system

$\nu'_{i,r}$ = stoichiometric coefficient for reactant i in reaction r

$\nu''_{i,r}$ = stoichiometric coefficient for product i in reaction r

$\aleph_i$ = symbol denoting species i

$K_{f,r}$ = forward rate constant for reaction r

$K_{b,r}$ = backward rate constant for reaction r

Equation 3-10 is valid for both reversible and non-reversible reactions (Reactions in FLUENT are non-reversible by default.) For non-reversible reactions, the backward rate constant, $K_{b,r}$ is simply omitted. The summations in Equation 3-10 are for all chemical species in the system, but only species that appear as reactants or products will have non-zero stoichiometric coefficients. Hence, species that are not involved will drop out of the equation. The molar rate of creation/destruction of species i in reaction r ($\hat{R}_{i,r}$ in Equation 3-9) is given by

$$\hat{R}_{i,r} = \Gamma(\nu''_{i,r} - \nu'_{i,r})(K_{f,r}\prod_{j=1}^{N_r}[C_{j,r}]^{\eta'_{j,r}} - K_{b,r}\prod_{j=1}^{N_r}[C_{j,r}]^{\eta''_{j,r}}) \tag{3-11}$$

N_r = number of chemical species in reaction r

$C_{j,r}$ = molar concentration of each reactant and product species j in reaction r (kgmol/m3)

$\eta'_{i,r}$ = forward rate exponent for each reactant and product species j in reaction r

$\eta''_{i,r}$ = backward rate exponent for each reactant and product species j in reaction r

Γ represents the net effect of third bodies on the reaction rate. This term is given by

$$\Gamma = \sum_{j}^{N_r}\gamma_{j,r}C_j \tag{3-12}$$

where $\gamma_{j,r}$ is the third-body efficiency of the jth species in the rth reaction. By default, FLUENT does not include third-body effects in the reaction rate calculation. You can, however, opt to include the effect of third-body efficiencies if you have data for them. The forward rate constant for reaction r, $K_{f,r}$ is computed using the Arrhenius expression

$$K_{f,r} = A_r T^{\beta_r} e^{-\frac{E_r}{RT}} \tag{3-13}$$

where

A_r = pre-exponential factor (consistent units)

β_r = temperature exponent (dimensionless)

E_r = activation energy for the reaction (J/kg mol)

R = universal gas constant (J/kg mol-K)

The user or the database provides values for $\nu'_{i,r}, \nu''_{i,r}, \eta'_{i,r}, \eta''_{i,r}, \beta_r, A_r, E_r$ and $\gamma_{j,r}$ during the problem definition in FLUENT.

If the reaction is reversible, the backward rate constant for reaction r, $K_{b,r}$ is computed from the forward rate constant using the following relation:

$$K_{b,r} = \frac{K_{f,r}}{K_r} \tag{3-14}$$

where K_r is the equilibrium constant for the rth reaction, computed from

$$K_r = \exp\left(\frac{\Delta S^0{}_r}{R} - \frac{\Delta H^0{}_r}{RT}\right)\left(\frac{p_{atm}}{RT}\right)^{\sum_{r=1}^{N_R}(\nu''_{j,r}-\nu'_{j,r})} \tag{3-15}$$

where p_{atm} denotes atmospheric pressure (101325 Pa). The term within the exponential function represents the change in Gibbs free energy, and its components are computed as follows:

$$\frac{\Delta S^0{}_r}{R} = \sum_{i=1}^{N}(\nu''_{i,r} - \nu'_{i,r})\frac{S^0{}_i}{R} \tag{3-16}$$

$$\frac{\Delta H^0{}_r}{RT} = \sum_{i=1}^{N}(\nu''_{i,r} - \nu'_{i,r})\frac{h^0{}_i}{RT} \tag{3-17}$$

where $S^0{}_i$ and $h^0{}_i$ are the standard-state entropy and standard-state enthalpy (heat of formation). These values are specified in FLUENT as properties of the mixture material.

For gas-phase reactions, the reaction rate is defined on a volumetric basis and the rate of creation and destruction of chemical species becomes a source term in the species conservation

$$\sum_{i=1}^{N_g} g'_{i,r} G_i + \sum_{i=1}^{N_b} b'_{i,r} B_i + \sum_{i=1}^{N_s} s'_{i,r} S_i \xleftrightarrow{K_r} \sum_{i=1}^{N_g} g''_{i,r} G_i + \sum_{i=1}^{N_b} b''_{i,r} B_i + \sum_{i=1}^{N_s} s''_{i,r} S_i \quad \text{(3-18)}$$

equations. The rate of deposition is governed by both chemical kinetics and the diffusion rate from the fluid to the surface. Wall surface reactions thus create sources (and sinks) of chemical species in the bulk phase and determine the rate of deposition of surface species. FLUENT treats chemical species deposited on surfaces as distinct from the same chemical species in the gas. Similarly, reactions involving surface deposition are defined as distinct surface reactions and hence treated differently than bulk phase reactions involving the same chemical species. Surface reactions can be limited so that they occur on only some of the wall boundaries (while the other wall boundaries remain free of surface reaction). The surface reaction rate is defined and computed per unit surface area, in contrast to the fluid-phase reactions, which are based on unit volume. We consider the rth wall surface reaction written in general form as follows:

$$\sum_{i=1}^{N_g} g'_{i,r} G_i + \sum_{i=1}^{N_b} b'_{i,r} B_i + \sum_{i=1}^{N_s} s'_{i,r} S_i \xleftrightarrow{K_r} \sum_{i=1}^{N_g} g''_{i,r} G_i + \sum_{i=1}^{N_b} b''_{i,r} B_i + \sum_{i=1}^{N_s} s''_{i,r} S_i \quad \text{(3-18)}$$

where, G_i, B_i, and S_i represent the gas phase species, the bulk (or solid) species, and the surface-adsorbed (or site) species, respectively. N_g, N_b, and N_s are the total numbers of these species. $g'_{i,r}$, $b'_{i,r}$ and $s'_{i,r}$ are the stoichiometric coefficients for each reactant species i, and $g''_{i,r}$, $b''_{i,r}$ and $s''_{i,r}$ are the stoichiometric coefficients for each product species i. Kr is the overall reaction rate constant. The summations in Equation (3-18) are for all chemical species in the system, but only species involved as reactants or products will have non-zero stoichiometric coefficients. Hence, species that are not involved will drop out of the equation.

The rate of the rth reaction is

$$R_r = k_{f,r} \prod_{i=1}^{N_g} [G_i]_{wall}^{g'_{i,r}} [S_i]_{wall}^{s'_{i,r}} \quad (3\text{-}19)$$

where, [ ]$_{wall}$ represents molar concentrations on the wall. It is assumed that reaction rate does not depend on concentrations of the bulk (solid) species. From this, the net molar rate of consumption or production of each species i, is given by

$$\hat{R}_{i,gas} = \sum_{r=1}^{N_{rxn}} (g''_{i,r} - g'_{i,r}) R_r \qquad \text{i = 1, 2, 3 …Ng} \quad (3\text{-}20)$$

$$\hat{R}_{i,bulk} = \sum_{r=1}^{N_{rxn}} (b''_{i,r} - b'_{i,r}) R_r \qquad \text{i = 1, 2, 3 …N}_b \quad (3\text{-}21)$$

$$\hat{R}_{i,site} = \sum_{r=1}^{N_{rxn}} (s''_{i,r} - s'_{i,r}) R_r \qquad \text{i = 1, 2, 3 …N}_s \quad (3\text{-}22)$$

The forward rate constant for reaction r (kf,r) is computed using the Arrhenius equation

$$k_{f,r} = A_r T^{\beta_r} e^{-\frac{E_r}{RT}} \quad (3\text{-}23)$$

where A_r = pre-exponential factor (consistent units)

β_r = temperature exponent (dimensionless)

E_r = activation energy for the reaction (J/kgmol)

R = universal gas constant (J/kgmol-K)

The user or the database provides the values of the coefficients.

(B). Boundary Conditions

A 2D axisymmetric model is solved for Zone 4. This is the only zone that we are solving the reacting case simulation for.

Velocity:

A no slip velocity boundary condition is applied at all wall surfaces.

Temperature:

The combustor wall is a zero heat flux zone. The catalyst thickness has a boundary condition of 1-D heat conduction. On one side of the catalyst wall, we have air in flow at 700K while on the other side we have the fuel air mixture in flow at 700k. Hence, boundary condition on either side of the catalyst is that of convective heat transfer.

Wall surface reaction Boundary condition:

As shown in Equations (3-15- 3-18), the goal of surface reaction modeling is to compute concentrations of gas species and site species at the wall; i.e., $[G_i]_{wall}$ and $[S_i]_{wall}$. Assuming that, on a reacting surface, the mass flux of each gas species is balanced with its rate of production/consumption, then

$$\rho_{wall} D_i \frac{\partial Y_{i,wall}}{\partial n} - \dot{m}_{dep} Y_{i,wall} = M_{w,i} \hat{R}_{i,gas} \qquad \text{i = 1, 2, 3 …Ng} \tag{3-24}$$

$$\frac{\partial [S_i]_{wall}}{\partial t} = \hat{R}_{i,site} \qquad \text{i = 1, 2, 3 …N}_s \tag{3-25}$$

The mass fraction Y_i, wall is related to concentration by

$$[G_{i,wall}] = \frac{\rho_{wall} Y_{i,wall}}{M_{w,i}} \tag{3-26}$$

$\hat{R}_{i,r}$, is the net rate of mass deposition or etching as a result of surface reaction; i.e.

$$\dot{m}_{dep} = \sum_{i=1}^{N_b} M_{w,i} \hat{R}_{i,bulk} \tag{3-27}$$

$[S_i]_{wall}$ is the site species concentration at the wall, and is defined as

$$[S_i]_{wall} = \rho_{site} z_i \tag{3-28}$$

where ρ_{site} is the site density and z_i is the site coverage of species i. Using Equations (3-24) and (3-25), expressions can be derived for the mass fraction of species i at the wall and for the net rate of creation of species i per unit area. These expressions are used in FLUENT to compute gas

phase species concentrations, and if applicable, site coverages, at reacting surfaces using a point-by-point coupled stiff solver.

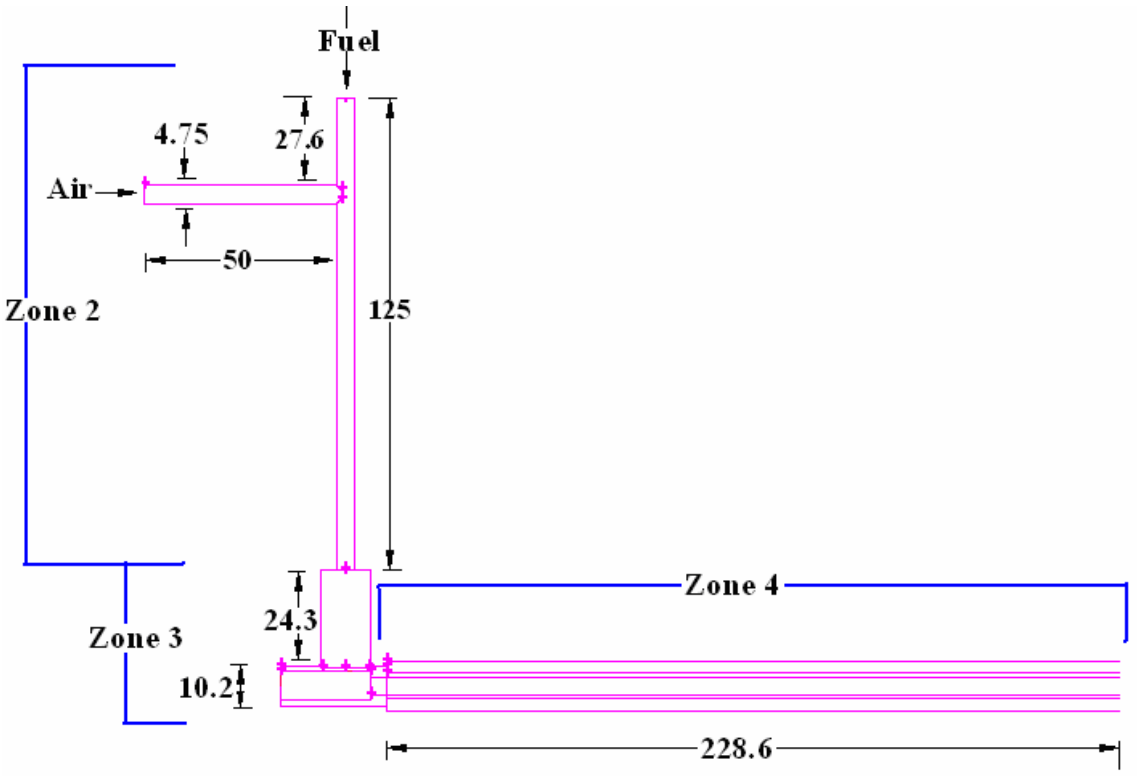

Figure 3-1. Model of the Catalytic Combustor: Zone 2 is the fuel-air mixing region, Zone 3 is the fuel-air mixture expansion in a CROSS and Zone 4 is the combustor section holding the catalyst and the annulus. All dimensions are in mm

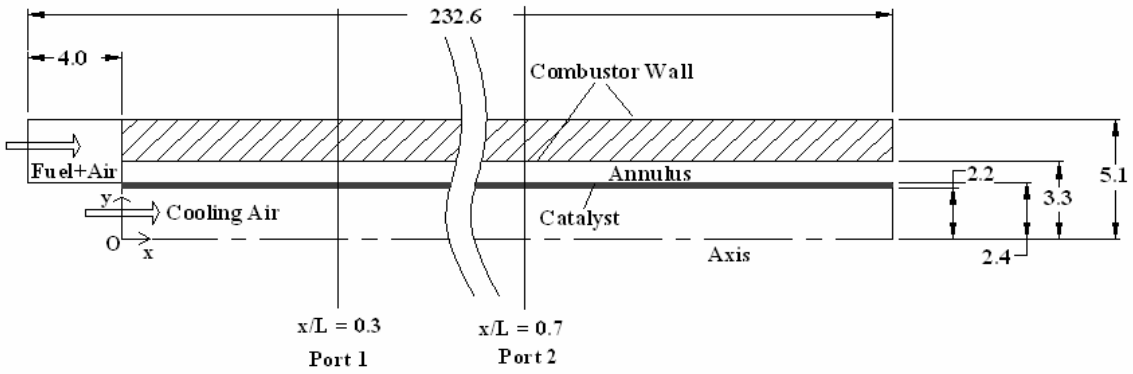

Figure 3-2. 2D-axisymmetric schematic of the Combustor section including catalyst and mass sampling ports 1 and 2. All dimensions are in mm

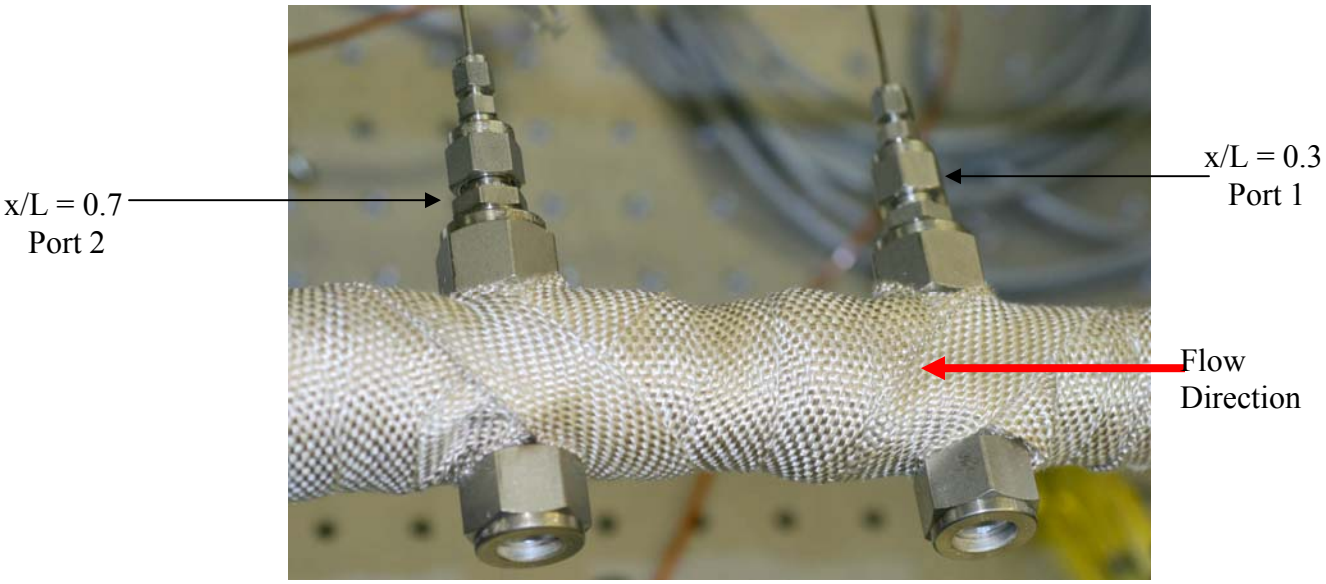

Figure 3-3. Mass Sampling Ports

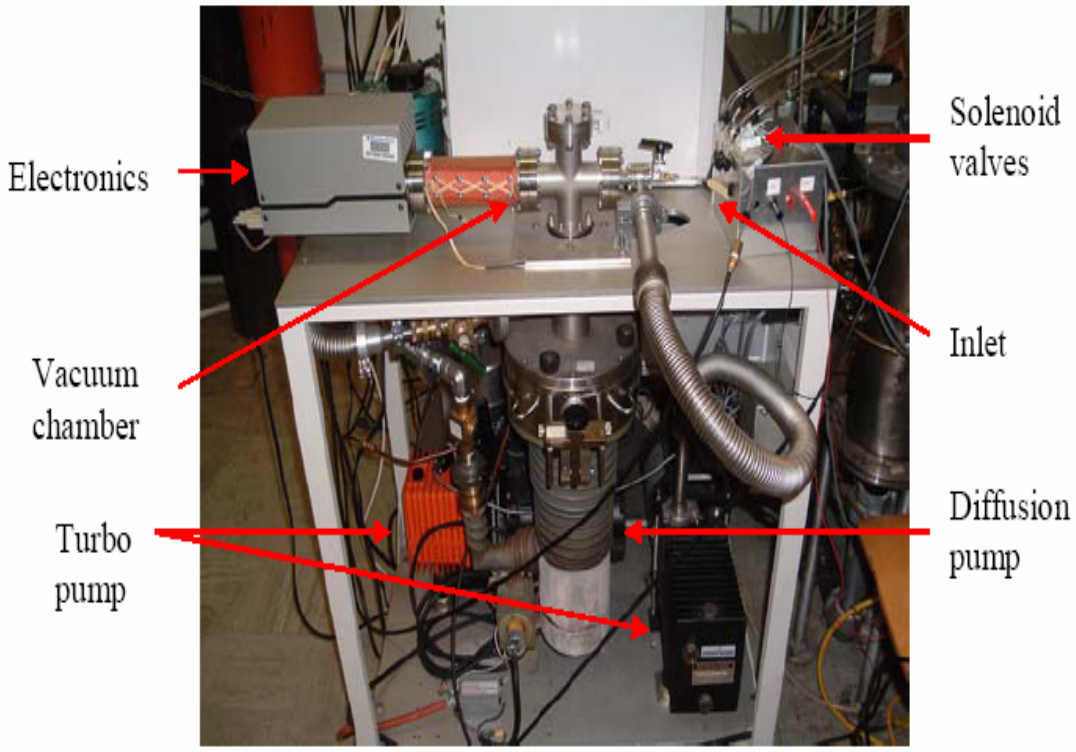

Figure 3-4. Mass Spectrometers for Species Concentration Measurement

Table 3-1. Operating Range for Mass Flow Controllers

Mass Flow Controllers	**Operating Range**
Air	0 – 10 SLPM
Air	0 – 60 SLPM
CH_4	0 – 50 SCCM
CO	0 – 5 SLPM
CO_2	0 – 1 SLPM
H_2	0 – 5 SLPM

CHAPTER 4
RESULTS AND DISCUSSION

Experimental and Computational analysis of the catalytic combustion was applied to the cases shown in Table 4-1. As seen in the table the computation using Deutschmann's surface chemistry model for CH_4/Air and (H_2+CH_4)/Air and an additional five step gas phase reaction mechanism for Syngas/Air covered the platinum smooth experimental cases. Since the composition of catalysts A and B is not fully characterized a surface reaction is not available at this time.

The experimental work measured the mole fraction of the products of combustion of hydrogen assisted methane/air and syngas/air on platinum catalysts. Mass spectroscopy was employed to measure the mixture composition of combustion at two axial locations.

The computational work provided detailed information including the mole fraction, velocity and temperature profiles at the two experimental axial locations. The reacting flow was modeled using Deutschmann's surface chemistry [1, 3, 21] shown in Table 4-2 and an additional five step gas phase reaction mechanism shown in Table 4-3.

A five step gas phase reaction was added to the 27 step surface reaction mechanism. The Deutschmann's model assumes the presence of atomic hydrogen and oxygen which required a pathway to their formation. Combustion temperatures were expected to be above 1000K which could lead to the dissociation of O_2 and H_2. This justifies the inclusion of the first two equations in the gas phase model. To keep the number of reactions to a computationally manageable size a simple reaction was introduced for CO oxidation in the gas phase.

The non-reacting flow was computed to infer mole fraction distribution, velocity and temperature profiles at various sections of the computational domain. These sections include the two mass sampling ports named as Port One and Port Two throughout our study. The mass

sampling experiments were carried out under steady premixed fuel-air mixture flow conditions. Two fuels and four catalysts were used for experimentation: methane ($\chi_{CH_4} = 0.24$), and syngas, which was primarily a mixture of methane ($\chi_{CH_4} = 0.002$), carbon monoxide ($\chi_{CO} = 0.29$), carbon dioxide ($\chi_{CO_2} = 0.06$), and hydrogen ($\chi_{H_2} = 0.16$). The inlet gas composition is shown in Table 4-4 and Table 4-5.

The two catalysts used were stainless steel hypodermic tubes coated with smooth Platinum and rough platinum respectively. The "mixing air" was kept at room temperature for all "cold flow" experiments with both fuels and on all catalysts. The "cooling air" was not passed during "cold flow" experiments. The "mixing" and "cooling air" (allowed to pass during combustion/reacting flow conditions) were both heated to 688 K during all experiments carried on all catalysts and with both the fuels. The fuels were always maintained at room temperature. Pressure conditions were atmospheric. The area weighted average velocity of the methane-air mixture at the entrance to the catalyst section was 3.1 m/s and that of the syngas-air mixture was 8.82 m/s respectively. These velocities lead to Mach Numbers of 0.01 and 0.026, thereby confirming the incompressible flow regime.

The composition of the gas (reacting as well as non reacting flow) in the combustor over the catalyst section was analyzed by the mass spectrometer in Partial Pressure of Species vs. Time mode. The species scanned were nitrogen (m/z=14 and 28), oxygen (m/z=16 and 32), methane (m/z=15 and 16) for non-reacting experiments with methane; nitrogen (m/z=14 and 28), oxygen (m/z=16 and 32), methane (m/z=15 and 16), hydrogen (m/z=1 and), carbon monoxide (m/z= 28) and carbon dioxide (m/z=44) with non-reacting syngas and nitrogen (m/z=14 and 28), oxygen (m/z=16 and 32), hydrogen (m/z=1 and 2), methane (m/z=15 and 16), carbon monoxide (m/z= 28), carbon dioxide (m/z=44) and water (m/z=17 and 18) for combustion experiments

with both fuels. There are two sampling ports at x/L = 0.3 and x/L = 0.73 respectively, where L = 21.8 cms denotes the length of the catalyst.

The mole fraction of a given species in the sample was determined from the partial pressures of all the component species recorded by the mass spectrometer. Further, the time-averaged fuel mole fraction at a port was obtained by averaging the mass fractions obtained over the sampling time period.

Experimental Results

For all reacting flow experiments, the temperatures of the mixing and cooling were maintained at a fixed 700 K. The surface temperature of the catalyst is measured when the air flows have reached a steady state.

Methane-Air Combustion: Mass Sampling in the Axial Direction

Methane inlet conditions are specified in the Table 4-4.Methane did not ignite when the platinum catalysts were used.

Syngas-Air Combustion: Mass Sampling in the Axial Direction

Syngas inlet specifications are shown in Table 4-5. The combustion of syngas was carried on platinum smooth and platinum rough Figures 4-1 through 4-6. Repeatability experiments were carried out performing two experiments at port two for each of the catalysts. The standard deviation between 10%-14% for the platinum catalysts is observed.

Unlike methane, syngas ignited on all the two catalysts. The axial distribution of the time averaged mole fraction of the species obtained from the combustion of syngas on platinum smooth and platinum rough catalysts are shown in Figures 4-1 through 4-6. Methane was in trace amount in the syngas composition used here and therefore for all practical purposes the methane presence can be neglected. The inlet conditions are shown in Table 4-5. Platinum rough shows better combustion traits than smooth. A considerable consumption of fuel and oxygen seems to

take place from port one to two and increased production of water and carbon dioxide on port two suggest increased combustion downstream.

A comparison between the performances of these two catalyst in converting reactants and yielding products during Syngas combustion is shown in Figures 4-3 through 4-6. An equilibrium calculation using STANJAN© was performed for syngas combustion with the same experimental conditions. The equilibrium mixture showed a mole fraction of 0.075% of H2 suggesting a conversion of 95% and a mole fraction of 11.3% for CO suggesting 65% conversion for CO. From our experiments it is found that the percentage conversion of H_2 on platinum smooth and 75% on platinum rough, whereas conversion of CO was found to 12% on platinum smooth and 30% on platinum rough are 39% and 42% respectively. Hence platinum smooth appears to convert H_2 better than any other catalyst and platinum rough converts CO than others.

Computational Results

Non Reacting Flow

The non reacting cases were computed to determine the mixture temperature and composition uniformity at the catalyst entrance. The computational domain is shown in Figure 4-7. The local mole fractions are shown in Figure 4-8 at selected cross sections as follows: Section ee is the exit from the computational zone 2 just after the fuel and air have mixed, section ff is the exit from the section of the cross which is computational zone 3, port 1 is section at experimental axial mass sampling location at x/L = 0.3 and port 2 is section at experimental axial mass sampling location at x/L = 0.73.

The bulk of the methane distribution above the catalyst surface shows a local equivalence ratio of 3.17 corresponding to a mole fraction of 0.249 as against a global input equivalence ratio of 3.04, thereby suggesting that the sampling port locations show an even fuel rich mixture. Other parts of the air passage show a local equivalence ratio of 2.95 corresponding to a mole

fraction of 0.237. Thus the computational results show a 5% non homogeneity. However, as the flow progresses downstream, the mole fraction distribution becomes more homogeneous as the flow reaches port one suggesting improved mixing.

The computational works accomplished so far with syngas, is shown as contours of mole fraction of H_2 and CO and velocity profiles at various sections. All these cases represent computational results for non reacting case. Sections are shown in figure 4-7. The mole fraction distribution of hydrogen and CO in Syngas at the sections ee, ff, port one and two are shown in Figure 4.9 and Figure 4.10.

Reacting Flow

Four separate computational reacting cases were studied in this research work, namely,

(a) Effect of catalyst surface site density on the formation of products,

(b) Catalytic Combustion of Methane on Platinum catalyst,

(c) Catalytic Partial Oxidation of Methane on Platinum: Hydrogen Addition,

(d) Catalytic Combustion of Syngas (a gas mixture of H_2, CO, CO_2 and CH_4) on Platinum,

(e) Effect of equivalence ratio on surface coverages of Syngas constituent species and product mole fractions, and

(f) Comparison between the experimental and computational results of Syngas combustion.

The basis of all the numerical investigations is a study of the surface coverage behavior of different species on platinum, and the effects that they have on the chemical kinetics of the heterogeneous combustion process. It is believed that the different surface coverage behaviors of different species on platinum are the key factor that initiates or truncates combustion.

(A). Effect of Catalyst Surface Site Density on the Formation of Products

Computations were also performed with the different values of the surface site density i.e. 1×10^{-8} Kgmol/m^2, 2×10^{-8} Kgmol/m^2, 2.7×10^{-8} Kgmol/m^2, 3×10^{-8} Kgmol/m^2 and 6×10^{-8}

Kgmol/m^2. Decreasing the site density from 2.7 x 10^{-8} Kgmol/m^2 shows a small change in the product % mole fraction, while increasing the site density shows almost no effect on product % mole fraction, since surface reactions are close to their mass transport limit as shown in Figure 4-11 through 4-16. The choice of temperature is random, since the trends of observations are the same at all temperatures. Only those temperatures are thus chosen in figures for which there were pronounced yield of the products. Temperatures of 1700K for Methane combustion, 900K for hydrogen assisted methane combustion and 1100K for syngas combustion was chosen since at these temperatures ignition is rapid and a trend of the reactions taking place with variations in site density can thus be established.

The surface characteristics of the two types of platinum catalyst used in experiments are shown below in Figures 4-17. Platinum was deposited on stainless steel tubes. Then one of the tubes was sand blasted. This tube is referred in what follows to as "Rough" platinum. The rough surface shows more grains per unit area and hence more exposed surface area than the smooth surface. The increased exposed surface area could result in an increased number of active free sites on the platinum which in turn would provide for increased probability of species adsorption and hence in turn increased surface reactions. The smooth surface appears to have reduced surface area. However, the range of site density values selected for the simulations (see Chapter 4 below) seems to produce no pronounced effect in combustion for all cases studied numerically a range of 1x10^{-8} Kgmol/m^2 to 6x10^{-8} Kgmol/m^2 for comparisons with previous studies[60]. Here the baseline was selected to be 2.7x10^{-8} Kgmol/m^2.

(B). Catalytic Combustion of Methane on Platinum Catalyst

Experimentally methane predominantly did not ignite on the platinum for surface temperatures below 1100K. There are two reasons: the melting point of stainless steel, which was the platinum substrate, is 1200K-1400K. Therefore the experiments were limited to 900K.

At a reduced surface temperature the adsorbed oxygen atoms do not leave the surface indicating higher surface coverage, and thus allow lesser vacancies for methane dissociation to take place. Hence, the surface temperature of the catalyst at higher equivalence ratio is not desirable for a surface ignition. Moreover, with more and more gas phase methane approaching the platinum surface and with surface temperature gradually decreasing the dissociation of methane into CH_3, CH_2, CH, H and C is greatly inhibited. Since the formation of these radicals is absolutely necessary for methane combustion on platinum, their inhibited formation at fuel rich conditions did not support combustion. This behavior requires a detailed explanation of the effects of species surface coverage on initiating and sustaining and/or extinguishing an ignition. This description is given below:

The role of surface coverage can be explained by assuming that before combustion is initiated, the surface is primarily covered with oxygen because the sticking probability of oxygen is higher than that of methane. This can be noticed in Figures 4.18 through 4.25 where the platinum surface is totally covered with oxygen as long as the surface temperatures does not exceed 1100K. In these cases the surface coverage value is close to 1 for oxygen on platinum and hardly any platinum vacancies are left. Hence no O atom is available to oxidize CH_4 and there is no CO_2 and H_2O formed along the entire catalyst length. With increasing surface temperatures conditions are reached where the adsorption/desorption equilibrium of oxygen shifts to desorption as shown in Figures 4.23 through 4.25 where the reducing surface coverage value of oxygen suggest desorption. As a result there are available bare surface sites where CH_4 can be adsorbed, an absolutely necessary step in initiating combustion of methane on platinum followed by H abstraction, which leads to adsorbed C(s) and H(s) atoms reacting with the surrounding O atoms to form CO(s) and OH(s). Significant amounts of CO(s) and OH(s) seem to be formed

only at and above 1100K, and hence their oxidation to form CO_2 and H_2O becomes predominant above 1100K followed by their desorption leaving more free surface sites for CH_4 adsorption. The pronounced behavior can be seen in figures 4-21 through 4-25 along with the corresponding product formation is shown in figures. The surface temperature distribution over the catalyst surface shown in Figure 4.26 suggests that not until the surface temperature reaches 1200K that the adsorption/desorption equilibrium of oxygen begin to shift towards desorption and it is then when the onset of O atoms leave the platinum surface, thus creating a possibility of vacant sites on the platinum surface upon which the adsorption of CH_4 becomes possible. However, the literature[56] indicates that the homogeneous i.e. gas phase reaction scheme is based on the reduction of a large set of hydrocarbon oxidation reactions to C1 species. Also, with the assumption of the absence of gas phase reactions, no CO was formed in the simulation. In order to capture the production of CO, the gas-phase reaction mechanisms must be included above 1200K. Research works based on the catalytic combustion of methane on platinum was conducted by Schwiedernoch[50] show that no significant influence on the conversion was observed. In the present computation the gas phase reactions set in not until the surface gets heated to 1200K. Therefore this numerical investigation confirms and explains why there was no ignition of methane on platinum in the experiments described here. The surface temperature distribution shown in Figure 4-26 indicates that there is hardly any adsorption taking place below 900K.

Adsorption is an exothermic process but a constant temperature below 900K suggests no adsorption. First significant signs of adsorption can be observed at 1100K. Pronounced gas phase reactions seem to take over at temperatures above 1500K and above. The mole fraction distribution of methane combustion at 1500K and 1700K are shown in Figure 4.27 and 4.28

respectively indicating more consumption of CH4 and O2 as the mixture flows further downstream. There is a simultaneous increase in product formation. At 1500K over 66% conversion of CH4 is observed and the mole fraction of H2O in the combustion mixtures is noticed to be 4.3%. At 1700K over 67% conversion of CH4 is observed and the mole fraction of H2O in the combustion mixtures is noticed to be 4.4%. The reactions taking place at 1500K and 1700K is largely contributed by the gas phase reactions than surface reactions. For all methane cases described here formation of molecular hydrogen was not observed.

(C). Catalytic Partial Oxidation of Methane on Platinum: Hydrogen Assisted

The addition of hydrogen can have a major influence on the reaction kinetics further complicating the methane dissociation pathway. H_2 is very likely to contribute more than only the heat for the ignition of CH_4. Since H_2 removes O(s) from the surface by formation of H_2O it is likely that H_2 has a great impact on the reaction kinetics of CH_4 combustion by hydrogen. Different conversions and yields of CO_2 indeed indicate an important role of H_2 on the kinetics causing considerable differences between hydrogen-assisted and thermally initiated reaction as seen in this work. Here, not only CH_4 and O_2 compete for free vacancies but also H_2, which occupies the surface first as shown in Figure 4.29 and 4.30. H_2 combustion on platinum heats up the catalyst surface and provides the adequate surface temperature to initiate CH_4 combustion. In case of H_2 addition water will be formed immediately by oxidation of H_2. Therefore, a certain amount of the surface area is always occupied by H_2O(s). This can be seen clearly by comparing these results with the surface coverage calculations in Figure 4.32 at 900 K, where with H_2 more surface sites are occupied by OH and H_2O than in absence of H_2. The adsorption of CH_4, dissociation as well as the reaction to CO and CO_2 respectively have to happen on the remaining vacancies downstream of the catalyst. This explains why more products are formed downstream

i.e. more at port two than at port one. However, with the addition of hydrogen first signs of formation of CO, CO_2 and H_2O are already to be seen at 700K as shown in Figures 4.31.

The added H_2 occupying the surface first under dissociation, reacts with the adsorbed O(s). The produced water leaves the surface continuously generating vacancies, which methane can occupy as well. At 400 K already traces of CO are formed and the surface is mostly covered by carbon. Compared to the catalytic combustion without H_2 the number of free adsorption sites on Pt seems to have increased by a factor of about 10^5. In order to simulate H_2-assisted catalytic combustion, the carbon coverage, C(s), plays an important role too. Here, also we see increase in the surface sites increase with the increase in temperature. The temperature distribution on the surface of the catalyst is shown in Figure 4.33.

The mole fractions at inlet, port one, port two and the combustor outlet is shown in figure 4-34 through 4-37. The surface temperature distribution shows no adsorption up to 600K and first signs of adsorption at 700K and above, suggested by an increase in temperature. The mole fraction distribution of hydrogen assisted methane combustion at 400K, 600K, 700K and 900K are shown in Figure 4.34 through 4.37 respectively. It is observed that there is no consumption of fuel and hence no noticeable product formation at 400K, 600K and 700K. At 900K it is observed that over 35% of CH4 and over 64% of H2 is consumed producing 10.6% and 1,3 % H2O and CO2 respectively. The trend established from the results is as expected, i.e. there is more consumption of reactants and more product formation as the flow goes further downstream.

(D). Catalytic Combustion of Syngas on Platinum

Catalytic Partial Oxidation i.e. hydrogen assisted as well as high temperature catalytic oxidation of methane shows a pathway of combustion that forms syngas. This is an expected trend in the numerical analysis; hence, the syngas catalytic combustion on platinum using the same Deutschmann's model. Since the pressure conditions are atmospheric and the adsorption of

methane on platinum is the rate determining step, this assumption appears reasonable. Syngas was a gaseous mixture of H_2, CO, CO_2 and CH_4, thus offering a competition between species to occupy vacant sites on the platinum surface. It was noticed that for the case of catalytic oxidation of methane the sticking coefficient of oxygen to be more than methane, hence the whole platinum surface was initially covered with O atoms. In the case of partial oxidation of methane with hydrogen addition the H atoms initially covered the whole of the Platinum surface. But in the case of syngas as the fuel, the H, O, CO, CO_2 and CH_4 molecules all compete to occupy the vacant sites on platinum surface. Interestingly, it can be noticed that at 400K see Figure 4.38 the entire platinum surface is covered with CO atoms thereby suggesting a greater sticking co-efficient of CO than any other participating species in the mixture. A dominant coverage of the C(s) is noticed, but no noticeable formation of OH(s), H_2O or CO2 seems to take place. In fact CO2 hardly adheres to the platinum surface, suggesting that CO_2 predominantly remains in the gas phase. At 600K see Figure 4.39, a similar trend is seen with no noticeable formation of OH(s), H2O or CO_2; however, the formation of OH(s) and H_2O(s) has increased 10^4 times.

At 700K see Figure 4.40, however, the first traces of OH(s) and H2O(s) formation are seen, the CO atoms still occupying the whole of platinum surface. This observation confirms the fact that the oxidation of CO to CO2 is relatively more difficult to achieve than the oxidation of OH(s) to H2O(s). Hence, with a syngas fuel one expects to see a greater yield of water due to the oxidation of H2 than the yield of CO2 due to the oxidation of CO. This behavior is also observed from figure where traces of H2O have already formed with no signs of increase in the CO2 mole fractions.

At 900K see Figure 4.41, the platinum surface coverage increases, suggesting that most of the other adsorbed species are loosely bound and have started leaving the surface. This is

observed from the figure where surface coverage of CO has decreased and that some of it has left the platinum surface. Thus H(s), OH(s) and CO(s) all competes with the available O atoms in the surrounding. However, with significant amount of H_2O noticeable on the surface, it means that the formation of H2O from O and OH is preferred over the oxidation of CO. More and more O(s) and OH(s) seem to cover the surface downstream from the mid point of the catalyst length, simultaneous decrease in the surface coverage of H(s) and H_2O(s) takes place, suggesting more formation of H_2O downstream. The bottle neck behavior can be explained as the transition between the heterogeneous and homogeneous reactions.

At 1100K see Figure 4.42, the surface of free platinum has increased and that of CO has decreased even further than at 900K, a trend is also noticed at 1100K, however, more and more OH(s) combines with O(s) and hence more H2O is formed with more CO leaving the surface and an augmented amount of CO2 is formed at 1100K. At this temperature, pronounced gas phase reaction is expected judging by the increased free sites of platinum and the bottle neck distribution of surface coverage. The surface temperature distribution shown in Figure 4.43 indicates no adsorption up to 600K and the first signs of adsorption appear at 700K due to an increase in temperature. Pronounced heterogeneous and transition into gas phase reactions are observed in the profiles at 900K and 1100K.

The mole fraction distribution of syngas combustion at 400K, 600K, 700K, 900K and 1100K are shown in Figure 4.44 through 4.48 respectively. . It is observed that there is no consumption of fuel and hence no noticeable product formation at 400K, 600K and 700K. At 900K it is observed that over 65% of H2 is converted and over 11% of H2O is formed. There is no significant consumption of CH4, CO and CO2 at 900K. At 1100K 67% of H2 is converted and 12% of H2O is formed. The mole fraction of CO2 in the combustion mixture was found to

be 7.4% suggesting a 2% increase in CO2 from inlet conditions. The trend established from the results is as expected, i.e. there is more consumption of reactants and more product formation as the flow goes further downstream.

(E). Effect of Equivalence Ratio on Surface Coverages in Syngas Combustion

The effect of temperature on the surface coverage is described below. The analysis was done for syngas mixture using Deutschmann's model[21]. Combustion occurred at 900K and above but no noticeable combustion was observed below 900K. An investigation of equivalence ratio effects on the combustion and surface coverage distribution of species at 900K followed including the surface behavior of species and their role in the reaction kinetics. Equivalence ratios were varied from fuel lean cases to fuel rich values including Φ = 0.47, 0.72, 1.0 and 1.2. One experimental case of equivalence ratio of 2.28 was compared to the numerical results. It is observed that the surface behavior is vastly different from the observations of our previous section where a fuel rich mixture was studied. The effects of equivalence ratios are shown in Figures 4-49, Figures 4-51, Figures 4-53 and Figure 4-55 and the corresponding mole fraction distribution is shown in Figure 4-50, Figures 4-52, Figures 4-54 and Figures 4-56. At Φ=0.47, shown in Figure 4-49, the fuel lean mixture results in altogether different surface coverages than the fuel rich conditions of Φ=2.28, for example as noticed in Figure 4-41. It is observed that at Φ=0.47, the entire platinum surface is covered mostly with O atoms and that CO is loosely bound to the surface. Traces of OH and H_2O have already been formed. The loosely bound CO atoms suggest their availability to combine with O atoms and thus form CO_2. Hence at this fuel lean condition there is a higher probability of CO meeting O and reacting. Thus both OH and CO now compete to abstract one O atom and oxidize to H_2O and CO_2 while at Φ=2.28 it was observed that whole of platinum surface was covered with CO, such that oxidation of CO to CO_2 seemed difficult to achieve. This is also noticed from the mole fraction distribution of CO in

Figure 4-47 where practically no conversion of CO to CO_2 is observed at ports 1 and 2 as against Figure 4-50 where a conversion of over 27% CO at port 1 and over 55% at port 2 is observed. Thus at Φ= 0.477 formation of both CO_2 and H_2O is observed whereas at Φ = 2.28 oxidation of CO is suppressed and formation of H_2O is dominant. From Figure 4-50 it is observed that there is a conversion of over 39% H_2 at port 1, 70% at port 2, 24% O_2 at port 1, 47% at port 2. 3.4 % and 6.2% H_2O. An increase of 47% and 96% in the mole fraction of CO_2 is observed at port 1 and port 2 respectively. The trend established from the results is expected, i.e. there is more consumption of reactants and more product formation as the flow goes further downstream.

The surface coverage and the mole fraction distribution at Φ=0.77 are shown in Figure 4-51 and Figure 4-52 respectively. The behavior of these parameters is the same as that at Φ=0.47 except that we have more production of CO2 at ports 1 and 2 is observed. So at a fuel lean condition, the oxidation of CO is favored because CO is loosely bound to the platinum and can thus abstract O atoms and oxidize. The percentage conversion and product formation are the same at Φ=0.47 and Φ=0.73.

However, a change in trend appears when mixture composition becomes stoichiometric and further richer. The surface coverage behavior and the mole fraction distribution at stoichiometric and fuel richer condition are shown in Figures 4-53 and 4-54. At Φ=1, the surface coverage of CO on platinum increases 1000 times and approaches unity suggesting that now the whole of platinum is predominantly covered with CO. This therefore translates in a very high sticking coefficient of CO and suggests that CO is no longer available to abstract the O atoms. Hence an inhibition in the oxidation of CO is observed which means that the conversion of CO is largely inhibited. Less than 10% and 26% conversion of CO is seen to occur at ports 1 and 2

respectively. Most of the O atoms are now abstracted by OH to form H_2O. This is suggested by over 6% and 10% production of H_2O at ports 1 and 2 respectively.

At Φ=1.21, the surface coverage of CO is observed to increase further and hence the conversion of CO is further inhibited. This is shown in Figure 4-55 and 4-56 where practically no CO conversion occurs at port 1 and port 2. All the O atoms are now available for to oxidize OH to form H_2O.

(F). Comparison between the Experimental and Computational Results of Syngas Combustion

The inlet specifications for both the experimental as well as the computational cases were identical. The mixture compositions are shown in Table 4-4 and 4-5. The study involved determining the mole fraction and the temperature distribution during both the experimental and computational studies and then comparing the two. The computational study was carried out in two stages. The first stage included the combustion simulation with only the heterogeneous surface reaction mechanism and the second stage included both the heterogeneous and the additional five step gas phase homogeneous reactions. This was done to magnify the difference from just the heterogeneous reactions and to bring about an improvement in the prediction of mole fraction and temperature distribution. The temperature distribution, shown in Figure 4.57, suggests good agreement between the experiment and the simulation that involved both surface and gas phase reactions. The temperatures at inlet, port one and port two agree within 5%, but at the outlet is affected by the computational artifact. There is a 12% error in the experimental and computational temperature at the outlet. During simulation, FLUENT requires a user specified temperature boundary conditions at the outlet. The outlet face was chosen to be a “pressure-outlet” face, wherein FLUENT requires for a backflow temperature. This temperature has to be somewhat of a similar value as the one which the computational domain i.e. combustor section

with catalyst in this case is expected to reach during combustion. If this is not done then there arise serious convergence issues due to a large gradient between the temperature reached during simulation and a default backflow temperature chosen by FLUENT.

In this study, a backflow temperature of 700K was chosen so that a slight decrease seems to appear in the temperature value from port two to the outlet.

Cooling air is used in the experiments to keep the catalyst from over heating. The computation models this flow and the conjugate heat transfer. Figure 4.58 through 4.60 shows a radial temperature profile of the cooling air for several cases at port 1 (x/L=0.3), port 2 (x/L=0.7) and outlet (x/L=1) respectively. The initial cooling air temperature is assumed the same as the initial reactant mixture temperature. These temperatures are shown on the y = 0 axis of the Figure 4.58 through 4.60. In the experiment the inlet temperature was limited to 700K. The computations were extended to higher values.

The heat transfer to the cooling air is evidenced by the temperature rise noticed at the catalyst proximity. At higher temperatures the metal surface reaches high temperature values indicating that cooling could be insufficient. Clearly in practice cooling air would be maintained at lower values. The amount of heat transferred to the cooling air in the case of 900K initial temperature was 75% for syngas and 90% for hydrogen assisted methane mixtures of the total heat released assuming equilibrium is reached at the catalyst exit. The difference in temperature along the catalyst from inlet to outlet was 331K for methane + hydrogen mixtures and 314K for syngas mixtures. This indicates a heat flux in an upstream direction of 23.4×10^3 W/m^2 and 22.2×10^3 W/m^2 respectively. Thermal conductivity of steel was taken to be 16.27 W/m-K.

The experiment and the simulation using heterogeneous reactions of syngas do not agree well, the later significantly lower than the values obtained in experiments. This validates the use

of additional gas phase reactions, which proceed with much heat release, thereby increasing the temperature. The % mass fraction distribution comparison between simulation and experiment at ports one and two is shown in Figure 4.61 through 4.63. There is a negligible yet noticeable decrease in the mass fractions of the incoming species during simulation. This is attributed to the fact that certain gas phase reaction is taking place before the fuel-air mixture actually reaches the catalyst. The Figure shows that the combination of heterogeneous and homogeneous reactions during simulations predicts the oxidation of H_2 quite well and thus provides an agreeable formation of water with the experiments. It does not however predict the oxidation of CO well.

This can be attributed to the high sticking probability of CO amongst all the species in the syngas composition. Since CO does not leave the surface, its presence and oxidation in the gas phase to form CO_2 is greatly inhibited. But in experiments there is considerable production of CO_2 and a corresponding consumption of CO. Hence another mechanism that predicts the oxidation of CO to CO_2 first on the catalyst surface followed by the desorption of CO_2 into the gas phase and subsequently additional gas phase reactions is needed to predict the formation of CO_2. Another reason for a good agreement in the prediction of H_2O can be attributed to the fact that the surface reaction mechanism shows the H(s) atoms are relatively mobile on the surface than CO (suggested by lower surface coverage of H than CO), hence abstraction of H and O atoms on the surface is easier than the abstraction of CO and O. Hence the mechanism supports the formation of H_2O. The simulation however predicts good agreement at higher temperatures, both with and without addition of gas phase reactions. This can be attributed to the fact that at higher temperatures, the adsorbed species including CO, tend to leave the surface and that the anticipation of the adsorbed species with an available O atom becomes more probable. Hence more CO_2 seem to be formed at higher temperatures, because of CO less strongly adhered to the

surface. H_2O however is seen to be formed more than CO at any temperature. The mass fractions of H_2O and CO_2 at port two found from experiment is 7.6% and 22.2% respectively, whereas those found from simulation is 8.2% and 12.05%.We thus find that the simulation predicts H_2O within less than 8% error but appears 45% offset in predicting CO_2. The robustness of the simulation scheme is best achieved at higher temperatures. Although the simulation does not validate experimental findings quantitatively, it does a good job to establish the correct trend qualitatively, namely, a decrease in the reactant composition with a simultaneous rise in the product composition while going downstream along the catalyst, thus providing valuable insight in the catalytic effect of the surface on the gas mixture combustion. A detailed study of the surface reaction behavior of CO on platinum as well as a reaction mechanism involving C1, C2, C3 etc species, which would capture the gas phase reactions of CO oxidation, is thus desired.

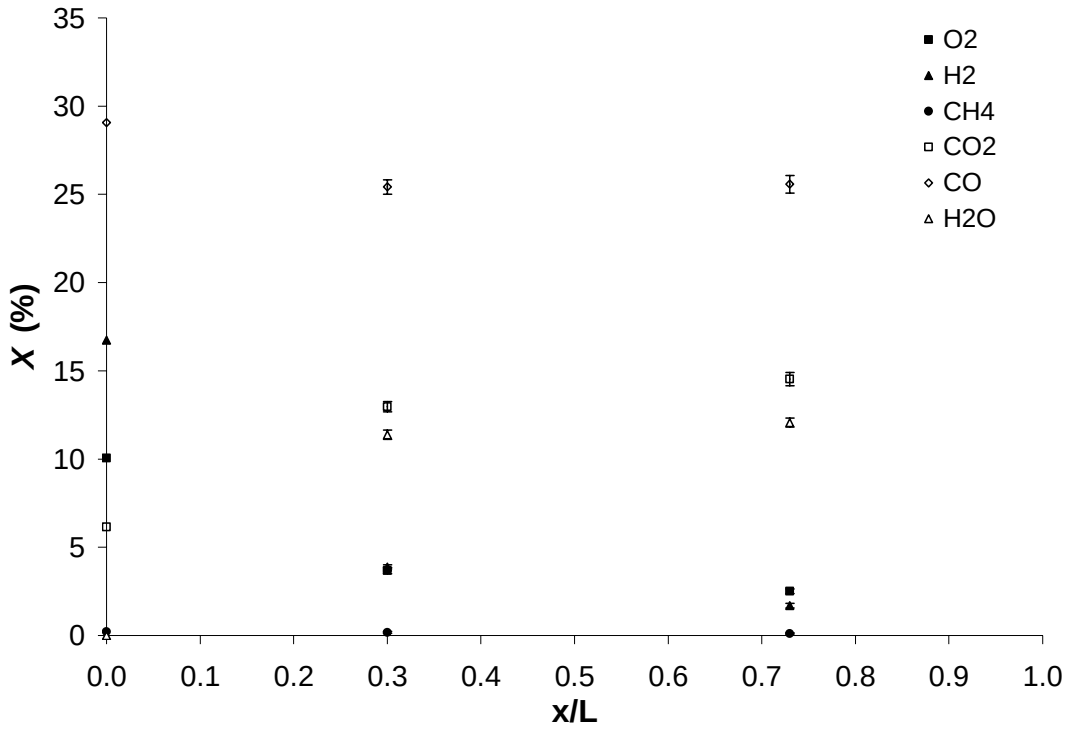

Figure 4-1. Mole Fraction Distribution of Syngas Combustion at Port One and Port Two on Platinum Smooth

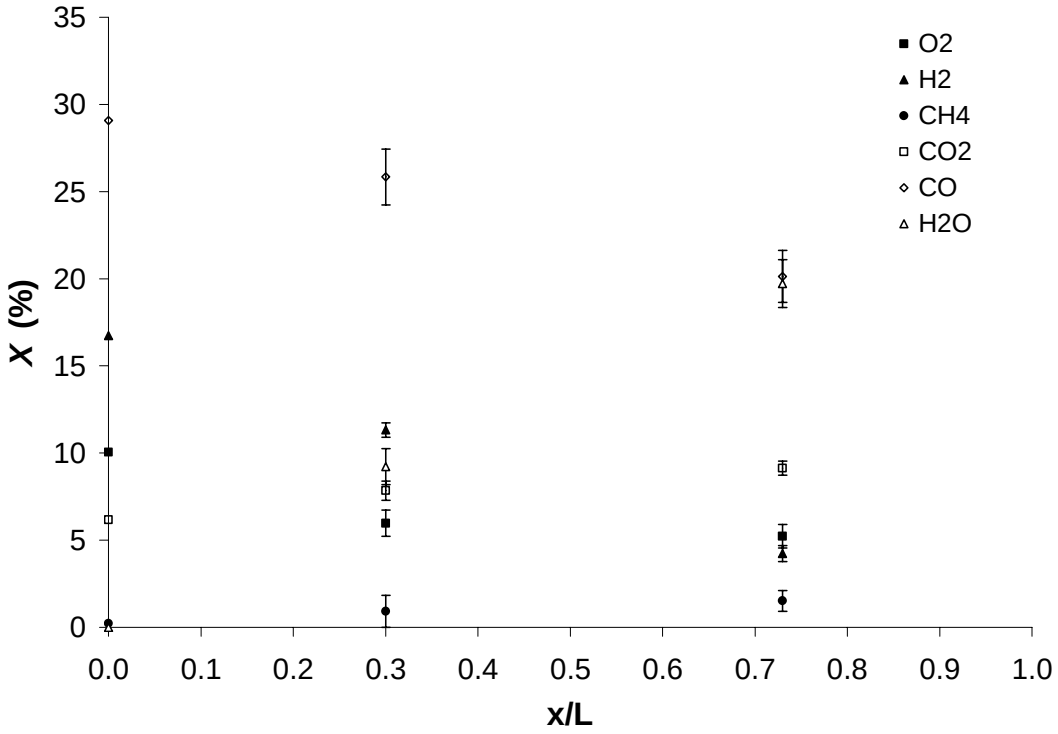

Figure 4-2. Mole Fraction Distribution of Syngas Combustion at Port One and Port Two on Platinum Rough

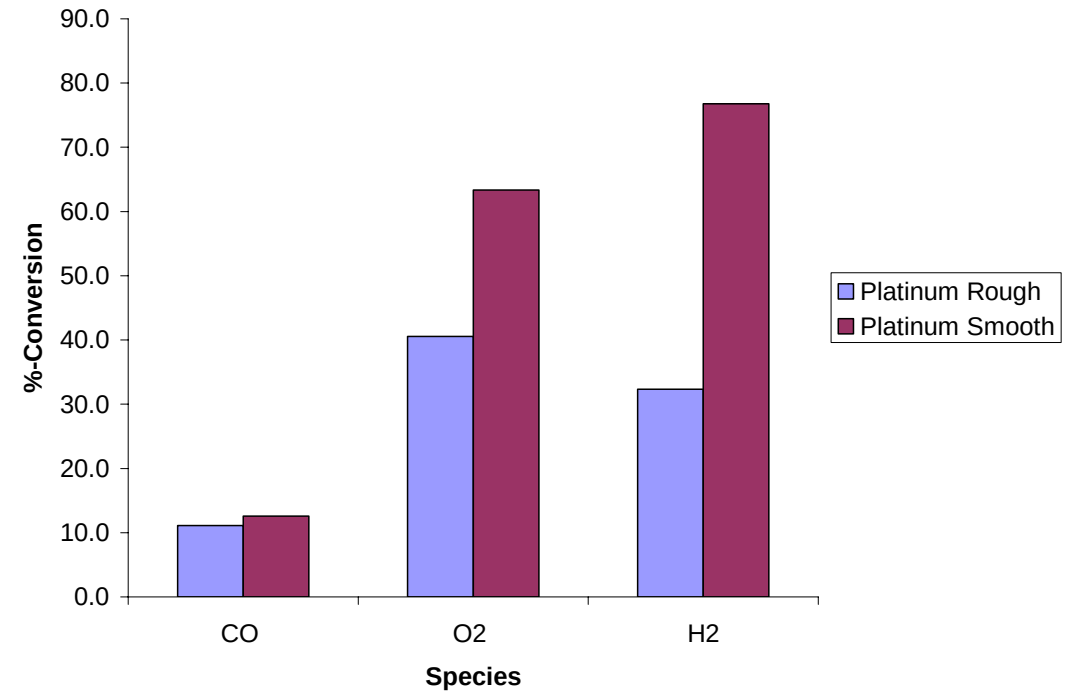

Figure 4-3. Comparison between Catalyst Platinum Smooth and Rough at Port 1 in Converting Reactants

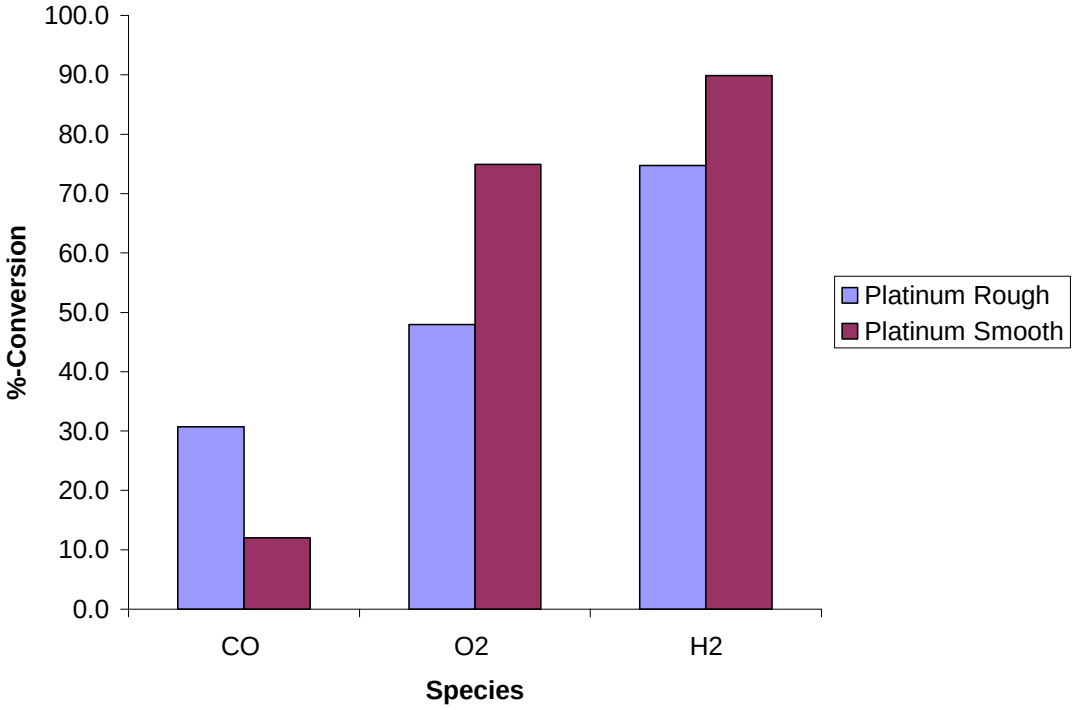

Figure 4-4. Comparison between Catalyst Platinum Smooth and Rough at Port 2 in converting reactants

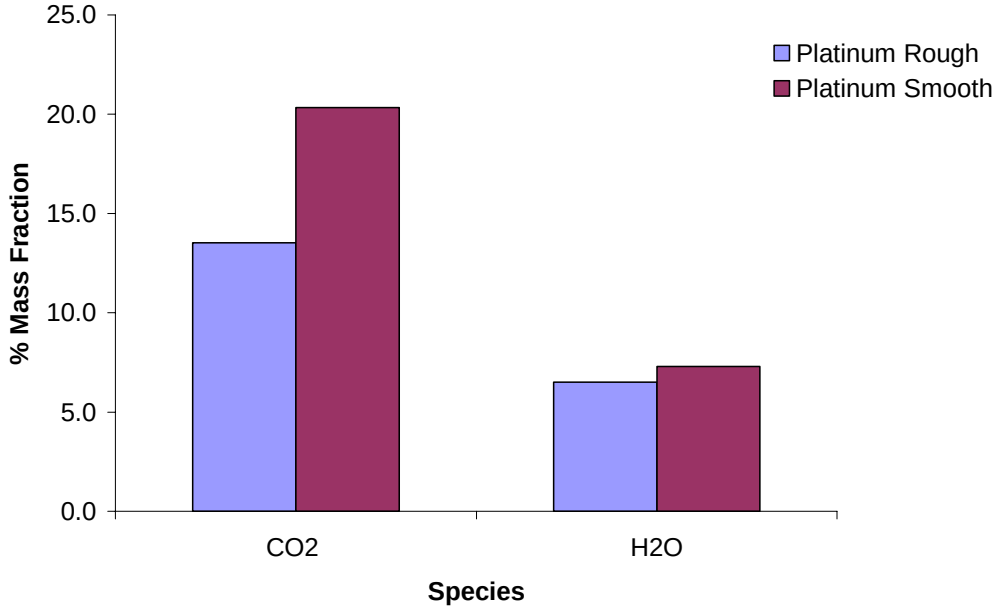

Figure 4-5. Comparison between Catalyst Platinum Smooth, Rough, A & B in Product Yield at Port One

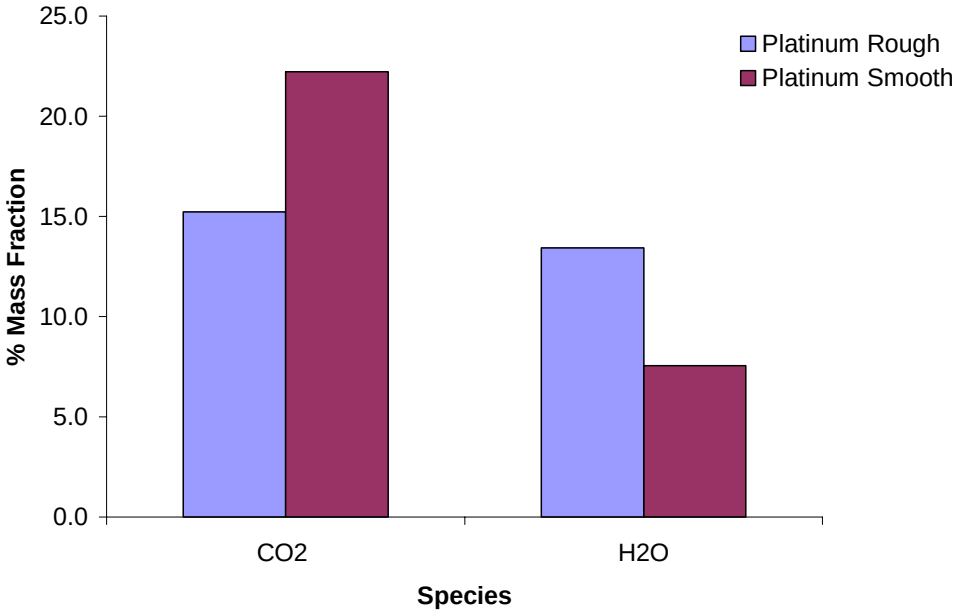

Figure 4-6. Comparison between Catalyst Platinum Smooth, Rough, A & B in Product Yield at Port Two

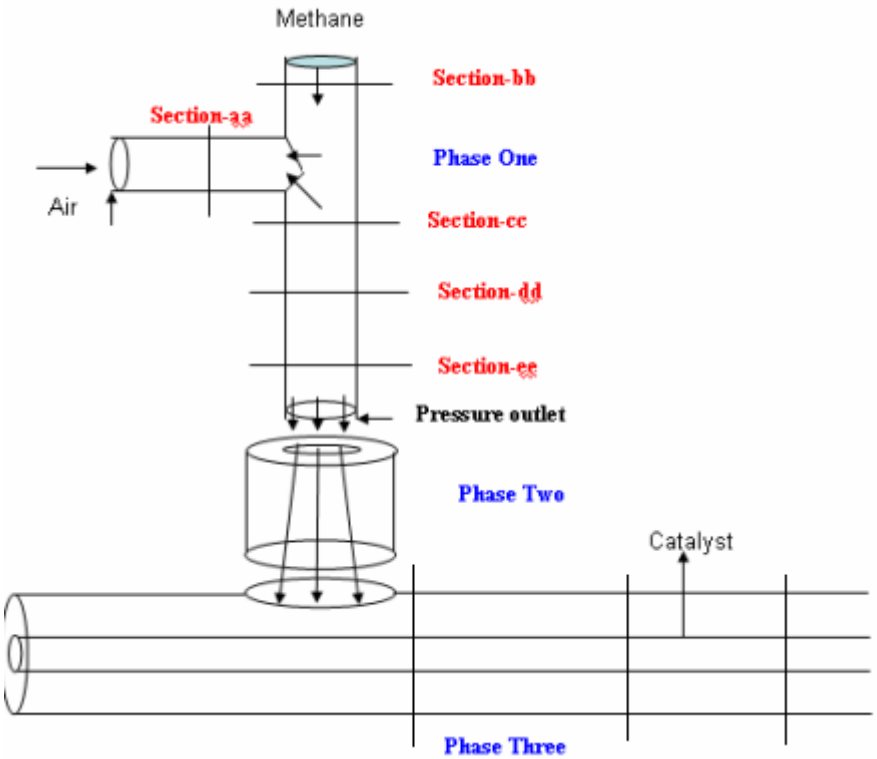

Figure 4-7. Schematic Diagram of the Computational Domain.

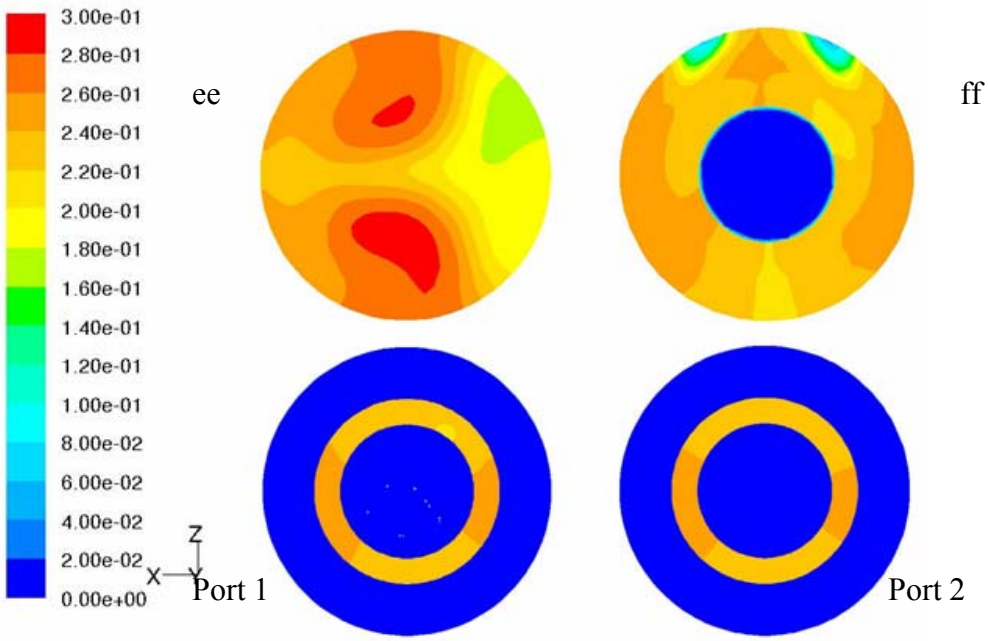

Figure 4-8. Non Reacting Mole Fraction Distribution of Methane at Section ee, ff, Ports One and Two

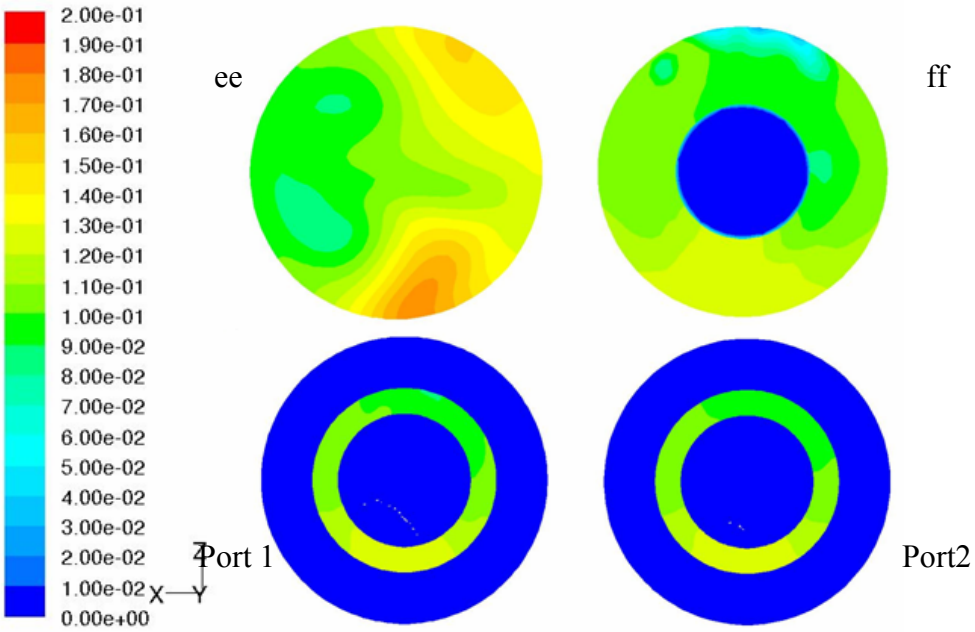

Figure 4-9. Non Reacting Mole Fraction Distribution of Hydrogen in Syngas at Section ee, ff, Ports One and Two

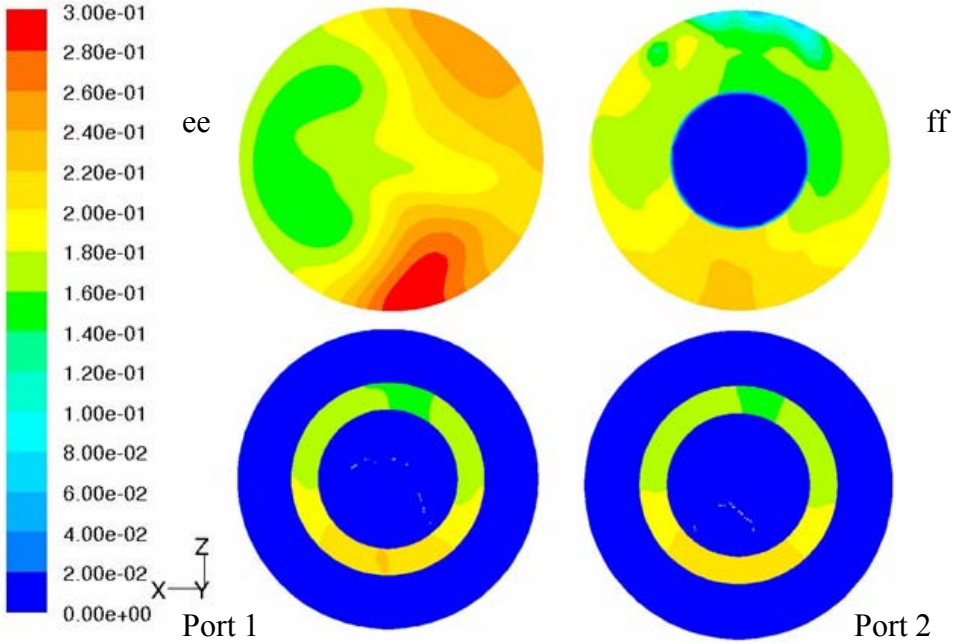

Figure 4-10. Non Reacting Mole Fraction Distribution of CO in Syngas at Section ee, ff, Ports One and Two

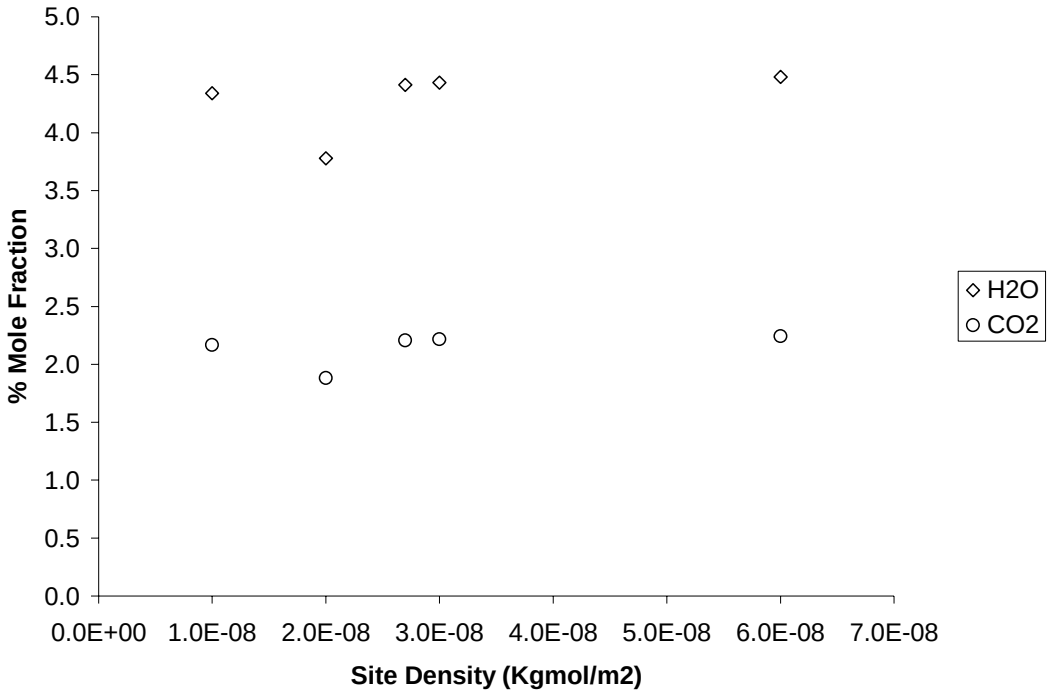

Figure 4-11. Mole Fraction Distribution with respect to Site Density for Methane Combustion at 1700K at Port 2

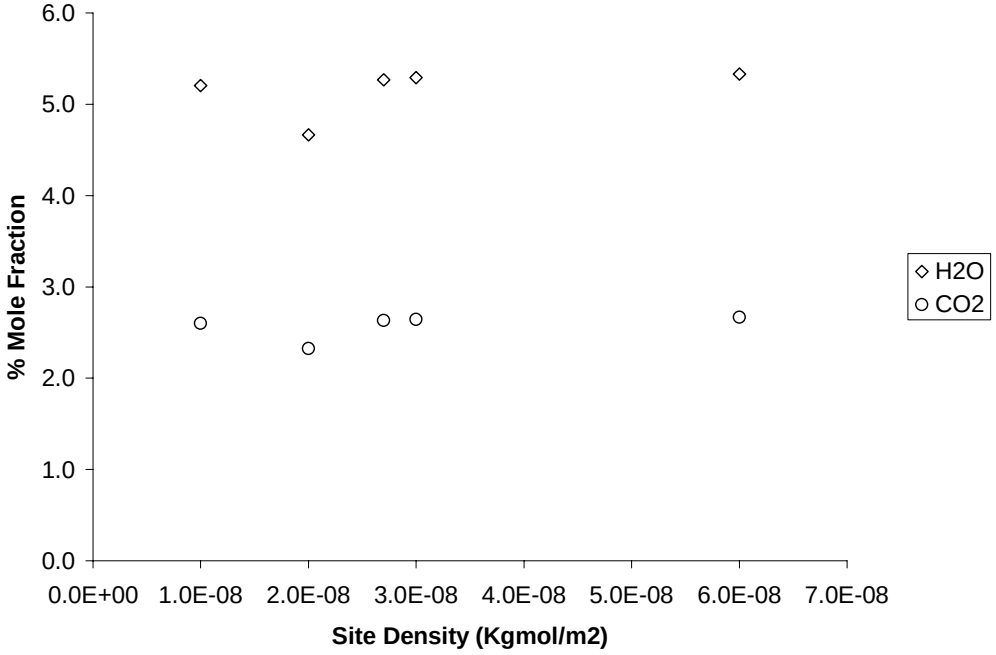

Figure 4-12. Mole Fraction Distribution with respect to Site Density for Methane Combustion at 1700K at Outlet

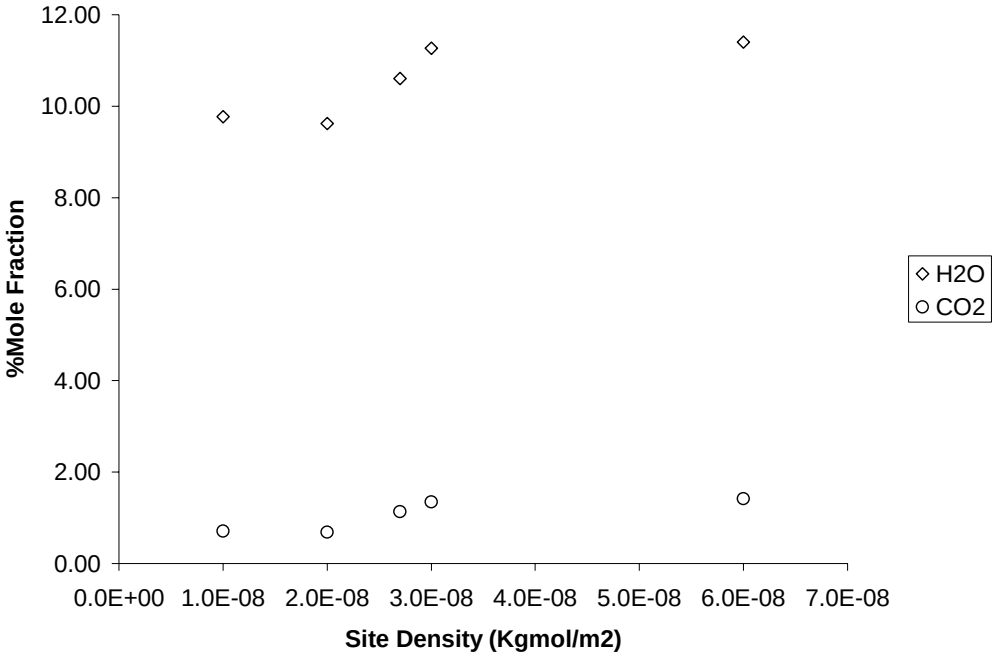

Figure 4-13. Mole Fraction Distribution with respect to Site Density for Hydrogen Assisted Methane Combustion at 900K at Port 2

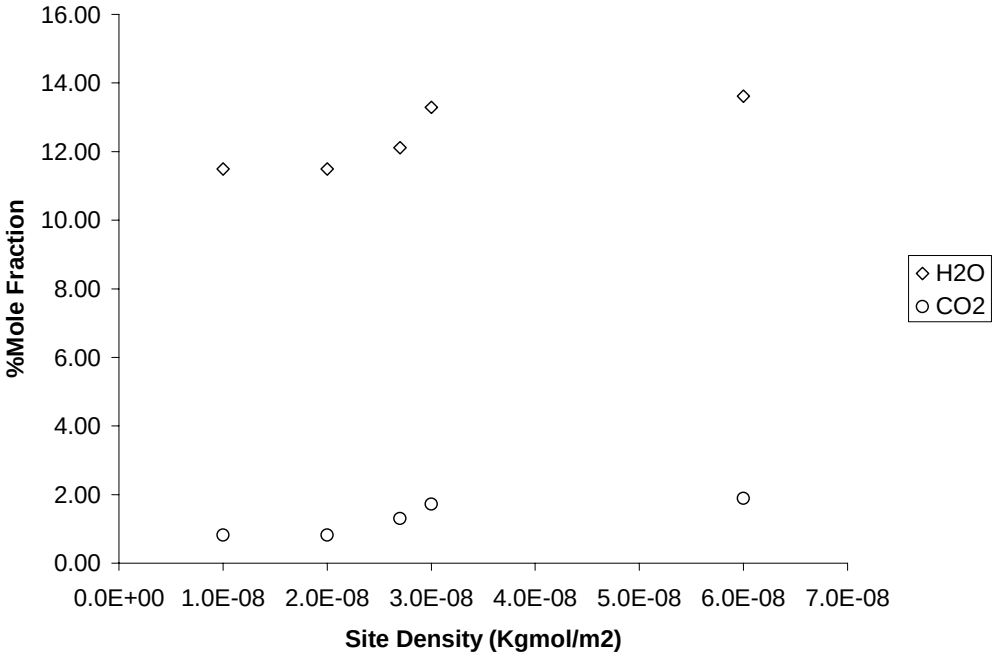

Figure 4-14. Mole Fraction Distribution with respect to Site Density for Hydrogen Assisted Methane Combustion at 900K at Outlet

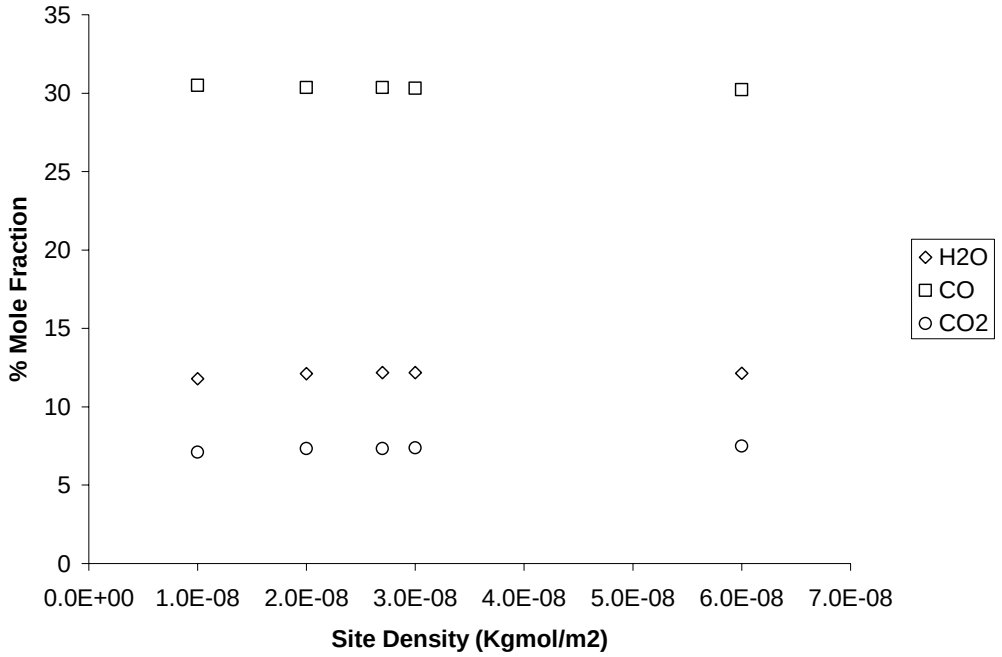

Figure 4-15. Mole Fraction Distribution with respect to Site Density for Syngas Combustion at 1100K at Port 2

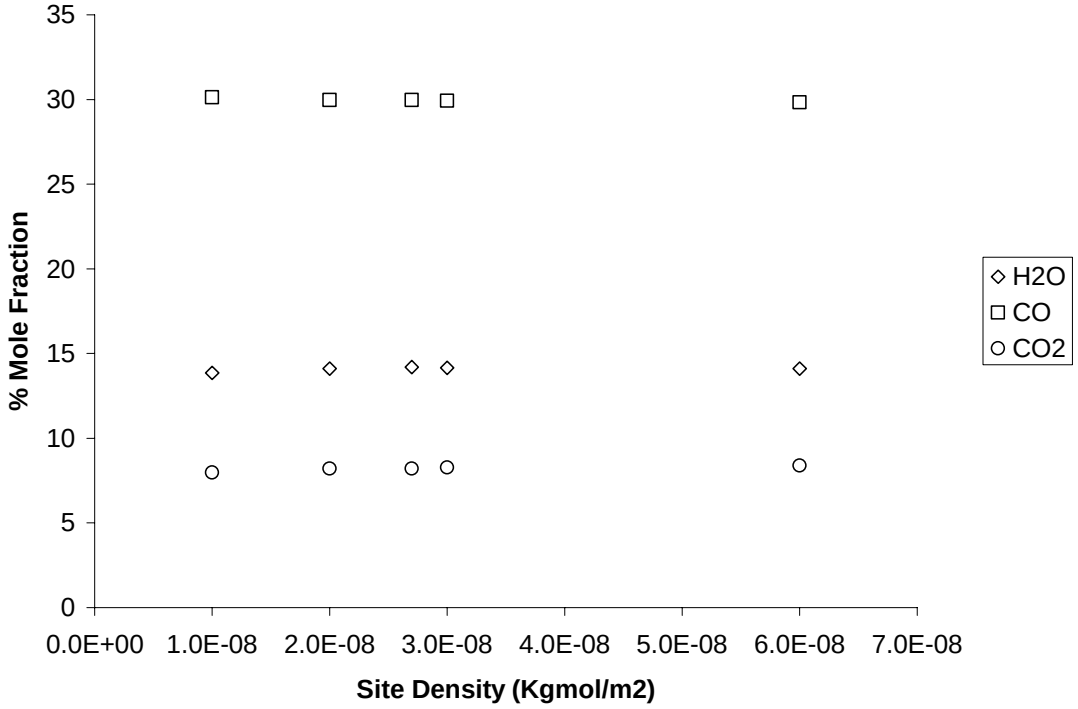

Figure 4-16. Mole Fraction Distribution with respect to Site Density for Syngas Combustion at 1100K at Outlet

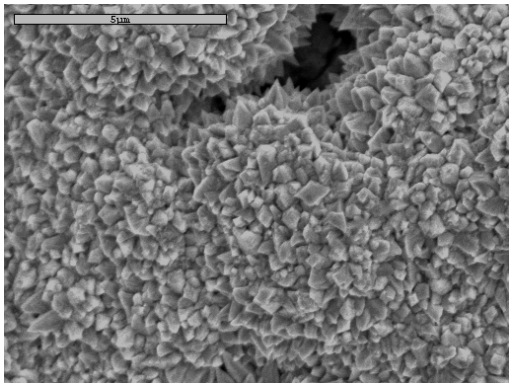

(A) M-10000 times: S- 5 µm

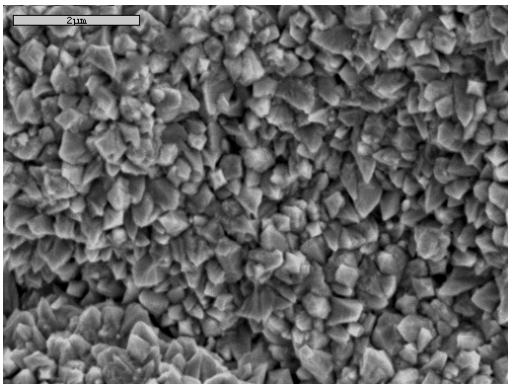

(B) M-15000 times: S- 2 µm

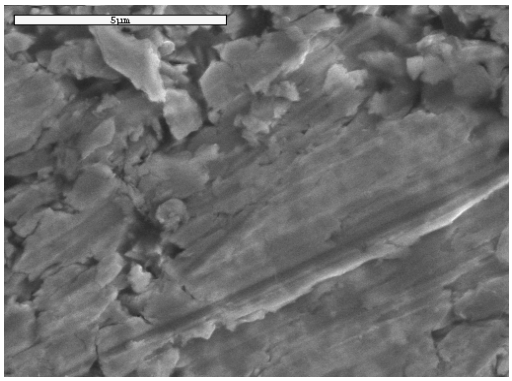

(C) M-10000 times: S- 5 µm

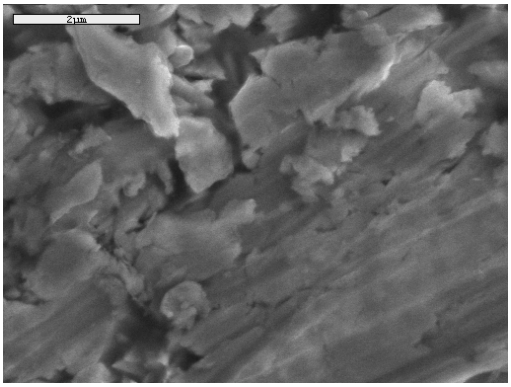

(D) M-15000 times: S- 2 µm

Figure 4-17. SEM images of Rough (A) and (B) and Smooth (C) and (D) magnified 10000 and 15000 respectively. Rough surfaces show more number of grains than the smooth surface per unit area. The exposed surface are is thus greater for rough surface and thus provides more active sites on platinum surface to allow adsorption. M: Magnification: S: Scale

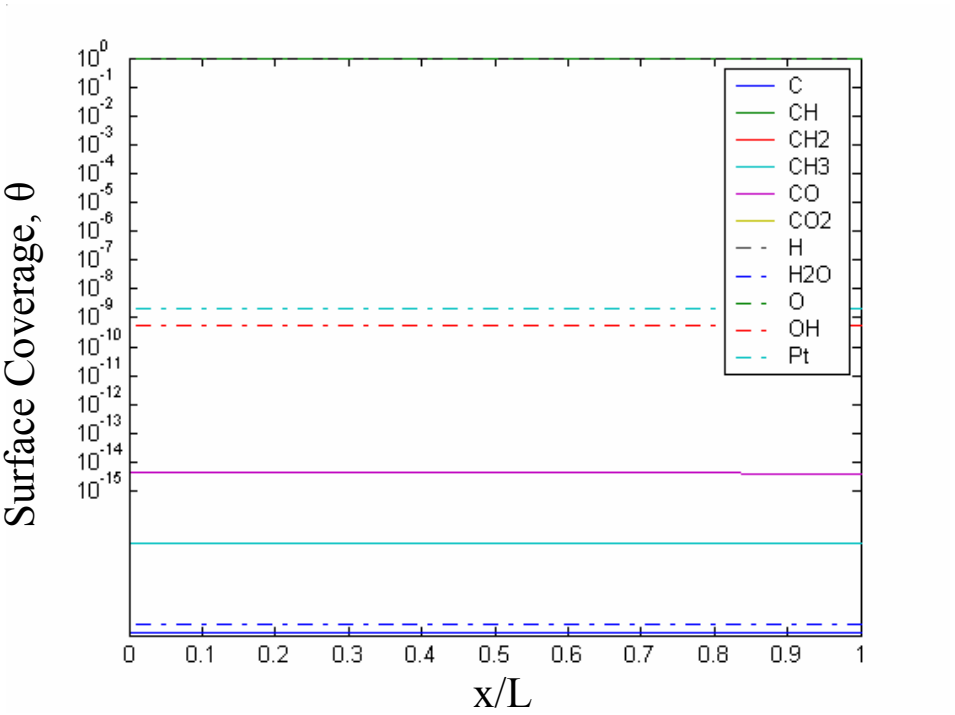

Figure 4-18. Surface Coverage Distributions along Catalyst for Methane Combustion at 400K

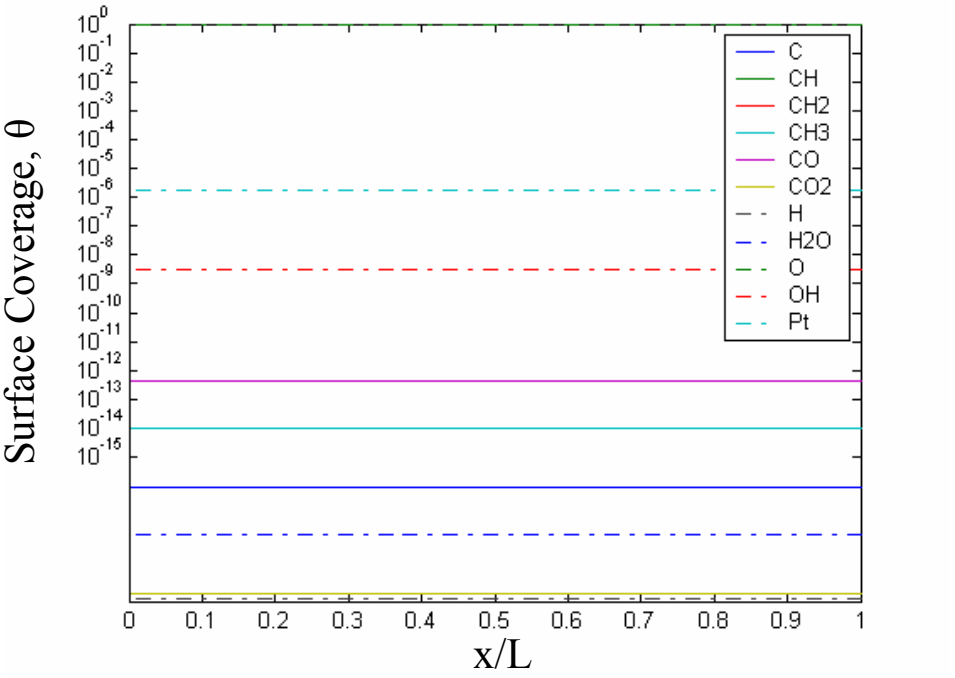

Figure 4-19. Surface Coverage Distributions along Catalyst for Methane Combustion at 600K

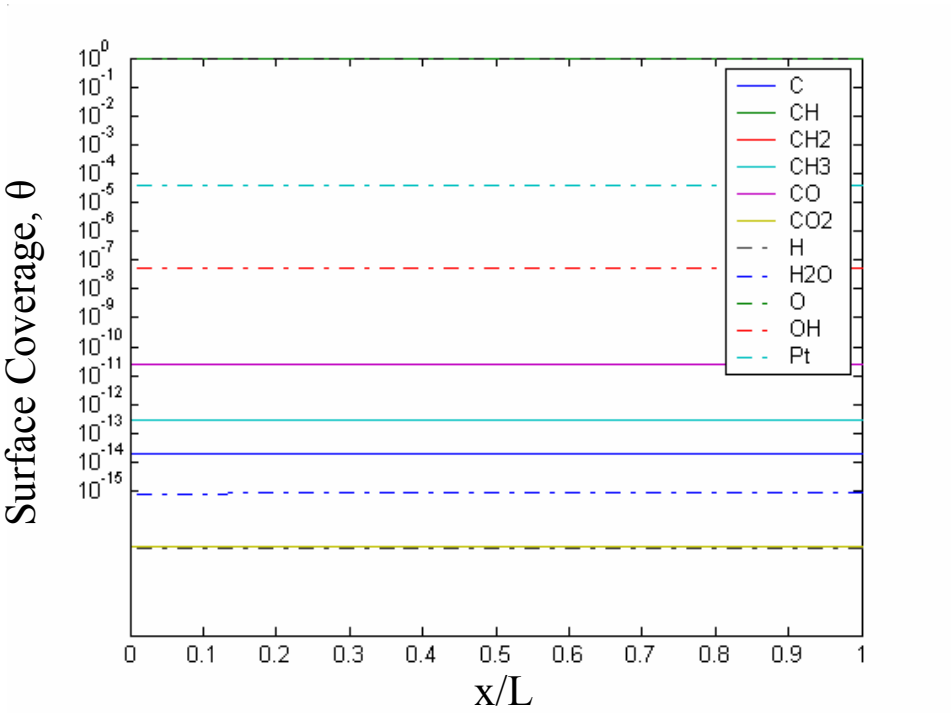

Figure 4-20. Surface Coverage Distributions along Catalyst for Methane Combustion at 700K

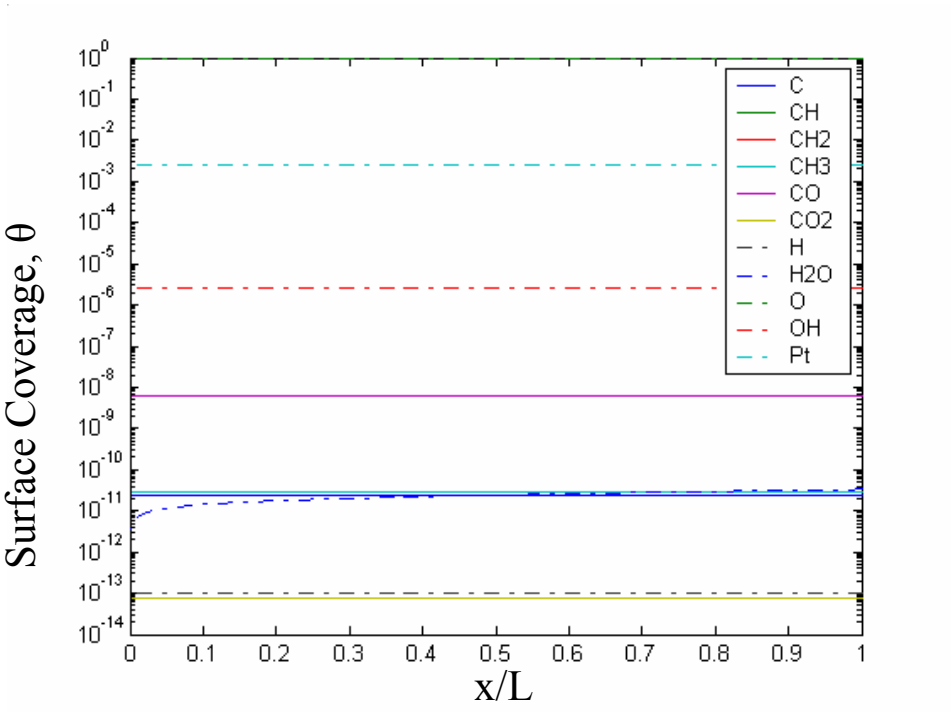

Figure 4-21. Surface Coverage Distributions along Catalyst for Methane Combustion at 900K

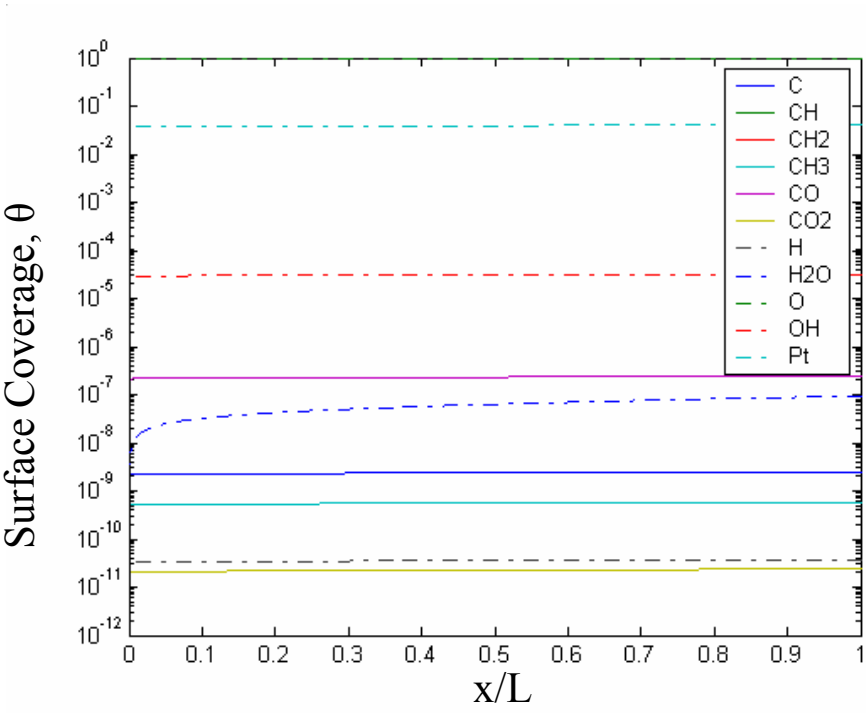

Figure 4-22. Surface Coverage Distributions along Catalyst for Methane Combustion at 1100K

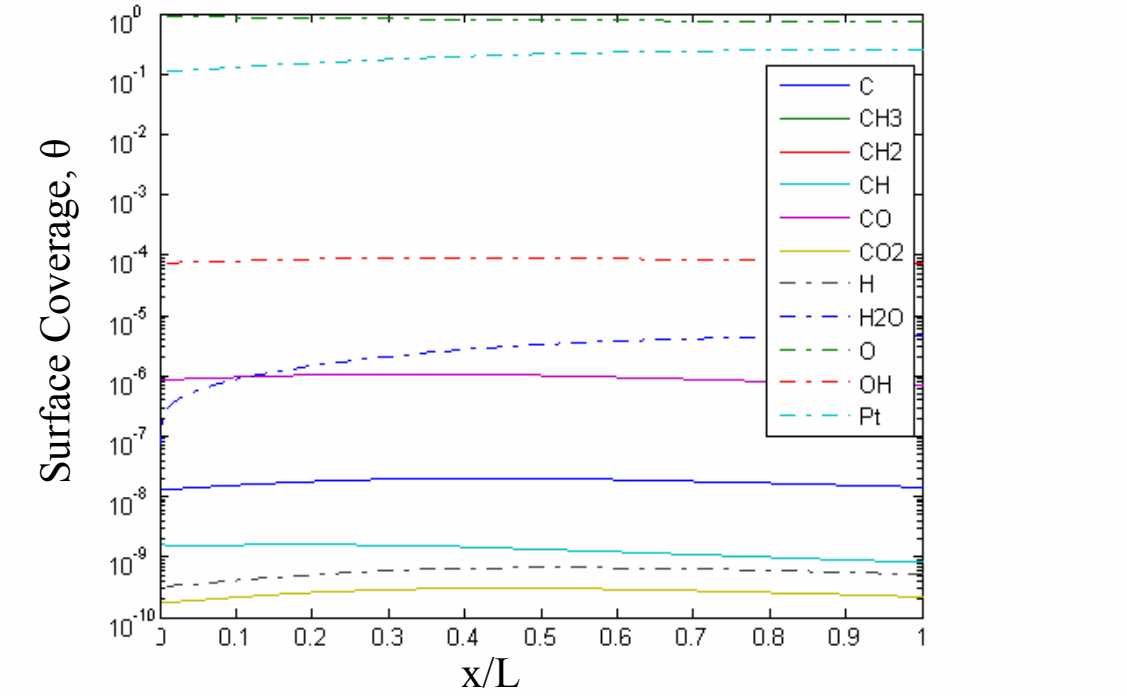

Figure 4-23. Surface Coverage Distributions along Catalyst for Methane Combustion at 1200K

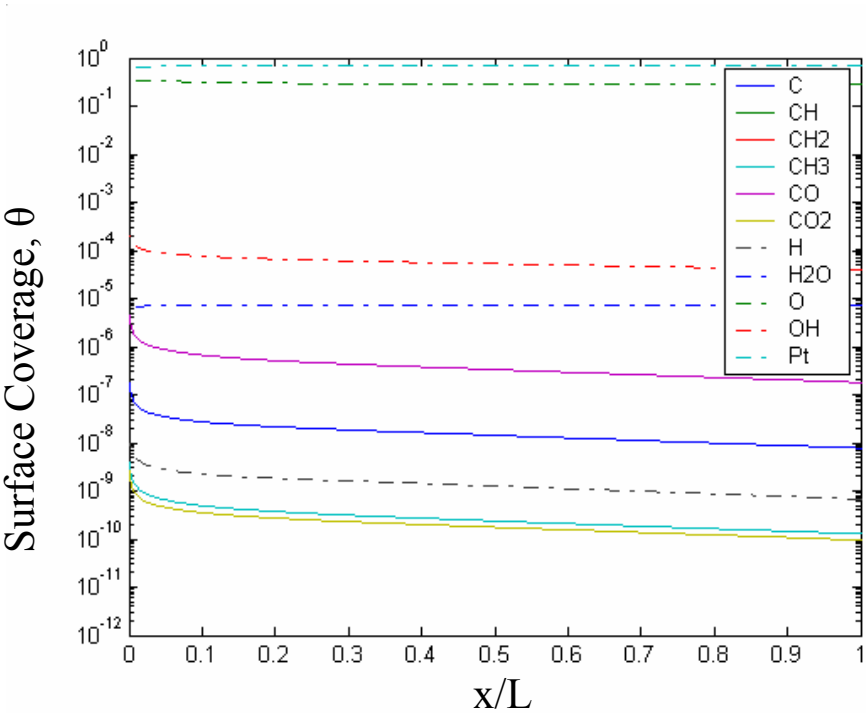

Figure 4-24. Surface Coverage Distributions along Catalyst for Methane Combustion at 1500K

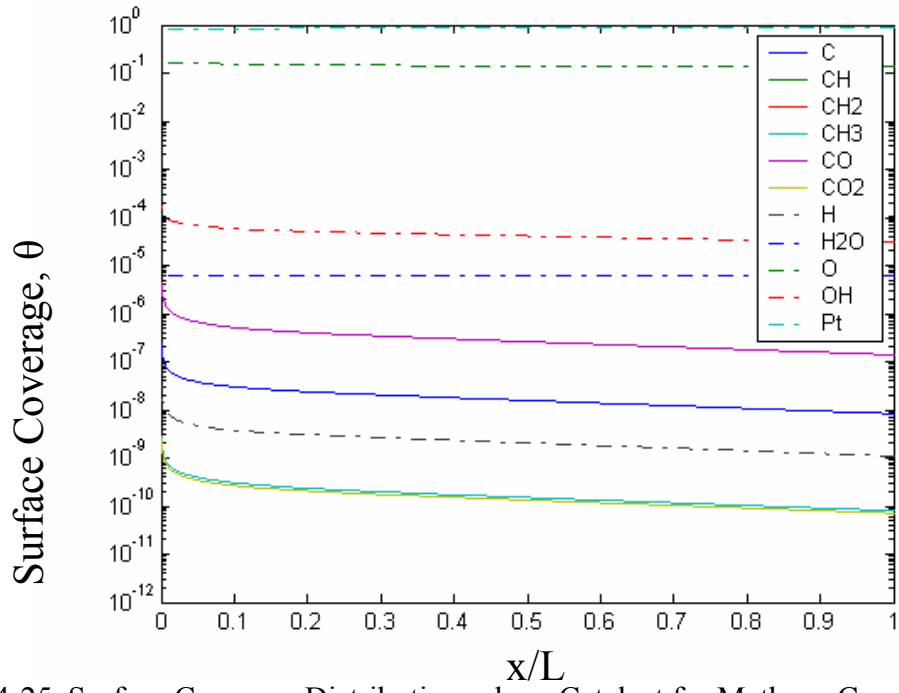

Figure 4-25. Surface Coverage Distributions along Catalyst for Methane Combustion at 1700K

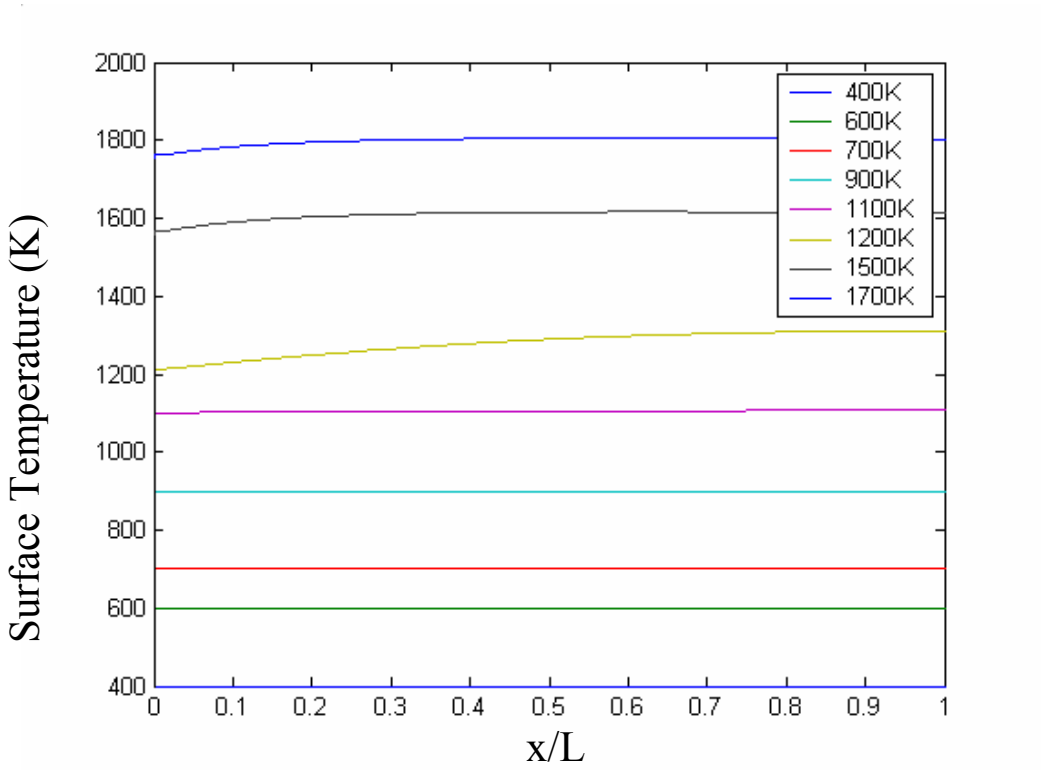

Figure 4-26. Surface Temperature Distribution along Catalyst for Methane Combustion at different Inlet Temperatures

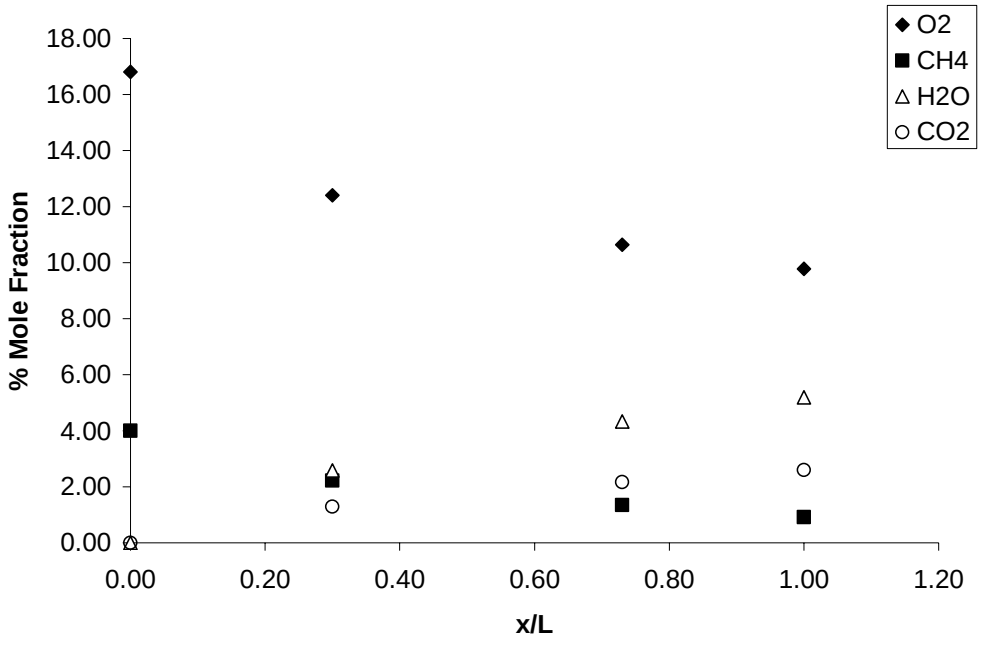

Figure 4-27. Mole Fraction Distribution of Methane Combustion at Inlet, Port One, Two and Outlet at 1500K

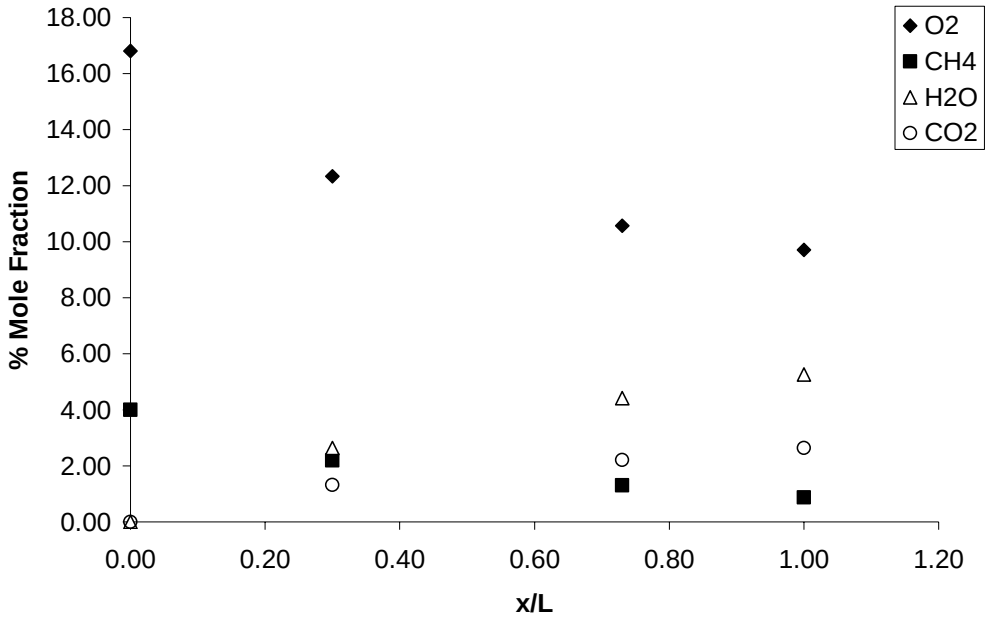

Figure 4-28. Mole Fraction Distribution of Methane Combustion at Inlet, Port One, Two and Outlet at 1700K

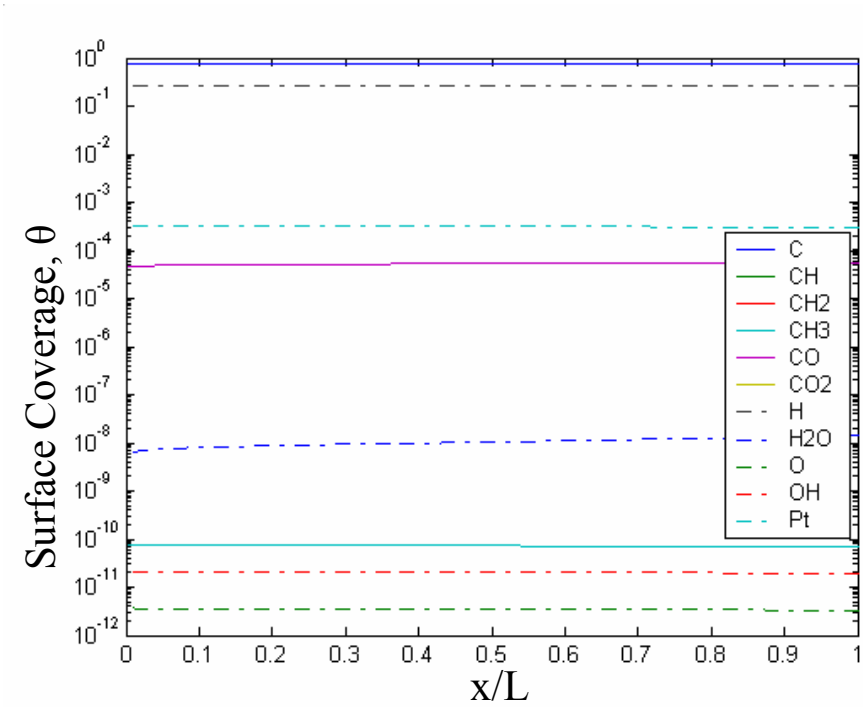

Figure 4-29. Surface Coverage Distribution along Catalyst for Hydrogen Assisted Methane Combustion at 400K

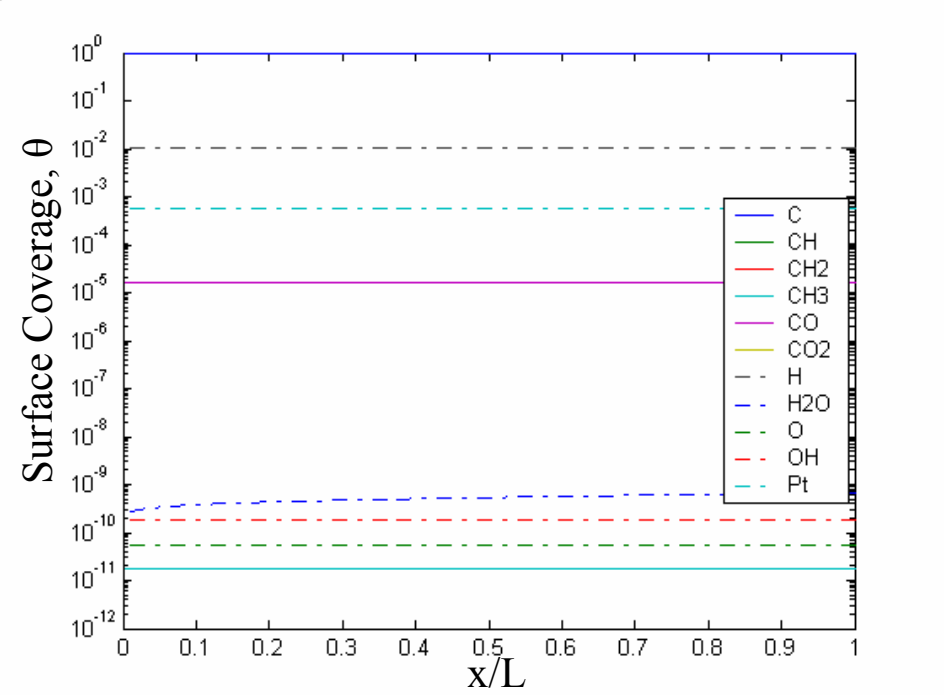

Figure 4-30. Surface Coverage Distribution along Catalyst for Hydrogen Assisted Methane Combustion at 600K

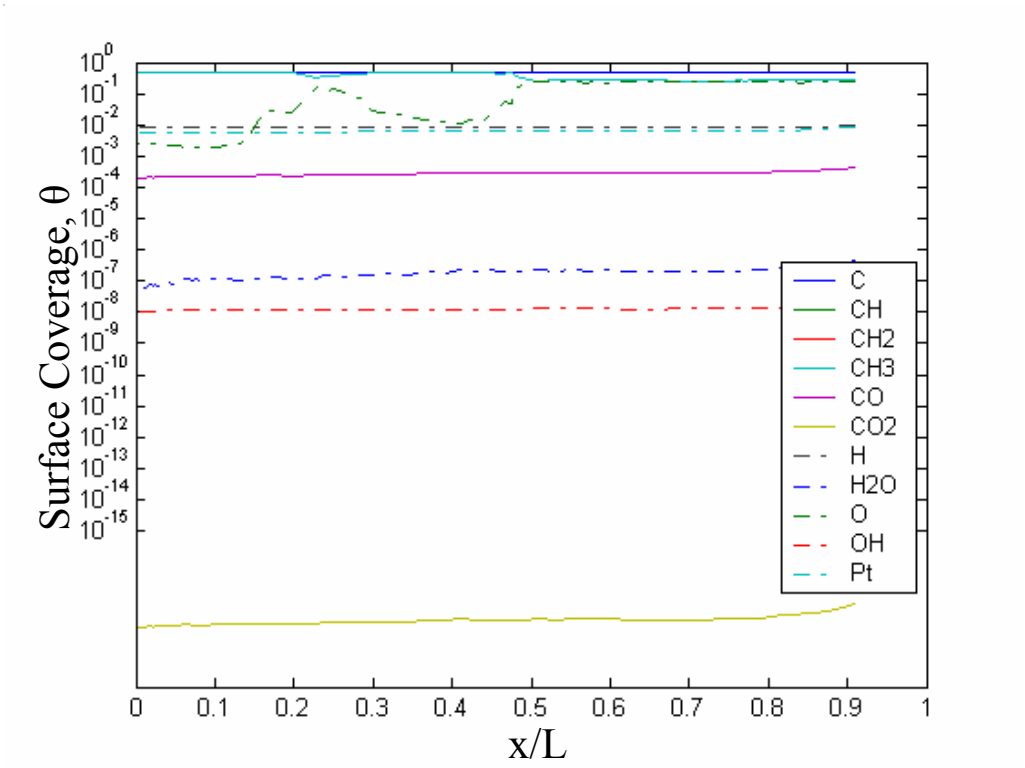

Figure 4-31. Surface Coverage Distribution along Catalyst for Hydrogen Assisted Methane Combustion at 700K

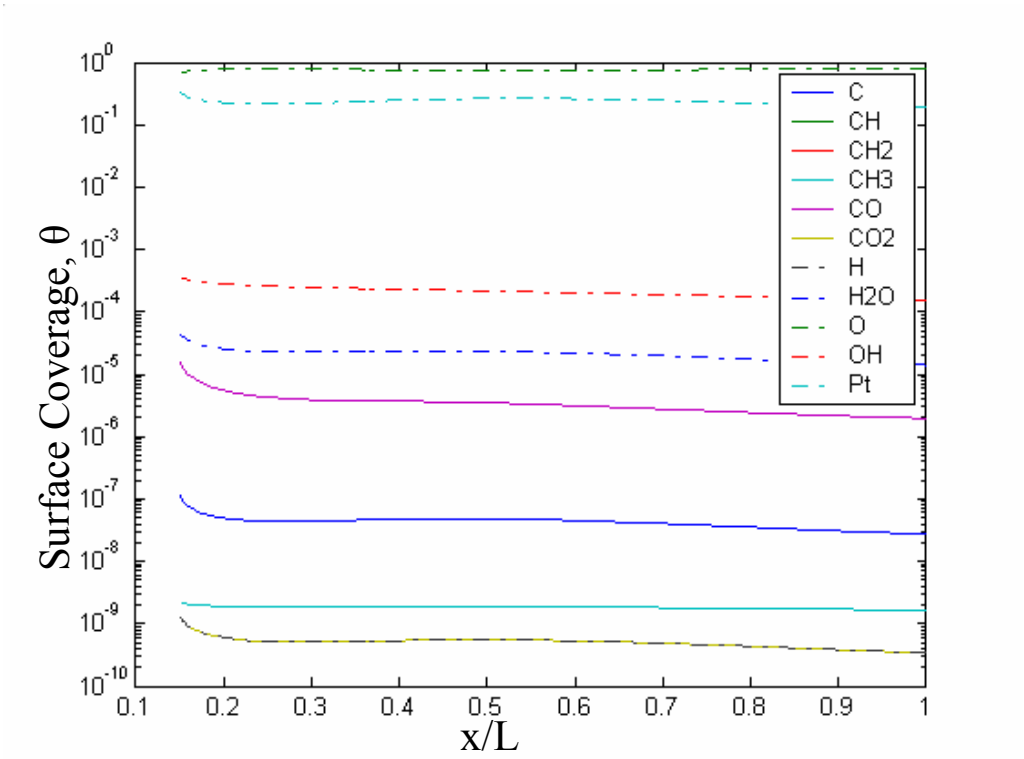

Figure 4-32. Surface Coverage Distribution along Catalyst for Hydrogen Assisted Methane Combustion at 900K

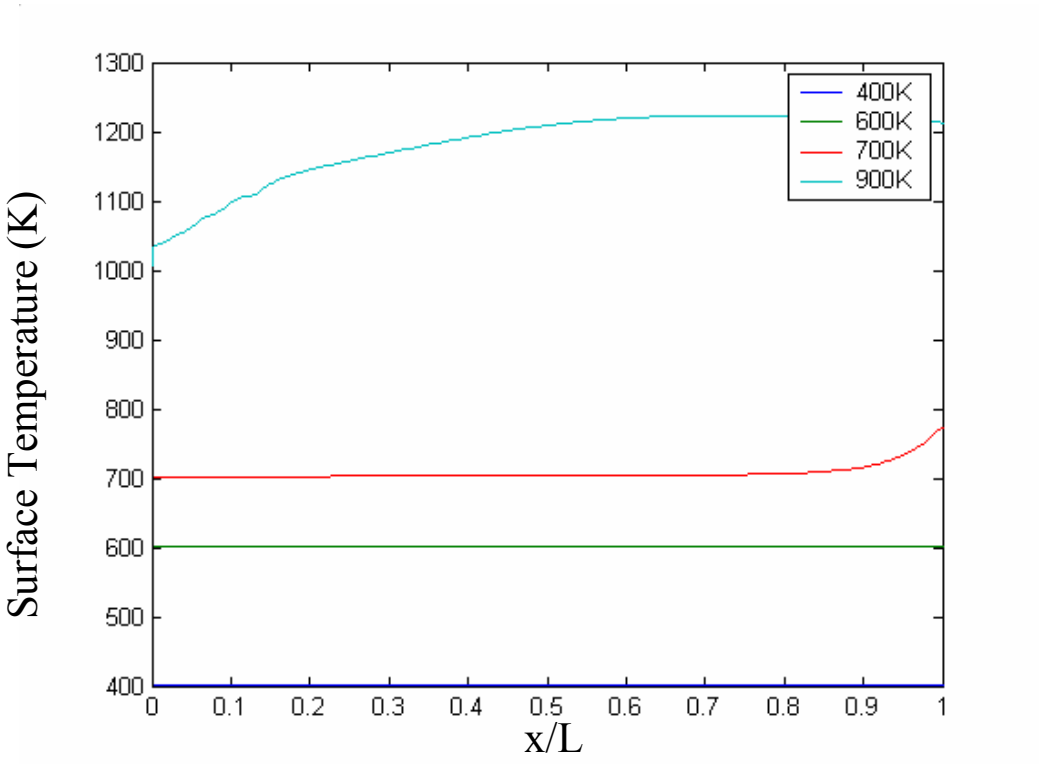

Figure 4-33. Surface Temperature Distribution along Catalyst for Hydrogen Assisted Methane Combustion at different inlet Temperatures

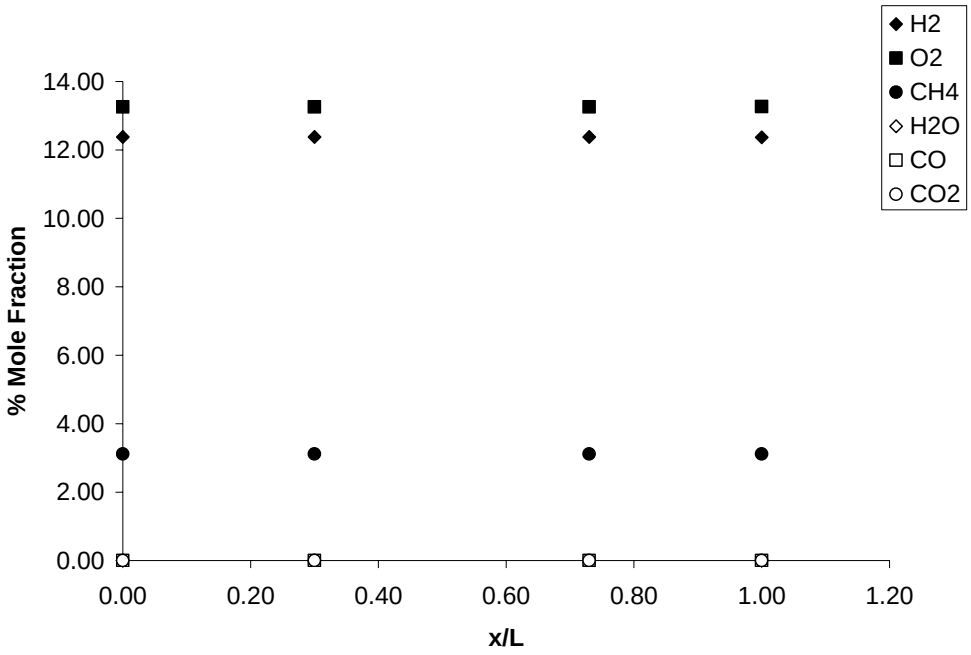

Figure 4-34. Mole Fraction Distribution of Hydrogen Assisted Methane Combustion at Inlet, Port One, Two and Outlet at 400K

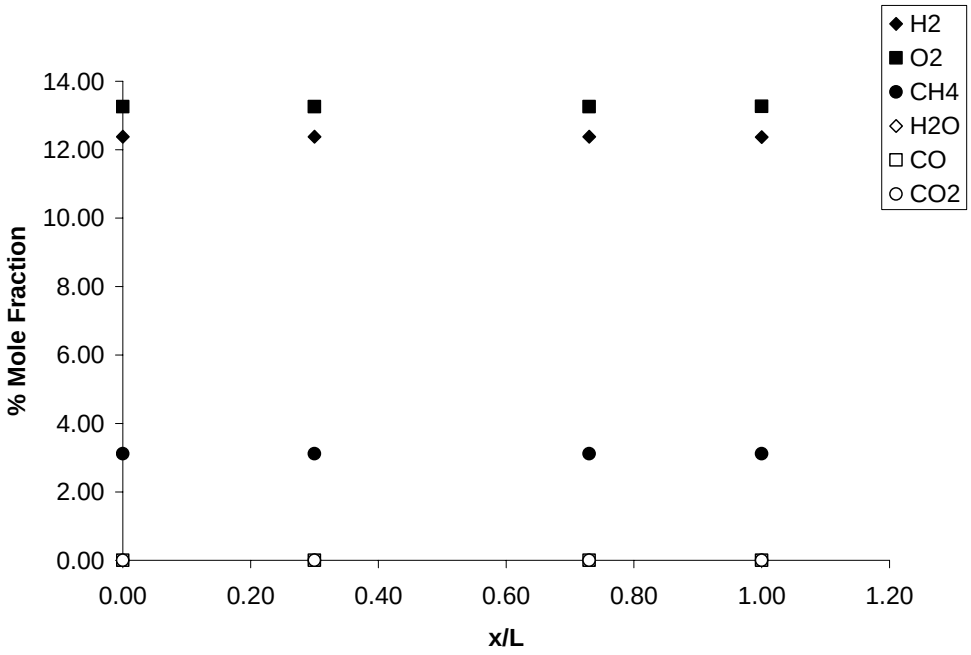

Figure 4-35. Mole Fraction Distribution of Hydrogen Assisted Methane Combustion at Inlet, Port One, Two and Outlet at 600K

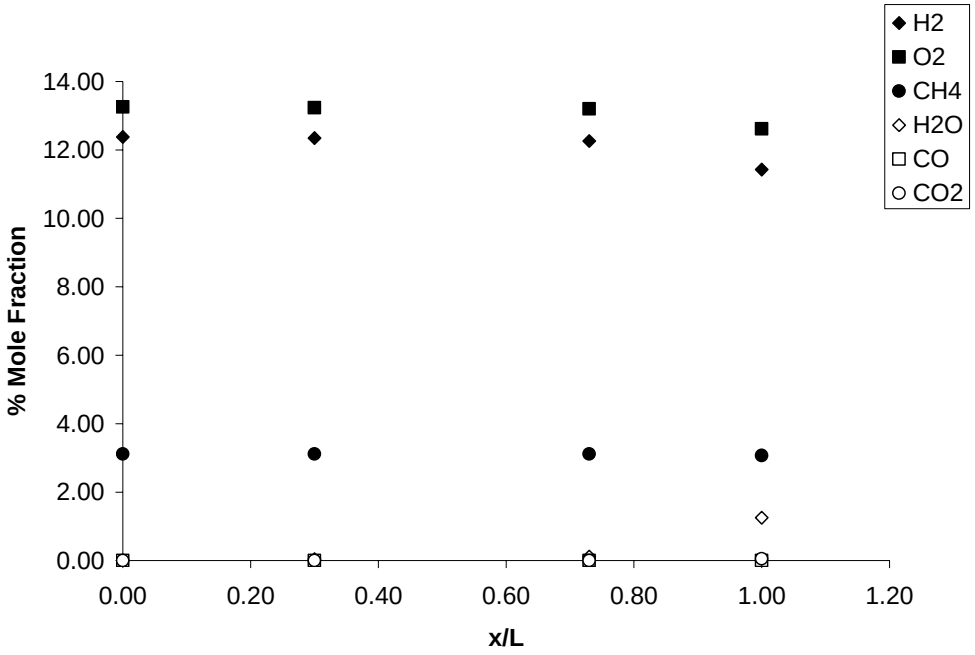

Figure 4-36. Mole Fraction Distribution of Hydrogen Assisted Methane Combustion at Inlet, Port One, Two and Outlet at 700K

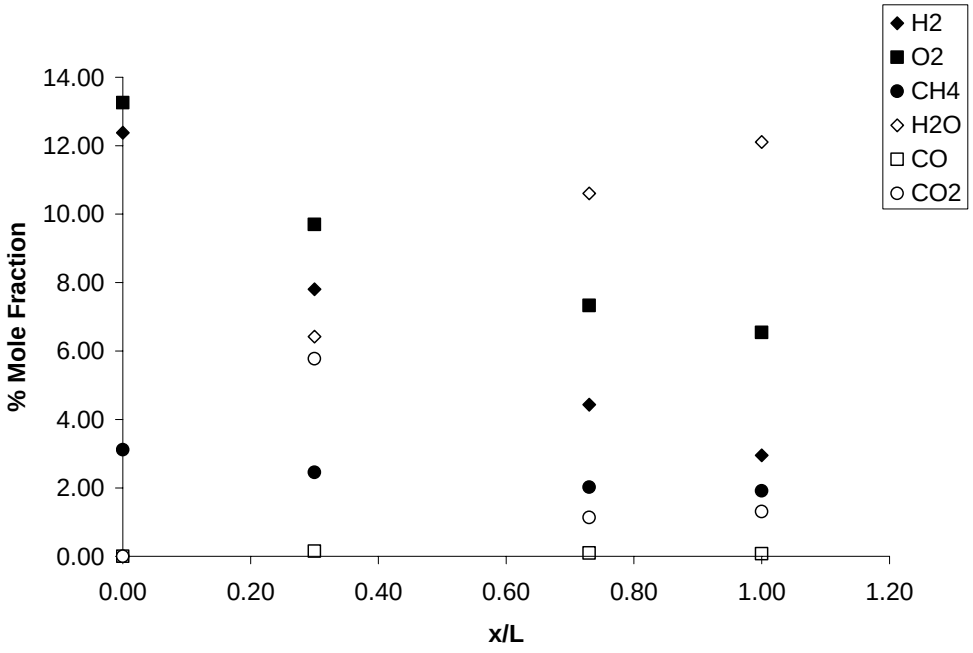

Figure 4-37. Mole Fraction Distribution of Hydrogen Assisted Methane Combustion at Inlet, Port One, Two and Outlet at 900K

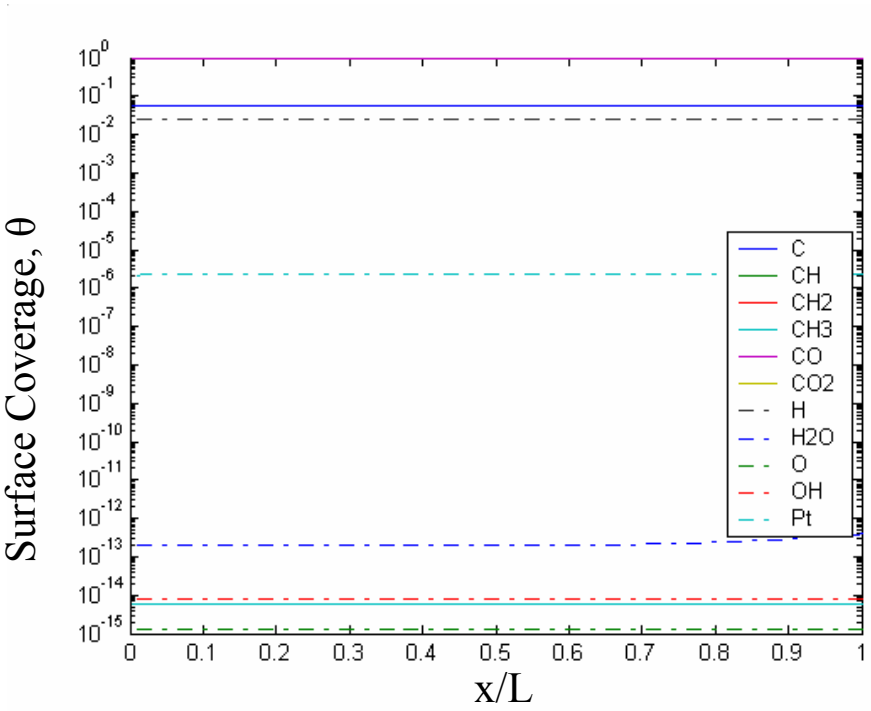

Figure 4-38. Surface Coverage Distributions along Catalyst for Syngas Combustion at 400K

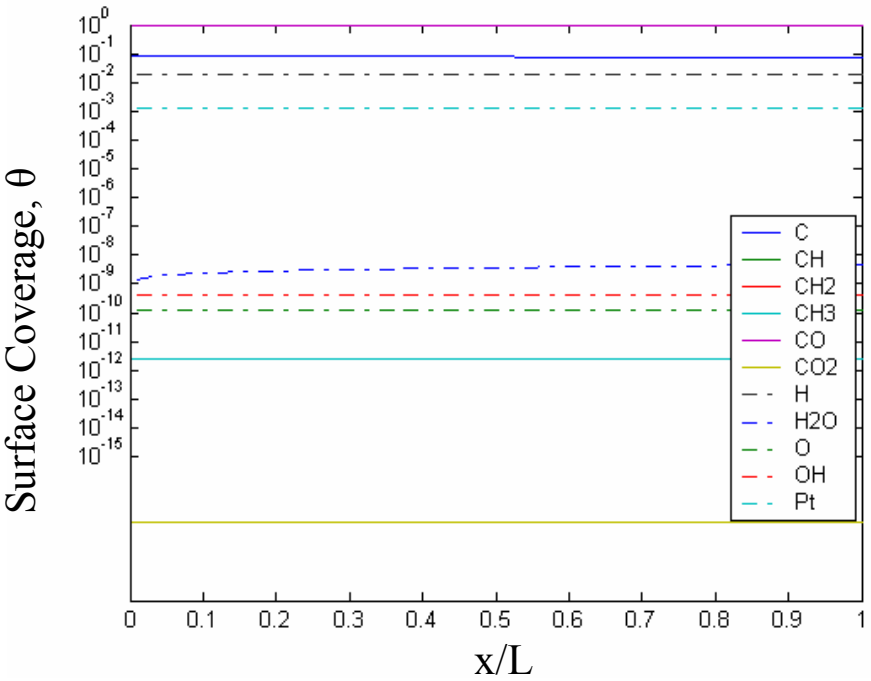

Figure 4-39. Surface Coverage Distributions along Catalyst for Syngas Combustion at 600K

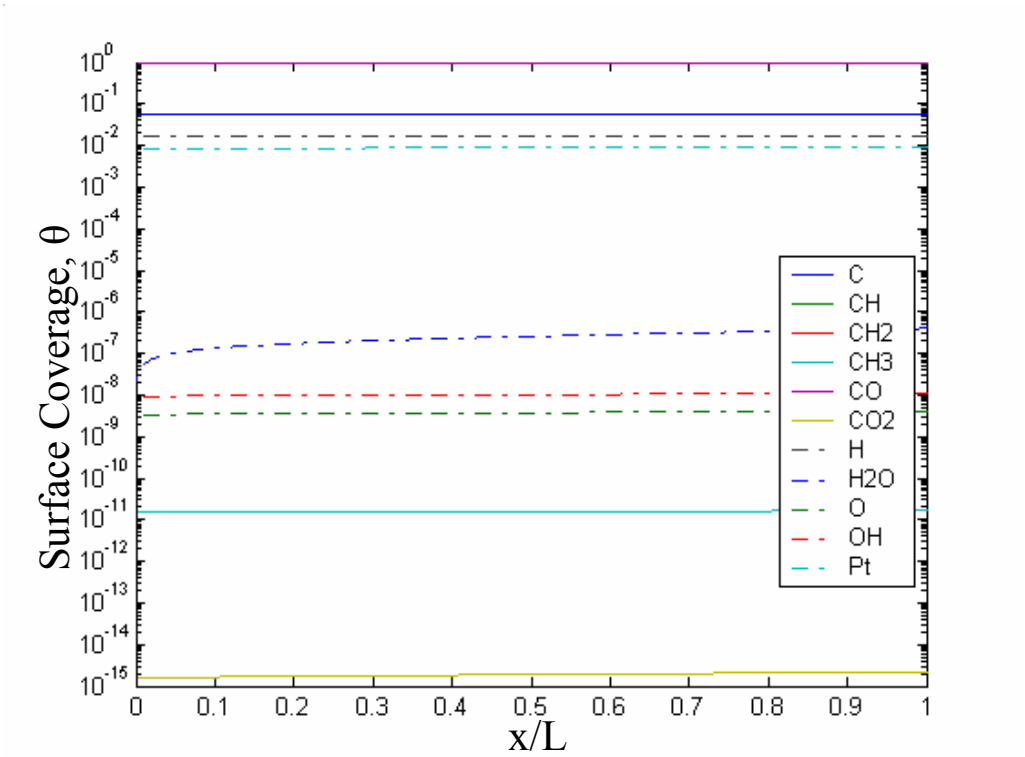

Figure 4-40. Surface Coverage Distributions along Catalyst for Syngas Combustion at 700K

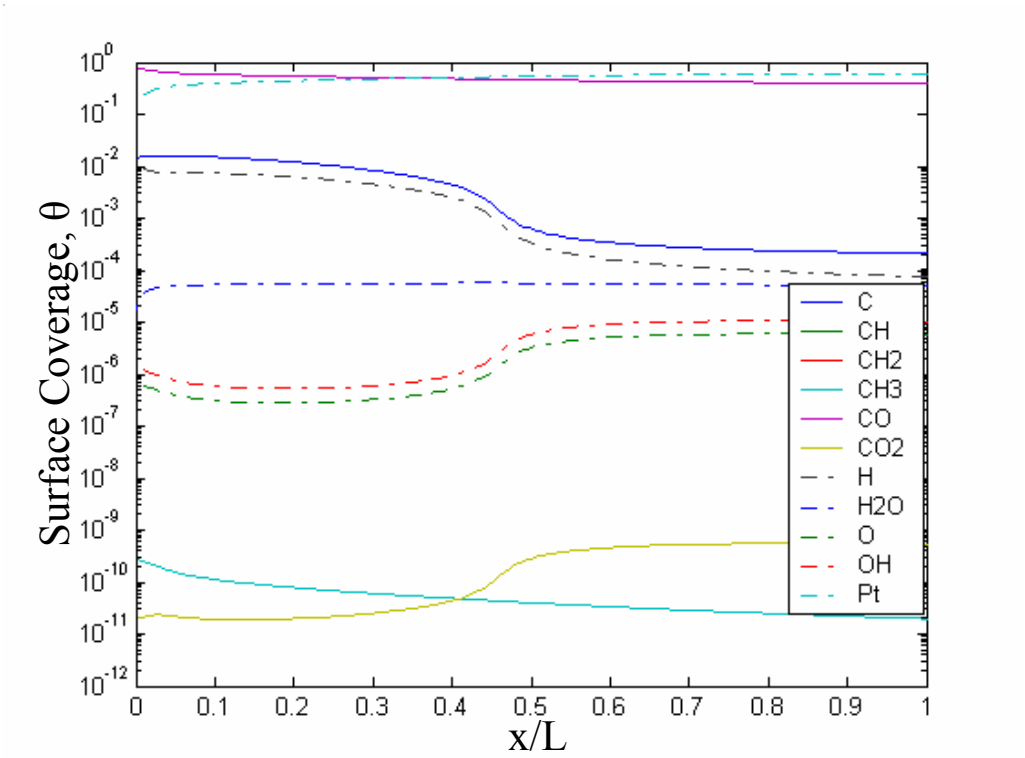

Figure 4-41. Surface Coverage Distributions along Catalyst for Syngas Combustion at 900K

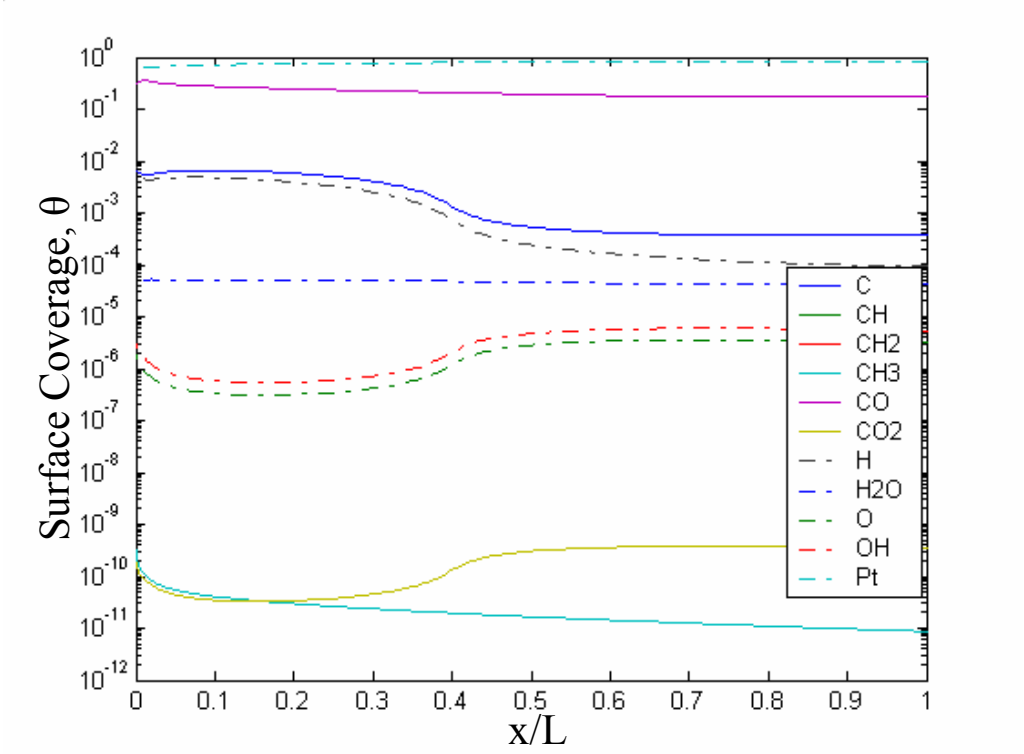

Figure 4-42. Surface Coverage Distributions along Catalyst for Syngas Combustion at 1100K

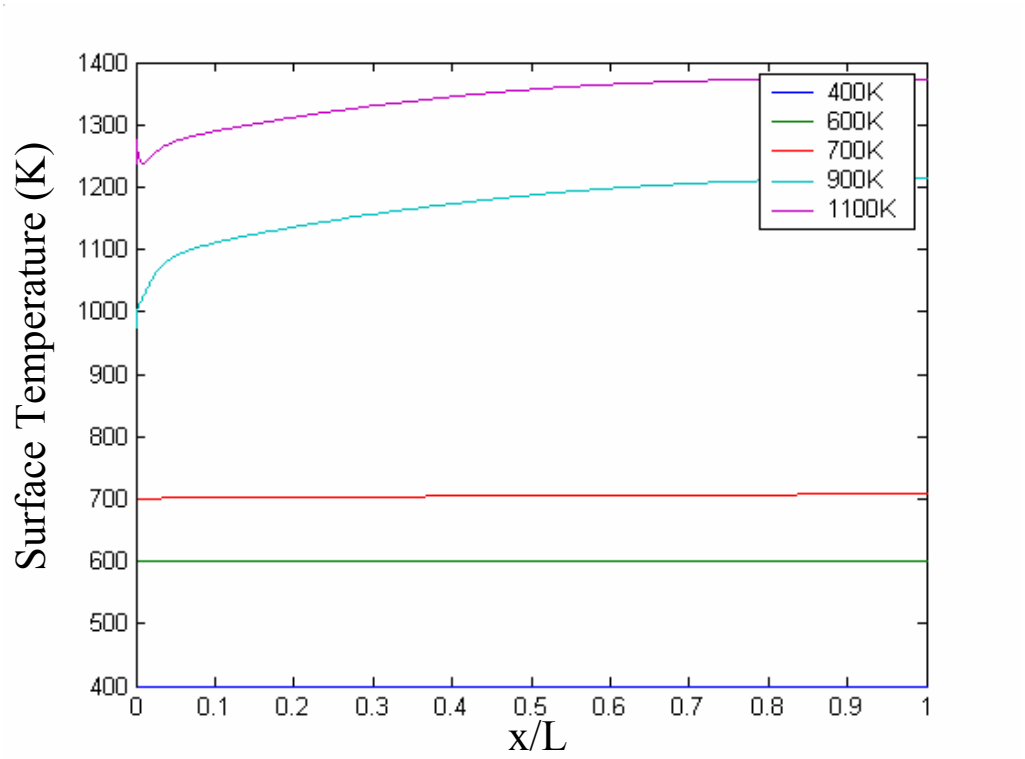

Figure 4-43. Surface Temperature Distribution along Catalyst for Syngas Combustion at different inlet Temperatures

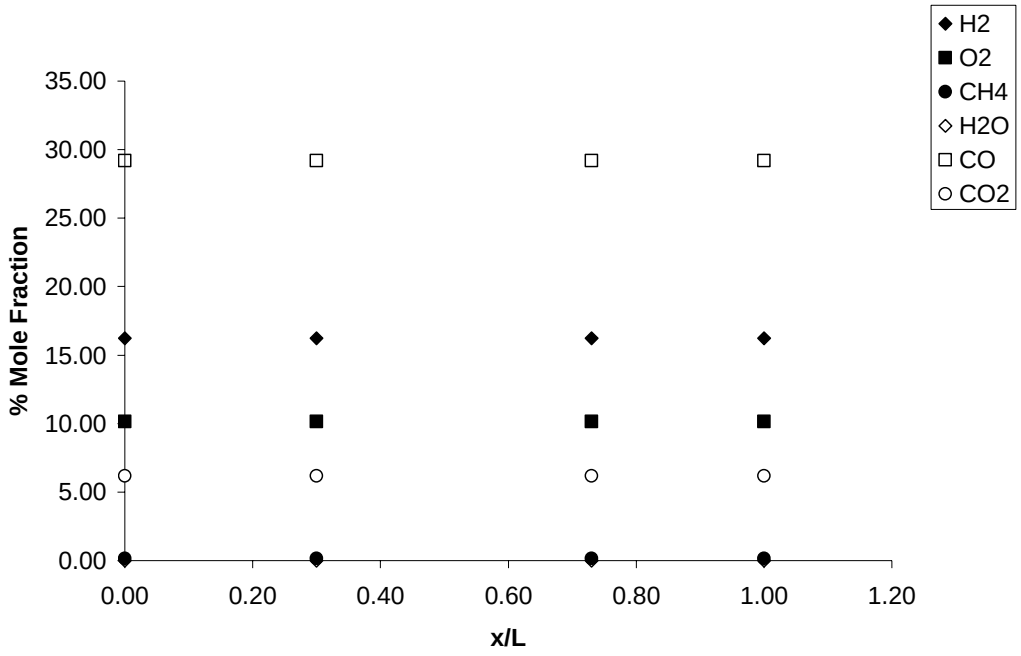

Figure 4-44. Mole Fraction Distribution of Syngas Combustion at Inlet, Port One, Two and Outlet at 400K

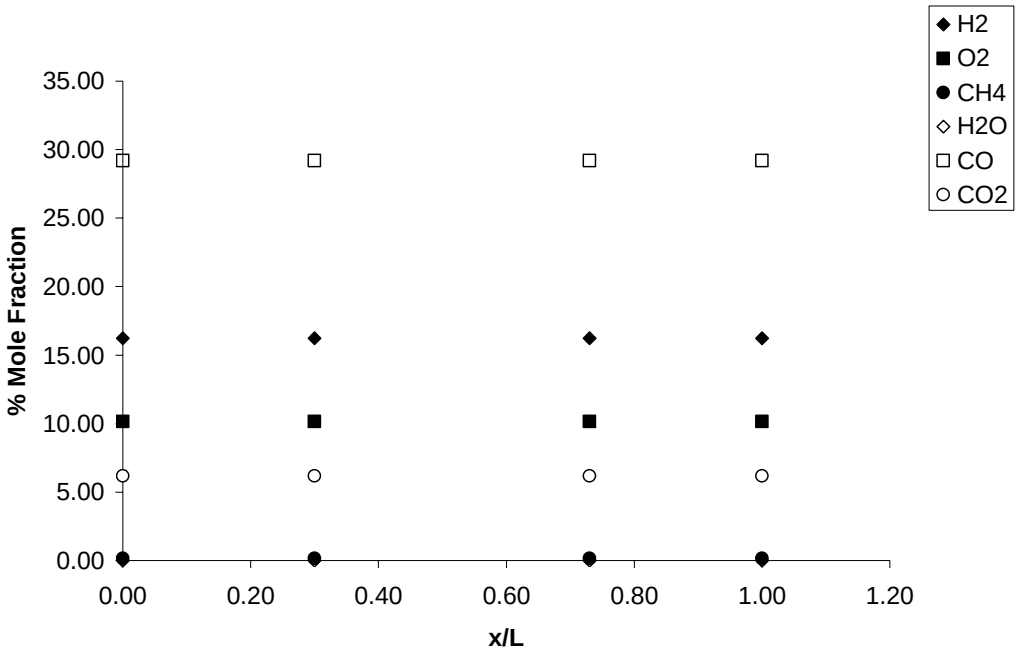

Figure 4-45. Mole Fraction Distribution of Syngas Combustion at Inlet, Port One, Two and Outlet at 600K

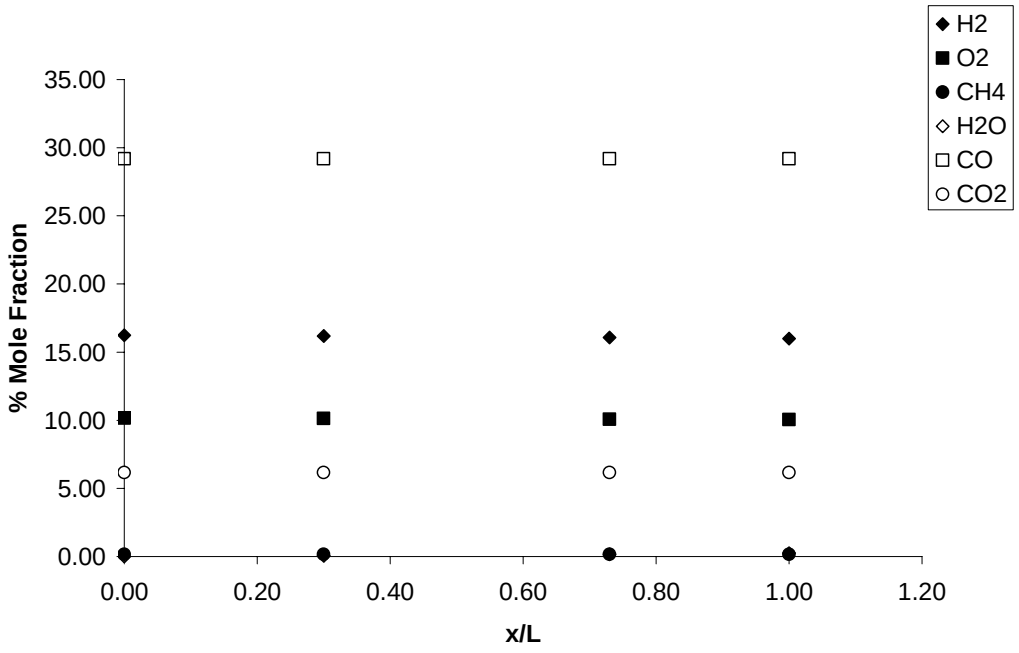

Figure 4-46. Mole Fraction Distribution of Syngas Combustion at Inlet, Port One, Two and Outlet at 700K

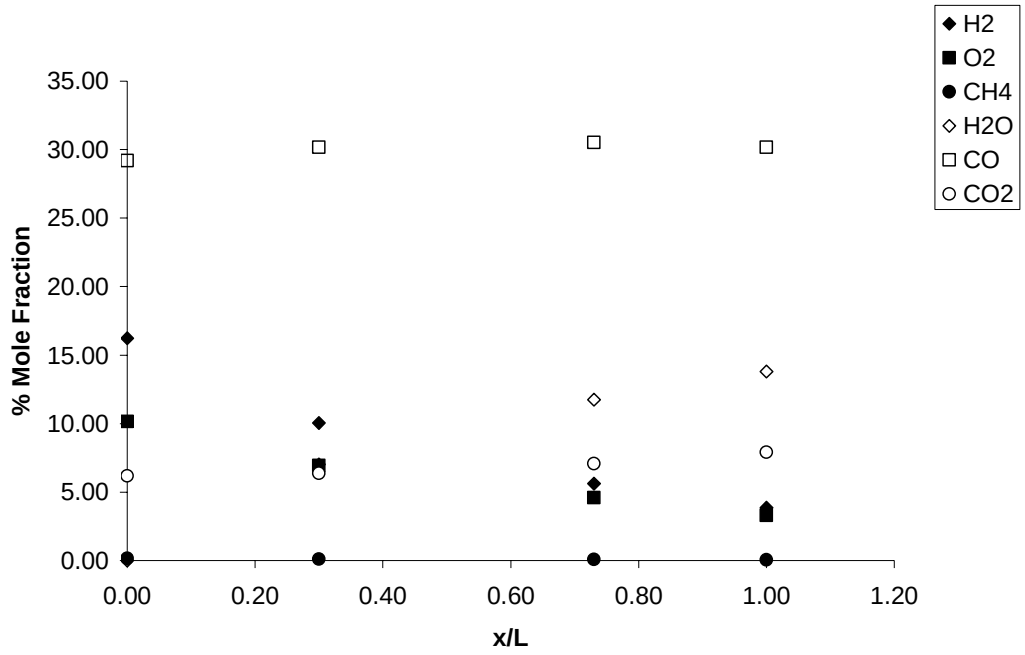

Figure 4-47. Mole Fraction Distribution of Syngas Combustion at Inlet, Port One, Two and Outlet at 900K

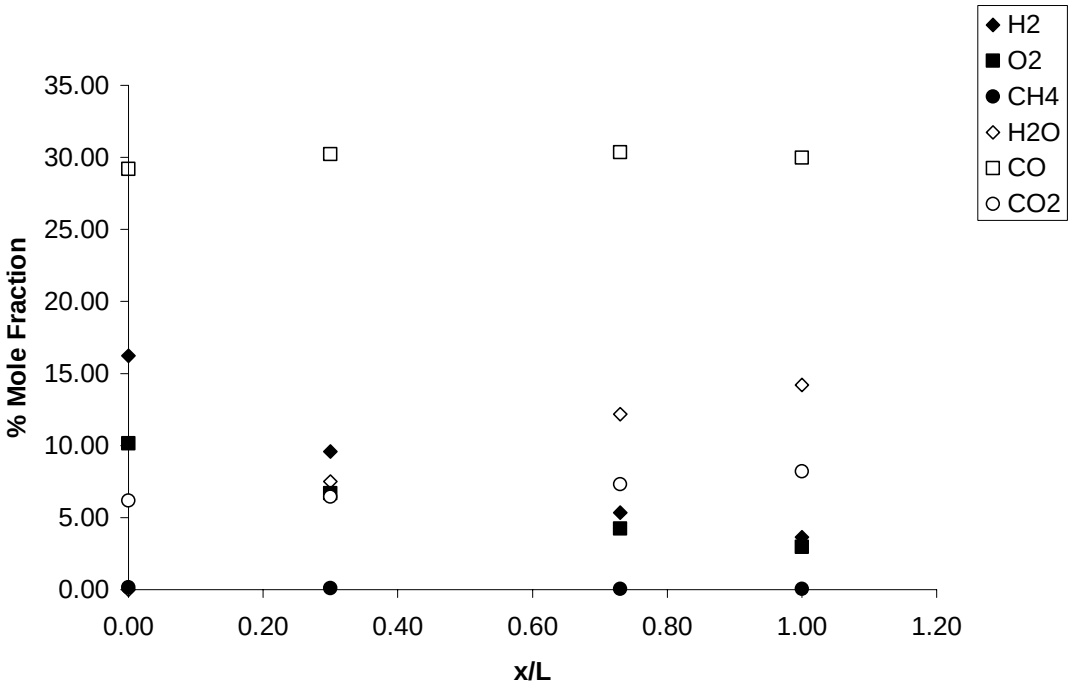

Figure 4-48. Mole Fraction Distribution of Syngas Combustion at Inlet, Port One, Two and Outlet at 1100K

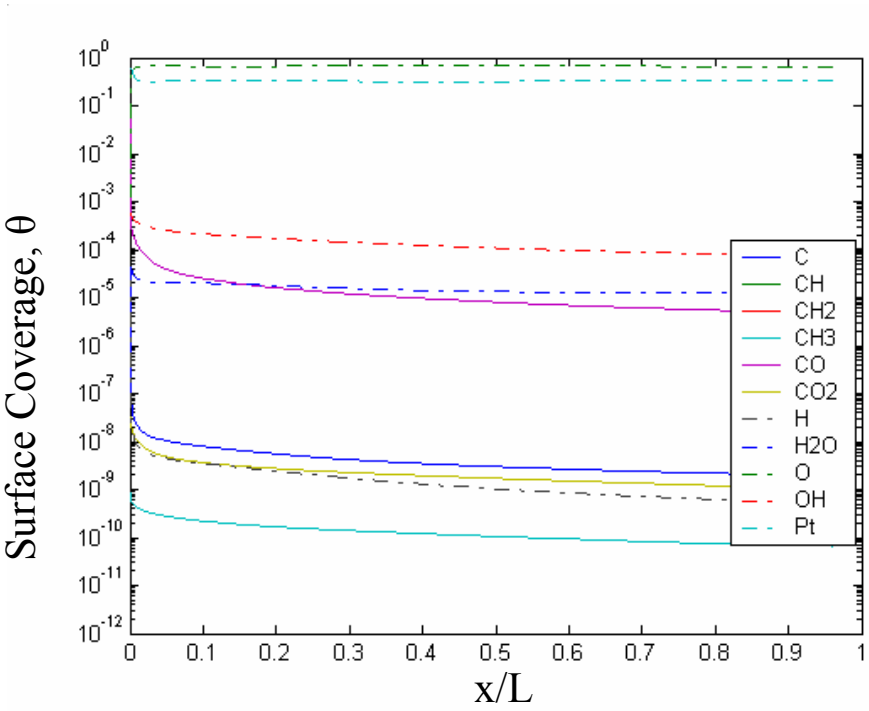

Figure 4-49. Surface Coverage Distributions along Catalyst for Syngas Combustion at 900K at Φ = 0.47

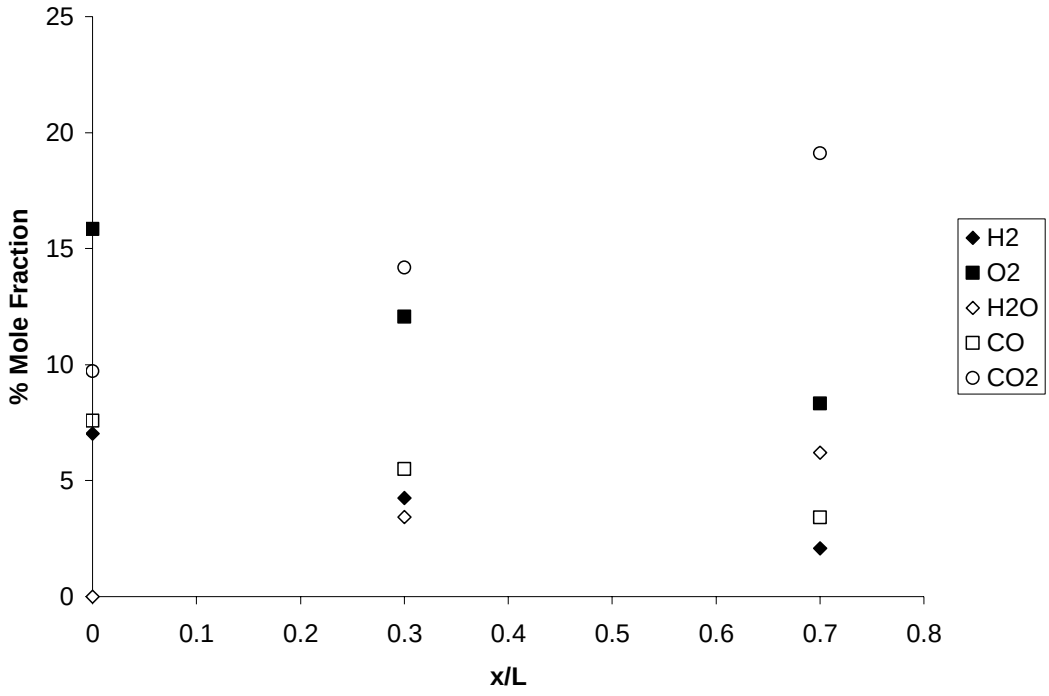

Figure 4-50. Mole Fraction Distribution of Syngas Combustion at Inlet; Port One and Two at 900K for Φ=0.47

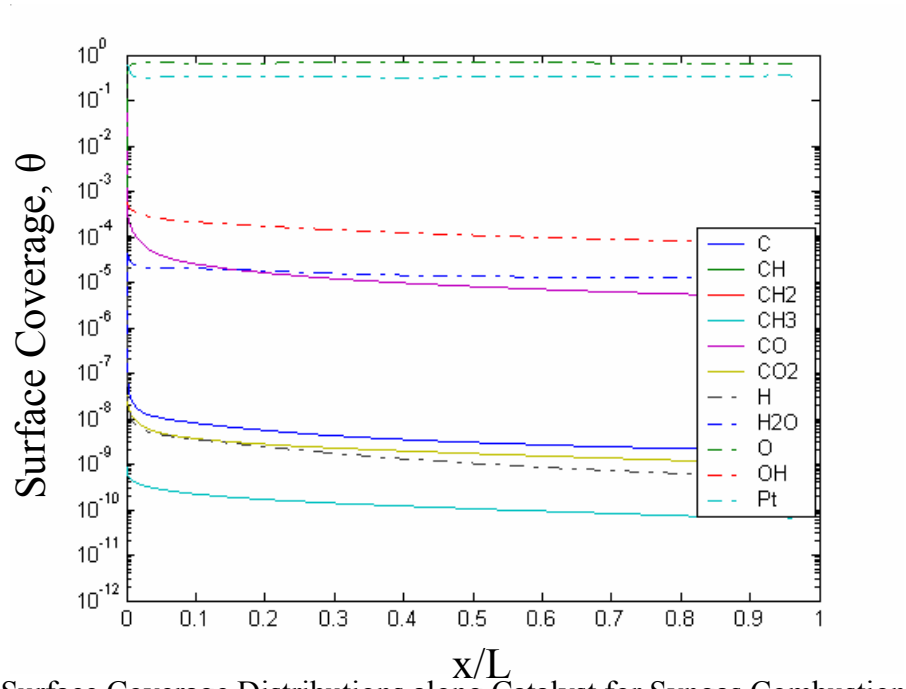

Figure 4-51. Surface Coverage Distributions along Catalyst for Syngas Combustion at 900K at Φ = 0.72

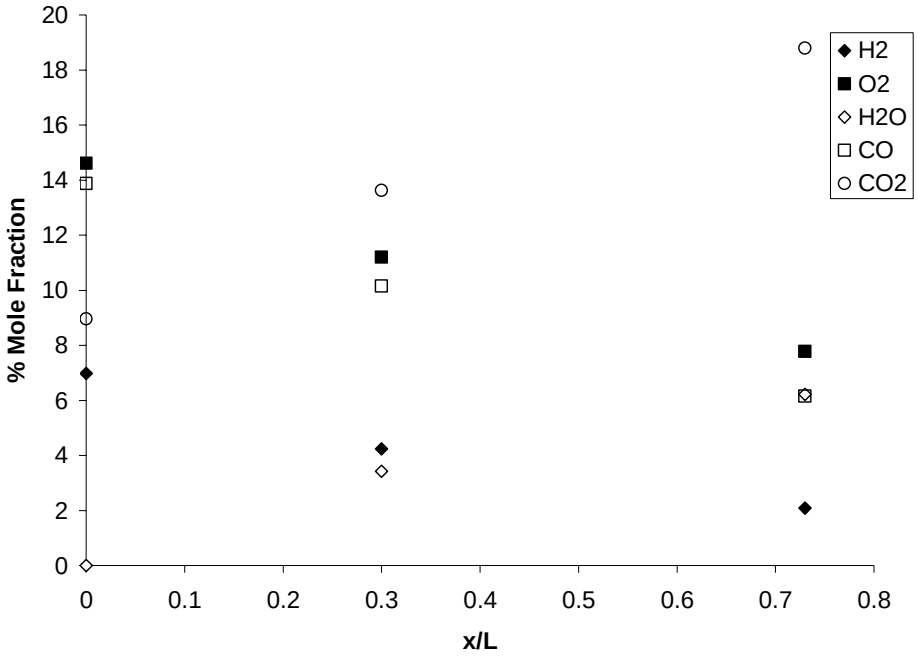

Figure 4-52. Mole Fraction Distribution of Syngas Combustion at Inlet; Port One and Two at 900K for Φ=0.72

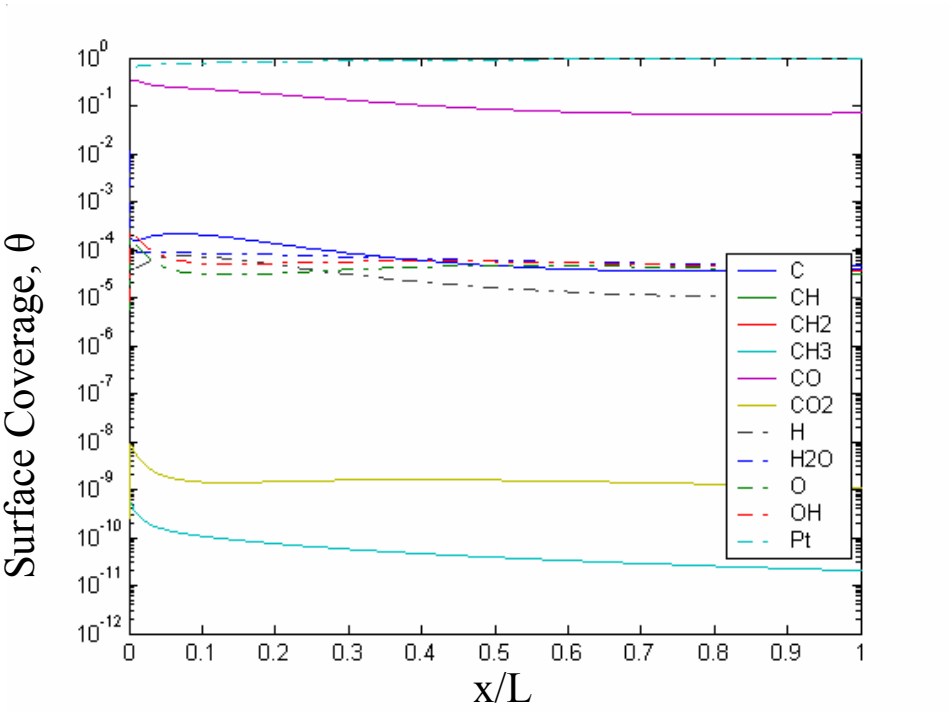

Figure 4-53. Surface Coverage Distributions along Catalyst for Syngas Combustion at 900K at Φ = 1.0

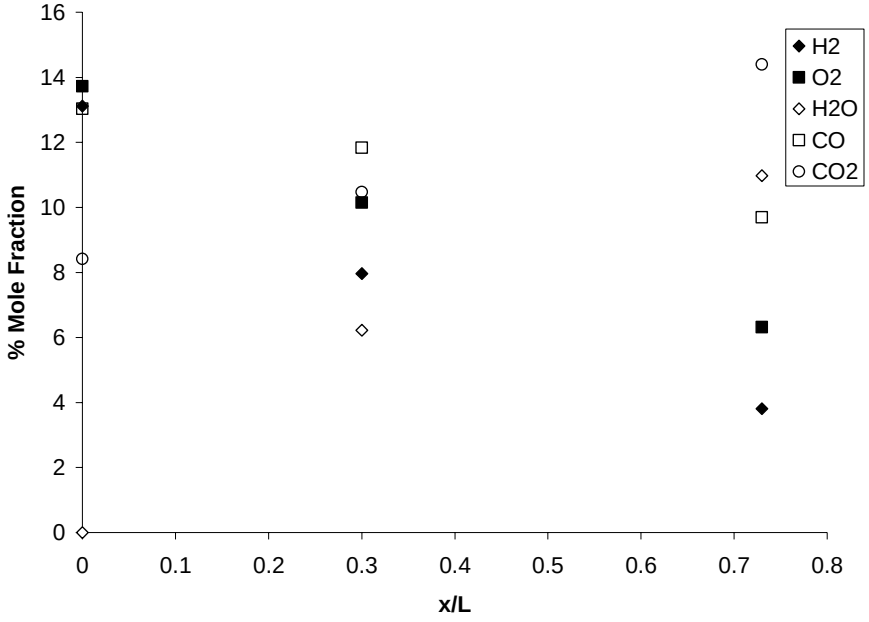

Figure 4-54. Mole Fraction Distribution of Syngas Combustion at Inlet; Port One and Two at 900K for Φ=1.0

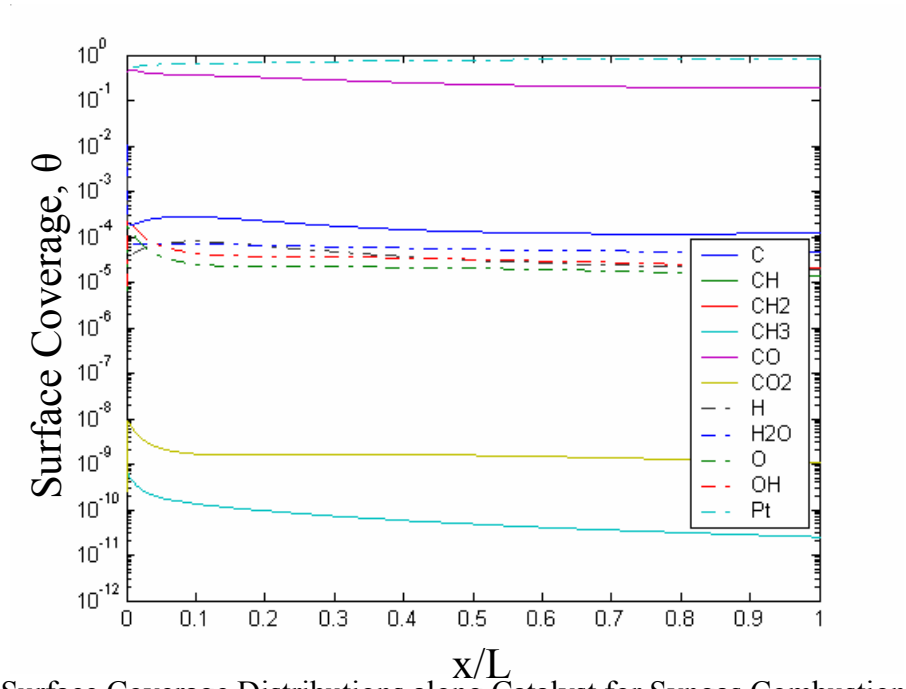

Figure 4-55. Surface Coverage Distributions along Catalyst for Syngas Combustion at 900K at Φ = 1.21

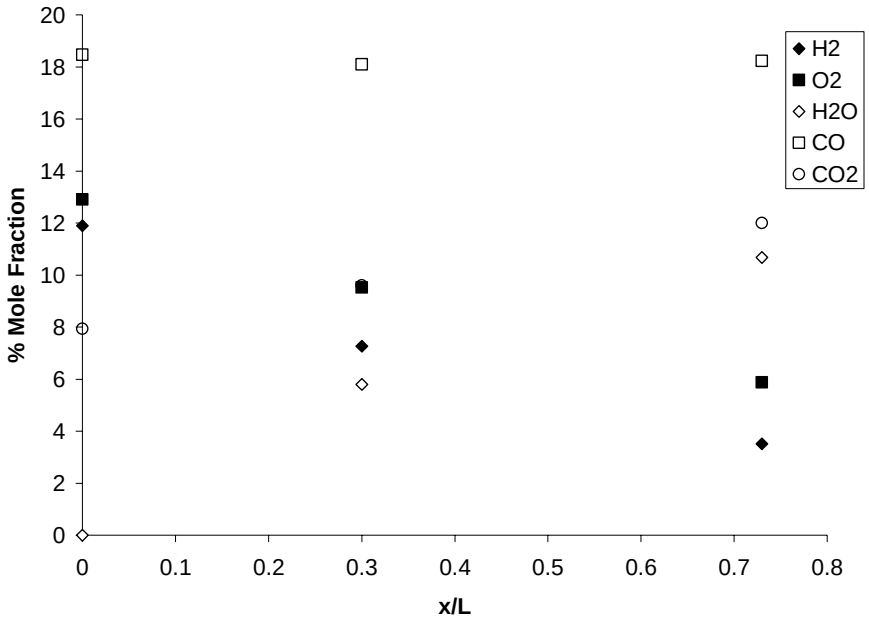

Figure 4-56. Mole Fraction Distribution of Syngas Combustion at Inlet; Port One and Two at 900K for Φ=1.21

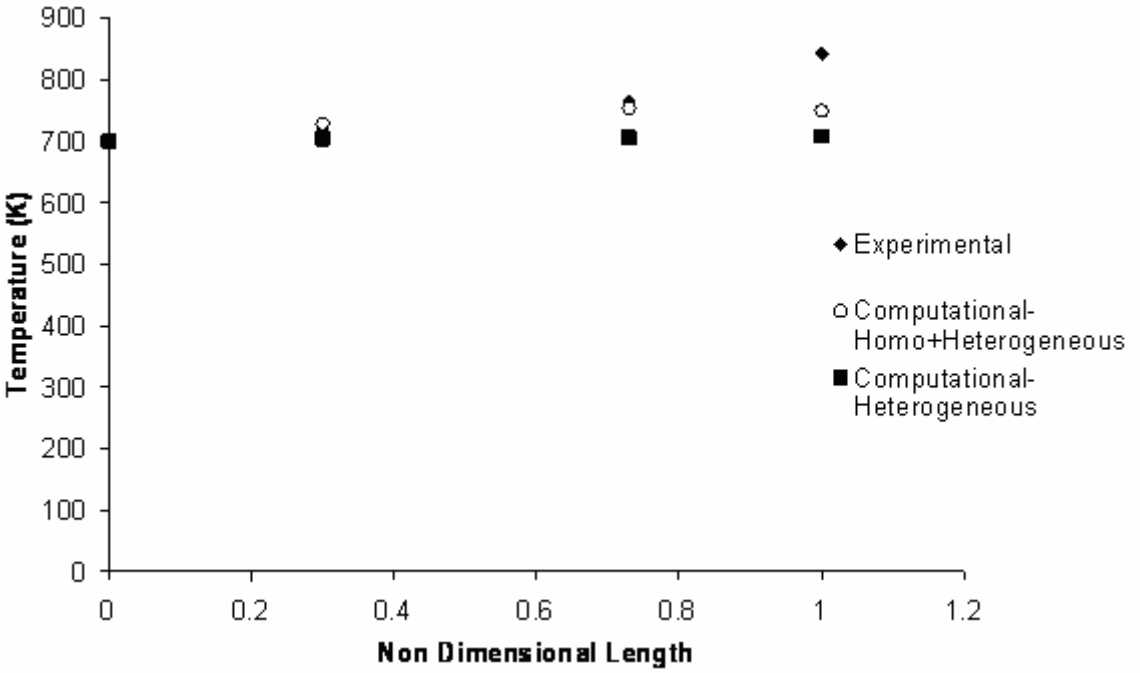

Figure 4-57. Temperature Comparison between Experimental, Heterogeneous and Heterogeneous combined with Homogeneous Mechanisms

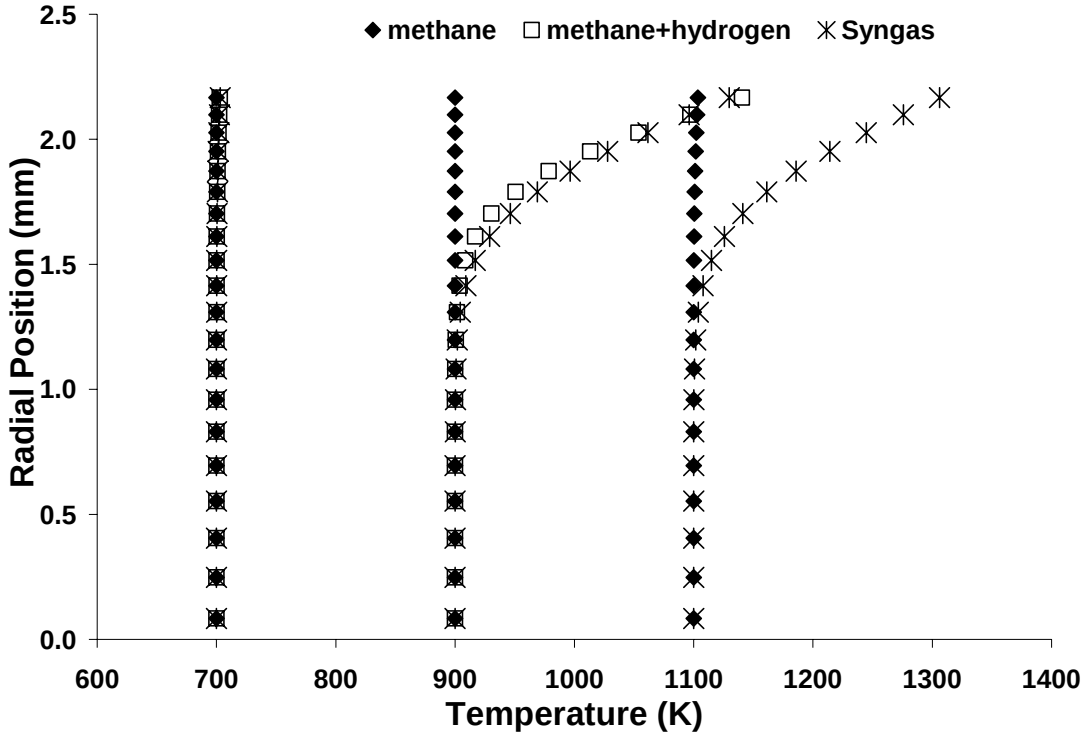

Figure 4-58. Temperature Comparison between Experimental, Heterogeneous and Heterogeneous combined with Homogeneous Mechanisms

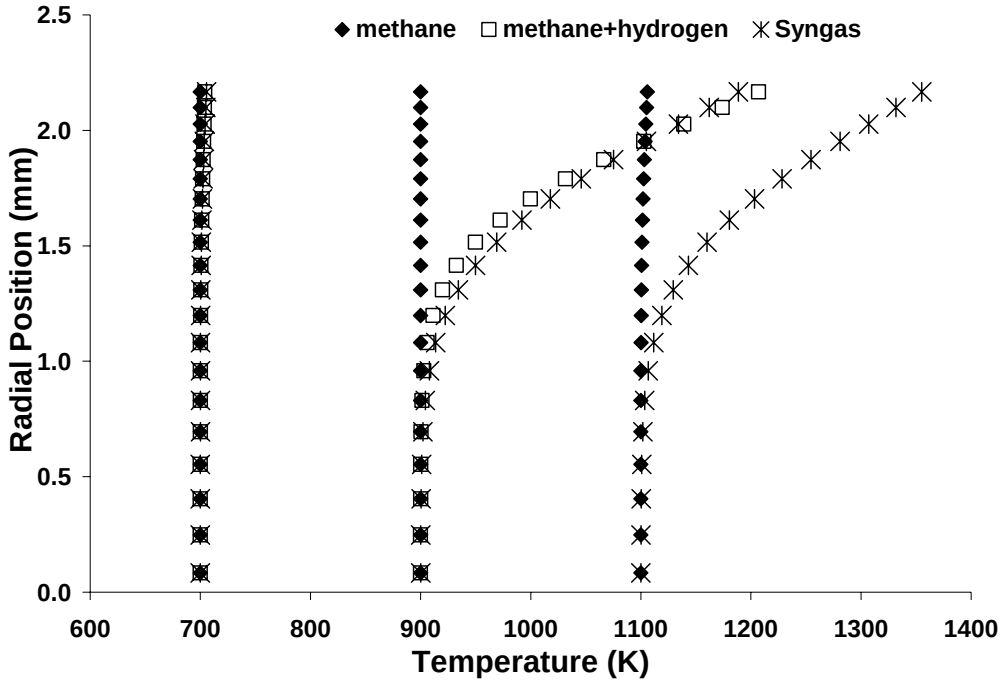

Figure 4-59. Temperature Comparison between Experimental, Heterogeneous and Heterogeneous combined with Homogeneous Mechanisms

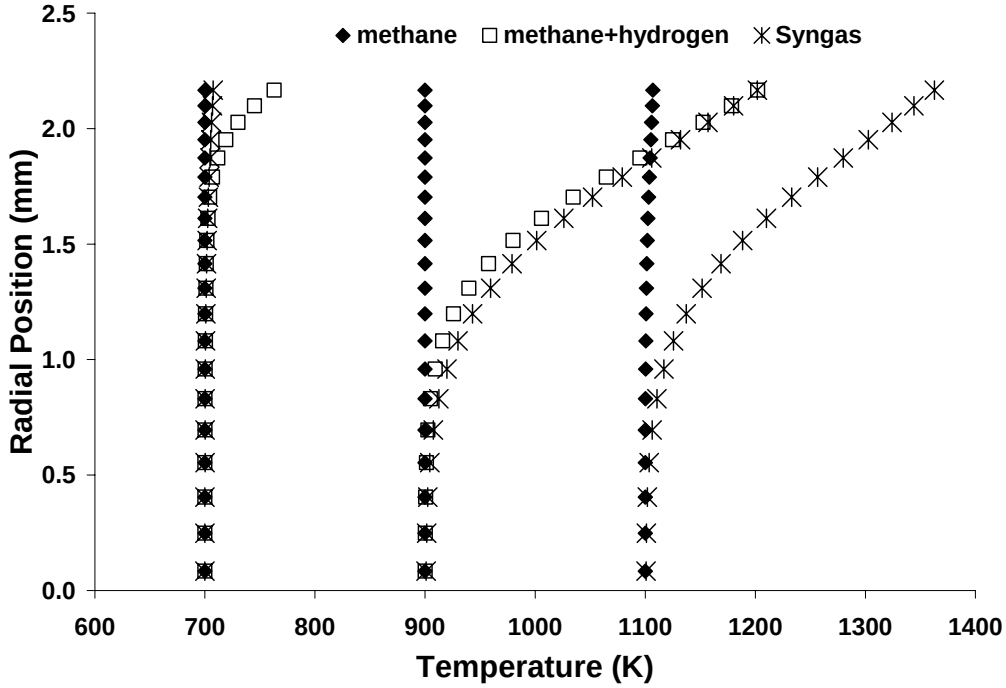

Figure 4-60. Temperature Comparison between Experimental, Heterogeneous and Heterogeneous combined with Homogeneous Mechanisms

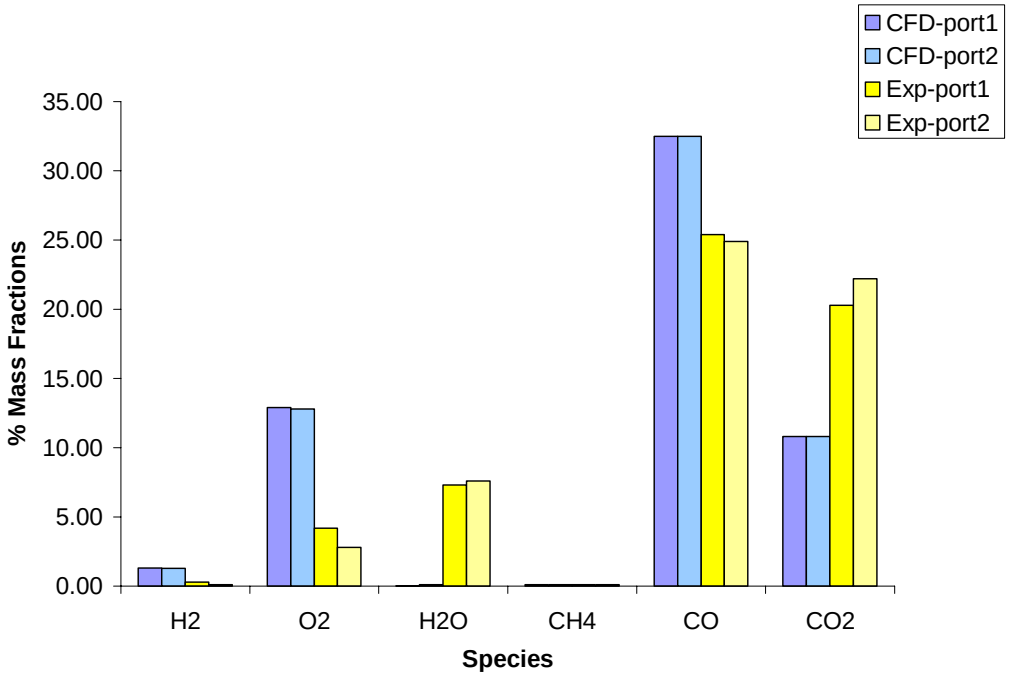

Figure 4-61. Comparison between Experimental and Computational % Mass Fractions for Syngas Combustion at Port One and Two

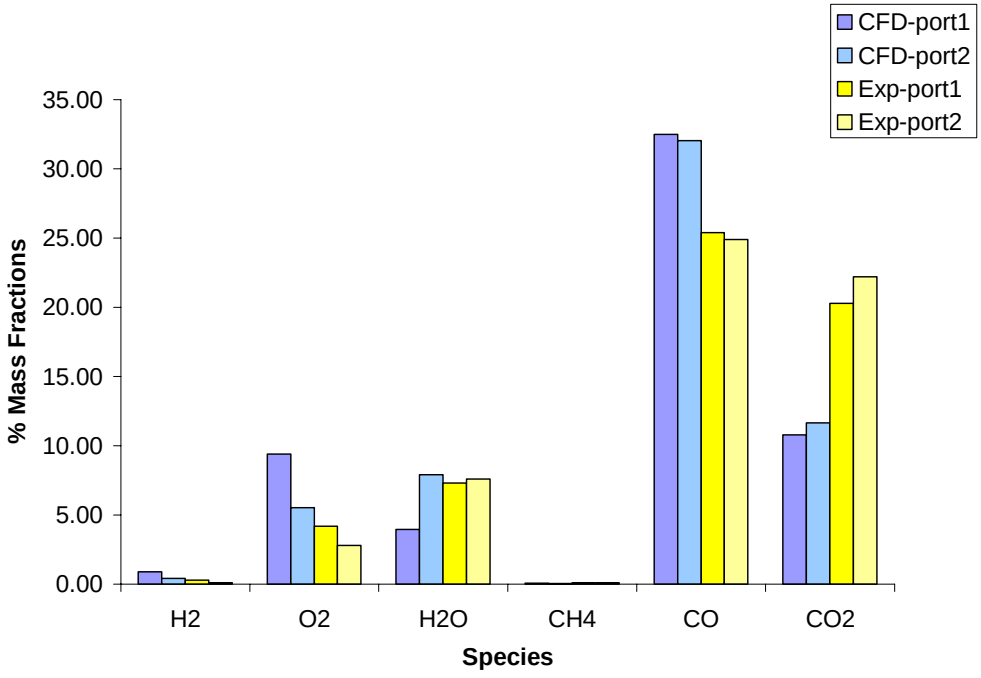

Figure 4-62. Comparison between Experimental and Computational % Mass Fractions for Syngas Combustion at Port One and Two

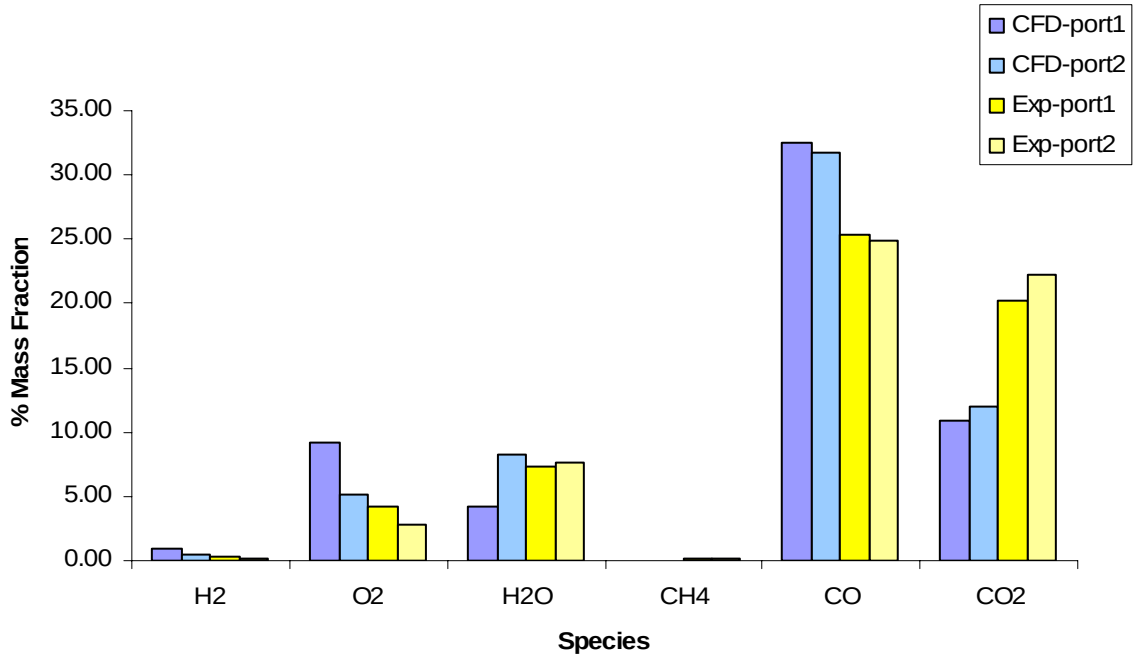

Figure 4-63. Comparison between Experimental and Computational % Mass Mole Fractions for Syngas Combustion at Port One and Two

Table 4-1. Experimental and Computational Case Matrix

Mixture Gases	Experiment		Computation								
			Pt-site density					Temperature			
	Pt-Sm	Pt-R	1	2	2.7	3	6	400	600	700	900
Syngas, $\Phi = 2.28^{\dagger}$	✓	✓	✓	✓	✓	✓	✓	✓	✓	✓	✓
$\Phi = 1.21$					✓			✓	✓	✓	✓
$\Phi = 1.0$					✓			✓	✓	✓	✓
$\Phi = 0.7$					✓			✓	✓	✓	✓
$\Phi = 0.4$					✓			✓	✓	✓	✓
Methane+H_2 $\Phi = 1.5$			✓	✓	✓	✓	✓	✓	✓	✓	✓
Methane $\Phi = 3.05$ ††	✓	✓	✓	✓	✓	✓	✓	✓	✓	✓	✓

Table 4-2. Deutschmann's Surface Reaction Mechanism, A is Pre Exponential Factor (cm.mol.sec), β is Temperature Exponent and Ea is activation energy(KJ/mol)

No.	Reaction	A (cm.mol.sec)	β	E_a (KJ/mol)
1	H_2+2Pt(s)=>2H(s)	4.60×10^{-2}	0	0
2	2H(s)=> H_2+2Pt(s)	3.70×10^{21}	0	67.4
3	H+Pt(s)=>H(s)	1.00	0	0
4	O_2+2Pt(s)=>2O(s)	1.8×10^{21}	-0.5	0
5	O_2+2Pt(s)=>2O(s)	2.30×10^{-2}	0	0
6	2O(s)=> O_2+2Pt(s)	3.70×10^{21}	0	213.2
7	O+Pt(s)=>O(s)	1.00	0	0
8	H_2O+Pt(s)=>H_2O(s)	0.75	0	0
9	H_2O(s)=>H_2O+Pt(s)	1.00×10^{13}	0	40.3
10	OH+Pt(s)=>OH(s)	1.00	0	0
11	OH(s)=> OH+Pt(s)	1.00×10^{13}	0	192.8
12	O(s)+H(s)<=> OH(s)+Pt(s)	3.70×10^{21}	0	11.5
13	H(s)+OH(s)<=> H_2O(s)+Pt(s)	3.70×10^{21}	0	17.4
14	OH(s)+ OH(s)<=> H_2O(s)+O(s)	3.70×10^{21}	0	48.2
15	CO+Pt(s)=> CO(s)	8.40×10^{-1}	0	0
16	CO(s)=> CO+Pt(s)	1.00×10^{13}	0	125.5
17	CO_2(s)=> CO_2+Pt(s)	1.00×10^{13}	0	20.5
18	CO(s)+O(s)=> CO_2(s)+Pt(s)	3.70×10^{21}	0	105.0
19	CH_4+2Pt(s)=>CH_3(s)+H(s)	1.00×10^{-2}	0	0
20	CH_3(s)+Pt(s)=>CH_2(s)+H(s)	3.70×10^{21}	0	20.0
21	CH_2(s)+Pt(s)=>CH(s)+H(s)	3.70×10^{21}	0	20.0
22	CH(s)+Pt(s)=>C(s)+H(s)	3.70×10^{21}	0	20.0
23	C(s)+O(s)=>CO(s)+Pt(s)	3.70×10^{21}	0	62.8
24	CO(s)+Pt(s)=>C(s)+O(s)	1.00×10^{18}	0	184.0

Table 4-3. Five Step Gas Phase Reaction Mechanism, A is Pre Exponential Factor (cm.mol.sec), β is Temperature Exponent and Ea is activation ebergy(KJ/mol)

No.	Reaction	A (cm.mol.sec)	β	E_a (KJ/mol)
1	O_2+H=>OH+O	2.00 x 10^{14}	0.00	70.3
2	H_2+O=>OH+H	5.06 x 10^4	2.67	26.3
3	H_2+OH=>H_2O+H	1.00 x 10^8	1.6	13.8
4	CO+OH=>CO_2+H	6.00 x 10^6	1.5	-3.1
5	H+OH=>H_2O	2.20 x 10^{22}	-2.0	0

Table 4-4. Methane Inlet Flow Rate Specification

Methane Air Composition	**Flow Rate in SLPM**
CH_4	1.6
Mixing Air	5
Cooling Air	30

Table 4-5. Syngas Inlet Flow Rate Specifications

Syngas Air Composition	**Flow Rte in SLPM**
H_2	1.75
CO	3.04
CO_2	0.664
CH_4	0.224
Mixing Air	5
Cooling Air	30

† Computational study was also performed at 1100 K, †† Computational study was also performed at 1100, 1200, 1500 and 1700 K, Φ is the equivalence ratio is the equivalence ratio.

CHAPTER 5
CONCLUSION

Mass spectrometry technique was used to determine the species concentration distribution inside the catalytic combustor at two selected locations. The experimental findings were validated using computational techniques that modeled heterogeneous catalysis. Non-reacting and combustion tests were conducted and fuel related parameters such as fuel mixtures were varied. Four different catalysts were used for each of these fuel types. Numerical investigation was conducted for each of these experimental cases. Additional numerical investigation was conducted by varying equivalence ratio, inlet temperature and site density of catalyst. The conclusions are summarized below.

Fuel type:

Methane Air mixture platinum smooth and platinum rough:

- Methane failed to ignite on both platinum smooth and rough catalysts below 1200K. This could be due to lower activation energy of surface reactions and higher bare sites on the surface of catalysts A and B where methane adsorption followed by reactions on the surface forming product-surface complex and desorption of the products is favored.

- Computational investigation carried out for methane air combustion on platinum surface consolidates this experimental observation. The model shows that almost all O atoms are strongly adsorbed on platinum surface and thus provide less or no bare site for CH_4 to adsorb below 1200K.

- Since adsorption of CH_4 is the primary step in initiating methane combustion on platinum, a higher sticking probability of O atoms over CH_4 suppresses any combustion. Since O atoms desorbs from the platinum surface at and above 1200K so that available sites for CH_4 adsorption are thus created and hence first signs combustion do appear to occur at and above 1200K.

- At even higher temperatures more and more O atoms leave the surface creating more opportunity for CH_4 adsorption and hence favoring more combustion.
- Gas phase reactions appear to be dominant at and above 1500K because there appears no adsorbed species on platinum at these temperatures and whole of the surface is just platinum only.

Methane Hydrogen- Air mixture on platinum smooth:

- C atoms have the highest sticking probability amongst all the constituent species. This would mean that the oxide of carbon formation is a difficult proposition.

- The H atoms are loosely bound thereby suggesting that formation of OH followed by H_2O formation is relatively easier. No products in the gas phase appear to be formed below 700K at which the first signs of product in the form of H_2O seem to be produced.

- Predominant product formation occurs at 900K and above when both C atoms and H atoms are loosely bound to the surface and they both compete to abstract O atoms to form CO and OH. However, combination of O and H atoms appears to dominate over CO abstracting an O atom and thus oxidation of OH to H_2O is preferred over CO forming CO_2.

- Simulations were performed by varying the site density of platinum. It was observed that changes in site density had no effect on the conversion of reactants as well as formation of products. This can be attributed to the fact that surface reactions take place at the mass transport limits.

Syngas Air mixture platinum smooth and platinum rough:

- Syngas ignited on the two catalysts. The conversion of reactants and formation of products appears to be the highest when using platinum smooth catalyst.

- Platinum appears to sustain combustion over the entire length of the catalyst. Numerical investigations performed using a five step gas phase reaction mechanism in addition to the Deutschmann's surface reaction mechanism suggest experimental and computational temperature within an error range of 5%-12%.

- The mass fraction is predicted with less than 8% error for H_2O at temperatures above 700K. However there is an error of 45% in predicting CO_2 formation. This can be attributed to the fact that for experimental conditions of a very rich fuel mixture, equivalence ratio of 2.28, the simulations show that out of the species comprising the syngas, CO has the highest sticking probability.

- CO remains adhered to platinum surface for as high as 900K. This inhibits O atoms being abstracted by CO and get oxidized to CO_2. However, H, OH and O atoms are loosely bound and thus H_2O is readily formed. This model predicts H_2O accurately and seems to model combustion better at temperatures at and above 900K.

- Numerical investigations performed to study effects of equivalence ratios show that oxides of carbon are formed at fuel lean conditions. This is attributed to a lower surface coverage of CO is lower at leaner conditions and increase as the equivalence ratio increases i.e. as the mixture becomes fuel rich.

- At lean conditions CO is loosely bound on the surface and H atoms occupy the whole of platinum surface. Hence formation of oxides of carbon eventually forming CO_2 is favored over formation of H_2O.

- Reverse conditions set in as the mixture becomes stoichiometric and richer. More of the surface would now be covered with CO and H atoms appear to be loosely bound. Hence more H_2O is formed with less or no CO_2.

- It is thus concluded that production of H_2O is preferred at fuel rich conditions and that of CO_2 at fuel lean conditions.

- Simulations were performed by varying the site density of platinum. It was observed that changes in site density had no effect on the conversion of reactants as well as formation of products. This can be attributed to the fact that surface reactions take place at the mass transport limits.

APPENDIX A
DETAILED COMPUTATIONAL SETUP

Boundary layer meshing is done by first selecting the edge wherever a boundary layer is required. These edges would be those places where the gradient in velocity, temperature and mass fractions are significant. The edge selected is then divided into "n" number of **nodes** followed by selecting the distance between the edge and the first row, called the "first distance" of the boundary layer. Since a boundary layer has a significant thickness, this thickness is modeled by selecting the number of rows that would constitute the overall thickness of the boundary layer. Finally we select a method of how the distance between one row to the other varies. In my selection, I have selected the distance between each layer of the boundary layer to grow exponentially by choosing a "factor" to be multiplied to the "first distance" to get the second row distance from the edge and so on. A typical boundary layer on a face is shown in Figure A-1.

Once the boundary layer is created, the face made out of the edge, has a diminished surface area now, the decrease in area being attributed to the area occupied by the circular boundary layer. Then we mesh this face.

Face mesh is generated by selecting the face which has already being meshed for boundary layer or otherwise. In either case the next step was to select the number of interval counts on this face. If a boundary layer exists on this face then this interval count would be distributed over the area left over after the boundary layer is created, if no boundary layer exists on that face, then the interval count would be distributed over the entire area available. A selection of the geometry of the elements of the mesh has to be made too. The two options out of possible many options are "Quad" and "Tri", which represent quadrilateral and trigonal shaped mesh elements respectively. Next we choose the pattern in which these elements would be swept

across the entire face. Possible options are “Map” and “Pave”. The quad-pave option results in a structured grid shown in Figure A-2. Once a face is meshed, we proceed to mesh the volume.

Volume mesh is generated by sweeping the face meshed previously across the entire volume that constitutes, as one of its faces, the one previously meshed. This was done using “hex/wedge” (suggesting hexahedral/wedge shape of the mesh elements) and the pattern of sweeping was selected to be “cooper” option. The limitation to this kind of volume meshing is that, it is available only if the faces are meshed using quad-pave option, if they are not (as in some complicated geometry) then we use “Tet/hybrid-Tgrid”. This type of volume meshing results in an unstructured pattern of grids shown in Figure A-3.

Boundary types used are “mass_flow_inlets” and “velocity_inlets” for the inlet faces of the three computational domain. The inlet face of the first domain uses “mass_flow_inlets” as inlet type while the inlet faces for the rest of the three domains use “velocity_inlets”, the outlet faces of all the four domains are specified as “pressure outlet” and the curved surface wall of all the domains are specified the boundary type “WALL”. Next we specify the Continuum type.

Continuum type specifies whether a given volume is a “fluid” or a “solid”. The “fluid” option is chosen when there is a fluid flow inside a hollow volume, while “solid” option specifies the entire volume as a solid.

Zone One is comprised of two 0.4 cm inner diameter tubes. One supplies the fuel and the other supplies the oxidizer. The fuel feed line is 40 cms long while the oxidizer line has a length of 116 cms. The mesh generated to capture boundary layer at the inlet face of the feed lines (both identical) is shown in Figure A-1. The first row distance is chosen to be 0.0001 m and the increment factor is 1.1. The number of rows selected is four. The face bearing the boundary layer is then meshed. A “quad-pave” option was chosen to mesh the faces. A total of 422 cells were

generated for this face. The volume was then meshed using “hex/wedge-cooper” option. Volume representing fuel flow was meshed into 834,128 nodes with 789,888 hexahedral elements whereas the volume representing the oxidizer flow was meshed into 1,742,720 with 1,641,158 hexahedral elements. The overall meshed volume is shown in Figure A-4.

Both the feed lines were meshed exactly the same except for the fact that the fuel line was modeled vertically while the oxidizer line horizontally. Inlets and outlets for both the volumes were specified as “mass_flow_inlet” and “pressure outlet” boundary type respectively. The curved surface was specified “WALL” boundary type.

Zone two shown in Figure A-5 is a region where the fuel and oxidizer is getting mixed. The incoming feeds as well as the mixing portion are all 0.4 cm inner diameter tubes. The oxidizer enters the domain from the left whereas the fuel enters vertically downwards. Since significant gradients in velocity, temperature and mass fractions are expected where the fuel and oxidizer start mixing, provisions for capturing these gradients are made by allowing boundary layer generation at the location of mixing shown in Figure A-6. This could be accomplished by subdividing zone two into three volumes (named as Volume 1, Volume 2 and Volume 3 and shown in [Figure A-7 (a), (b) and (c) shown in red]) and then generating boundary layers where the edges of these three volumes meet. Boundary layers are also made on the two inlet faces. Faces for all these three volumes as well as the volumes themselves, were meshed using the same schemes adopted for zone one. Figure A-8 shows the meshed zone two.

The entrance faces and the pressure outlet face have 1177 cell elements and 892210 hexahedral cells combining the three volumes. Oxidizer and fuel entrance faces were specified as “velocity_inlet”, mixture outlet face as “pressure outlet” and the curved surface as “WALL”

boundary type respectively. The X direction span is 5.23 cm, Y direction span is 12.5 cm and the Z direction span is 0.4 cm (inner diameter of the tube)

Zone three shown in Figure A-9 is a region where the fuel-oxidizer mixture after mixing over a length of 9.5 cm (mixing length in zone two), expands over a CROSS joint. The span length of the CROSS in the X-direction is 2.7 cm; in the Y direction is 3.4 cm and has a 0.635 cm inner diameter. Zone three was subdivided into regions of three volumes, named as Volume 1, Volume 2 and Volume 4 shown in Figure A-10 (a), (b), (c) in red. Volume 2 models the catalyst holder. The incoming mixture after expanding over the CROSS hits the holder and turns right angles and continues flowing out of the third zone in to the fourth zone. Faces for all these three volumes as well as the volumes themselves, were meshed using the same schemes adopted for zone one. The mixture entrance face is specified as "velocity_inlet", mixture outlet face as "pressure outlet" and all curved surfaces as well as other solid surfaces as "WALL" boundary type. Figure A-11 shows the meshed zone three. Volume 1 has 13,000 nodes with 10,800 hexahedral elements; Volume 2 has 73911 nodes with 70770 hexahedral elements and Volume 4 has 194,641 nodes with 917,544hexahedral elements, i.e. a total of 281,552 nodes and a total of 999,114 hexahedral elements.

Zone four shown in Figure A-12 is a region where the mixture after leaving the CROSS, flows through the annular passage of the catalytic combustor and over the surface of the catalyst. Zone four was subdivided into regions of five volumes, namely, Volume 4, Volume 7, Volume 10, Volume 11 and Volume 13 shown in Figure A-13 (a), (b), (c), (d) and (e) in red. Volume 4 models the annular passage (22.8 cm length in the X-direction and 0.9145 mm width in the Y-direction) through which the fuel-oxidizer mixture is allowed to pass, Volume 7 models the combustor wall, Volume 10 models the cooling air flow through the inside of the catalyst,

Volume 11 models the catalyst, which is 22.8 cm long and Volume 13 models the entrance. The catalyst thickness is 0.01875 cm, and the combustor thickness is 0.84455 cm. Zone four has a total of 110,751 nodes with a total of 232,041 hexahedral elements. Figure A-14 shows the meshed zone four.

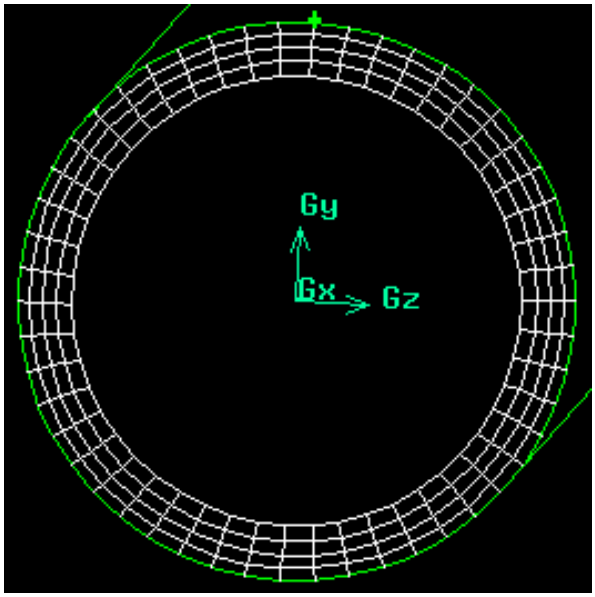

Figure A-1 Boundary layer on Face

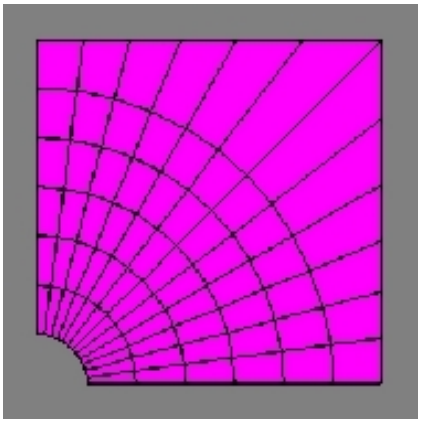

Figure A-2 structured grid

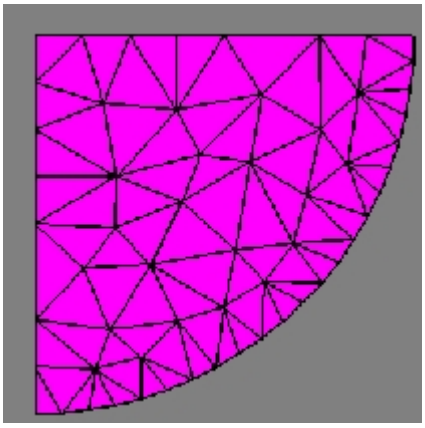

Figure A-3 Unstructured grid

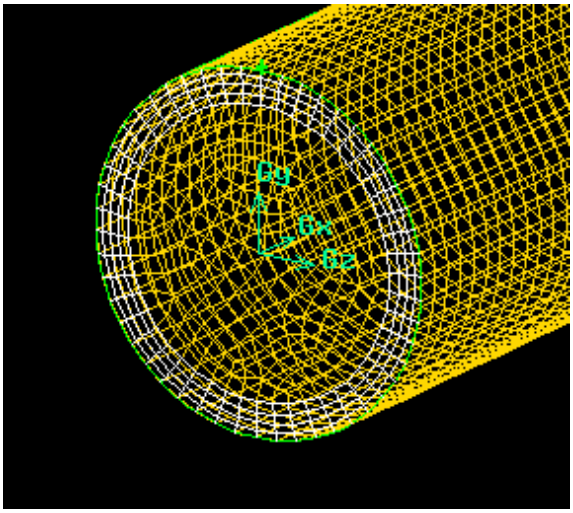

Figure A-4 Face and Volume Mesh

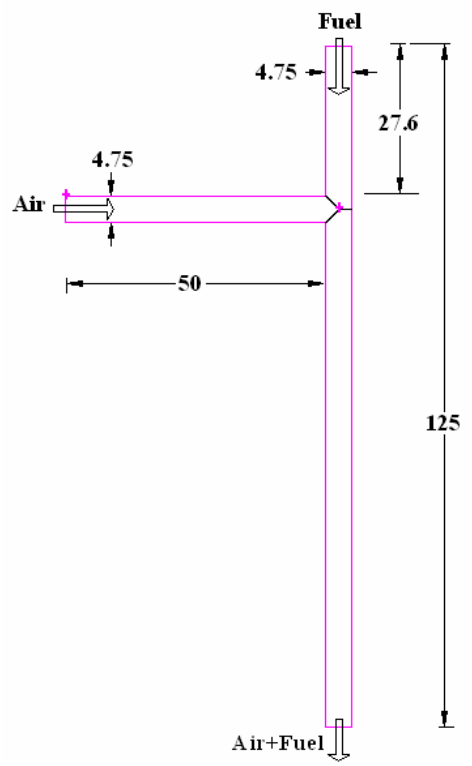

Figure A-5 Computational Model of Zone Two

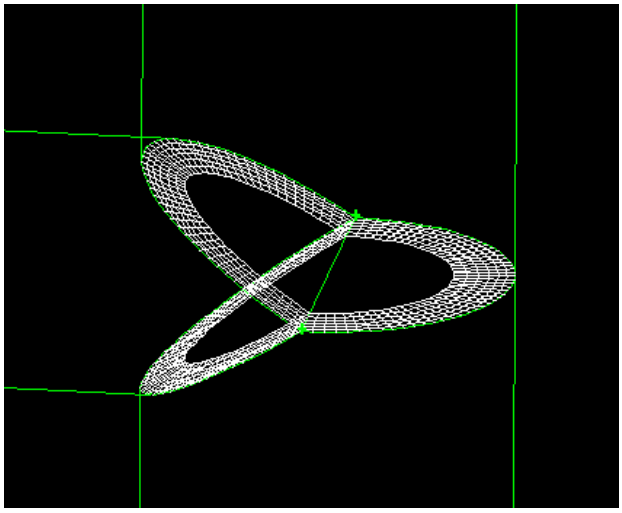

Figure A-6. Boundary Layer capturing mixing

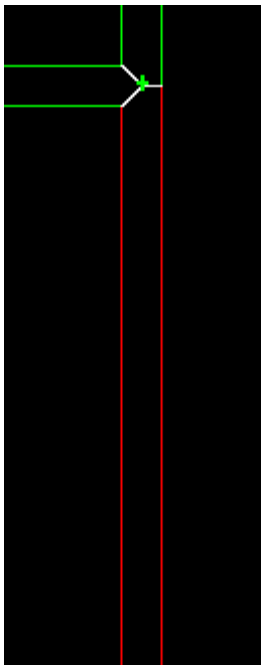

(A)

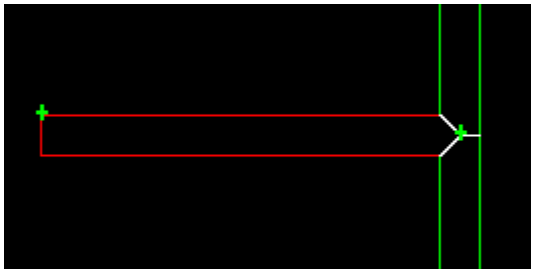

(B)

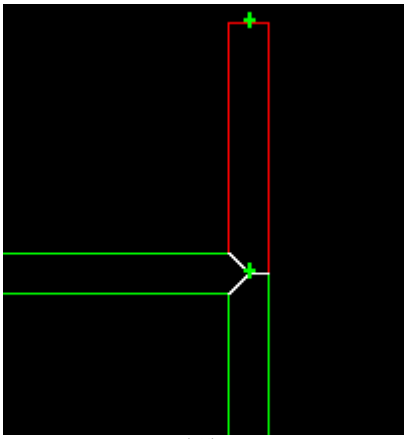

(C)

Figure A-7 Three separate Volumes that makes Zone Two (A) Volume 1 (B) Volume 2 and (C) Volume 3

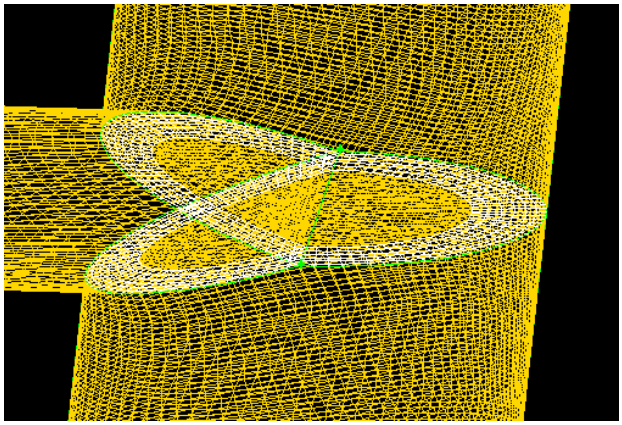

Figure A-8 Meshed Zone two

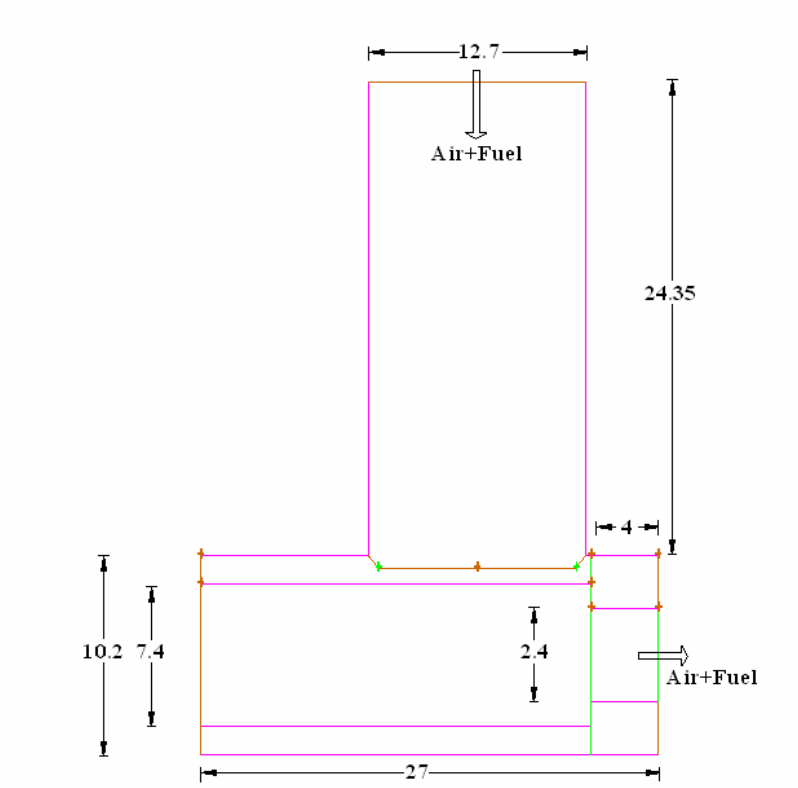

Figure A-9. Computational Model of Zone three

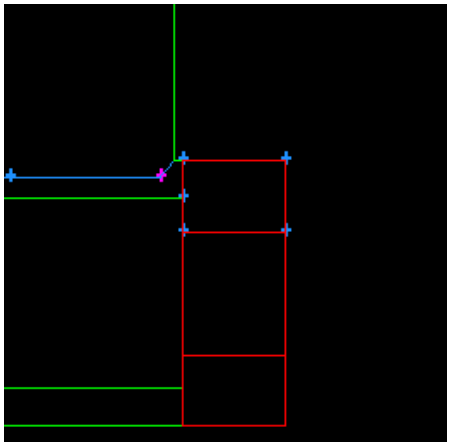

(A)

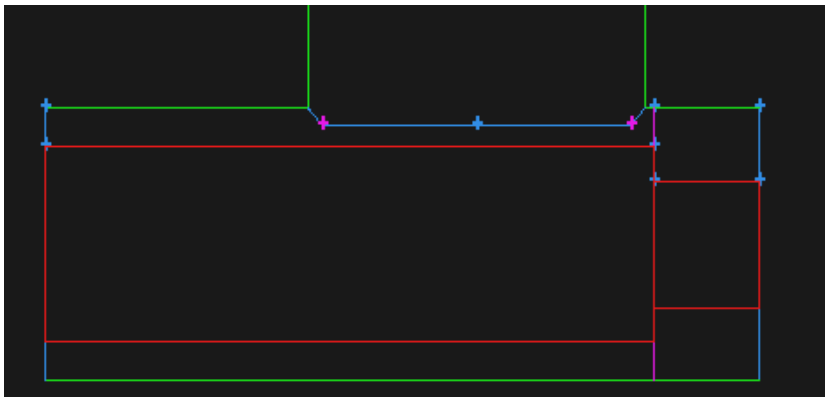

(B)

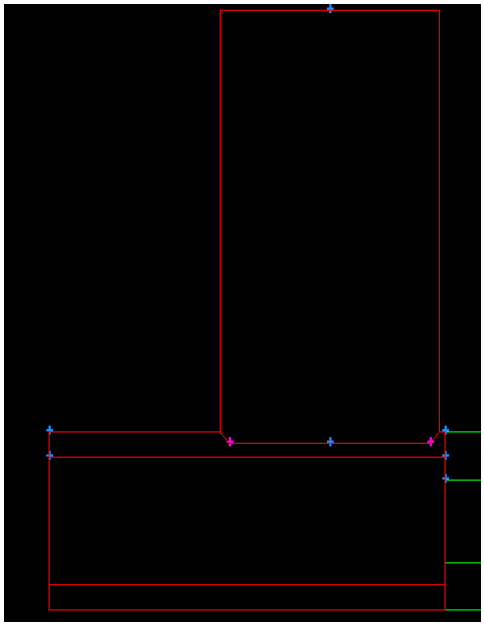

(C)

Figure A-10 Three Volumes that make Zone Three (A) Volume 1 (B) Volume 2 and (C) Volume 4

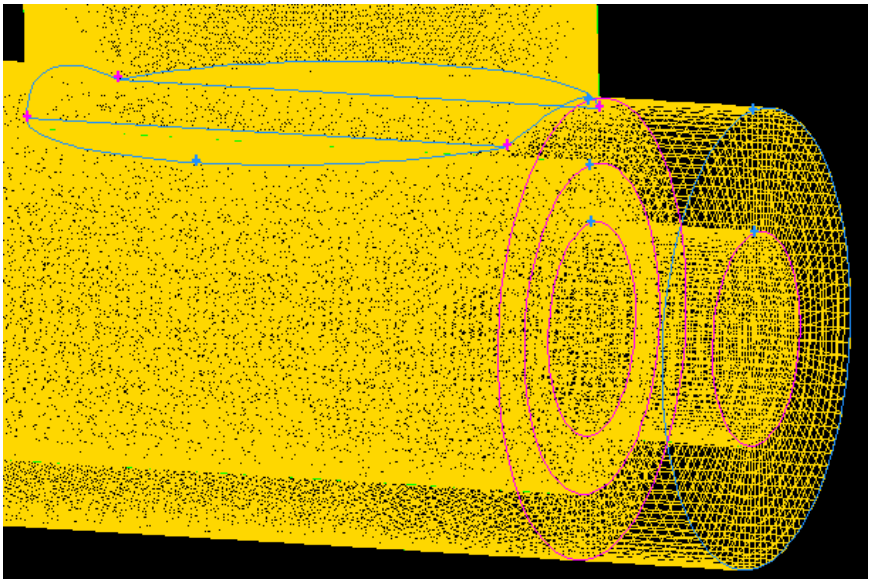

Figure A-11 Meshed Zone three

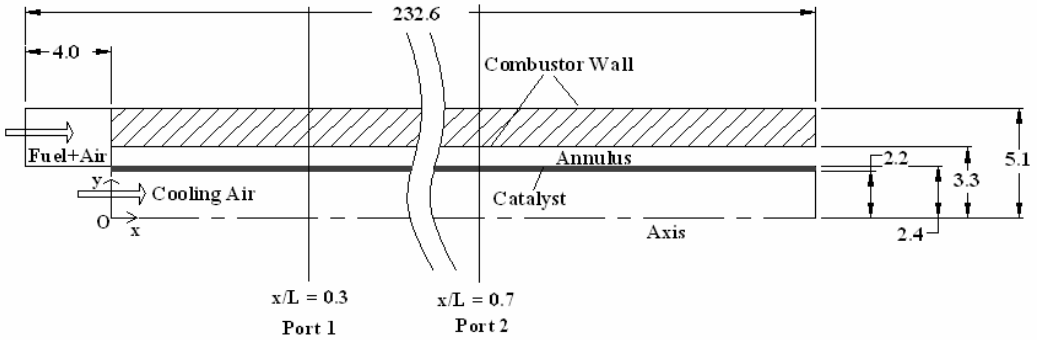

Figure A-12 Computational Model of Zone three

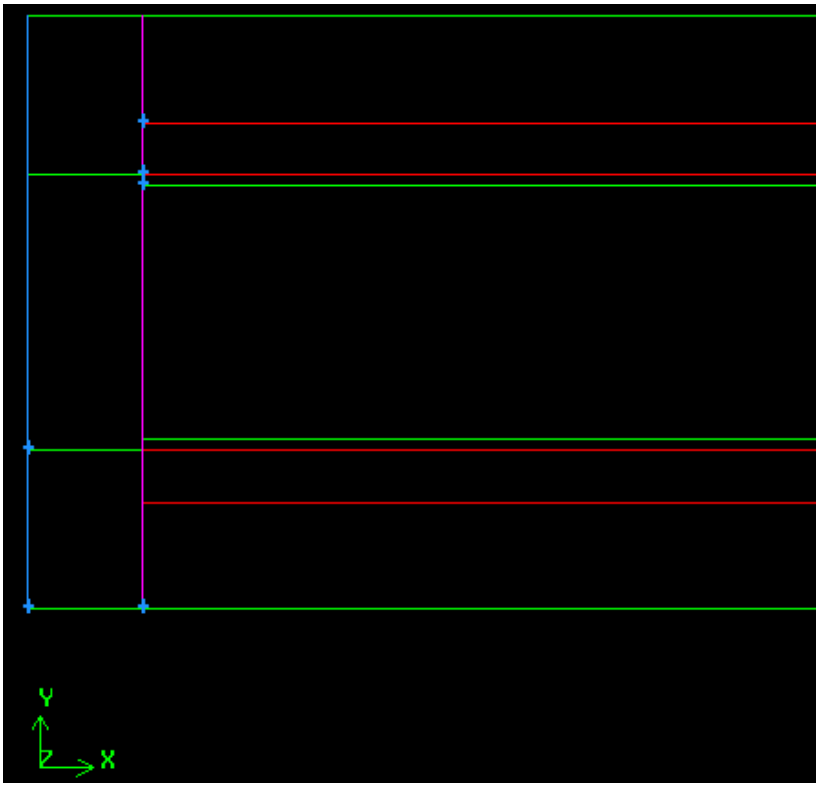

(A)

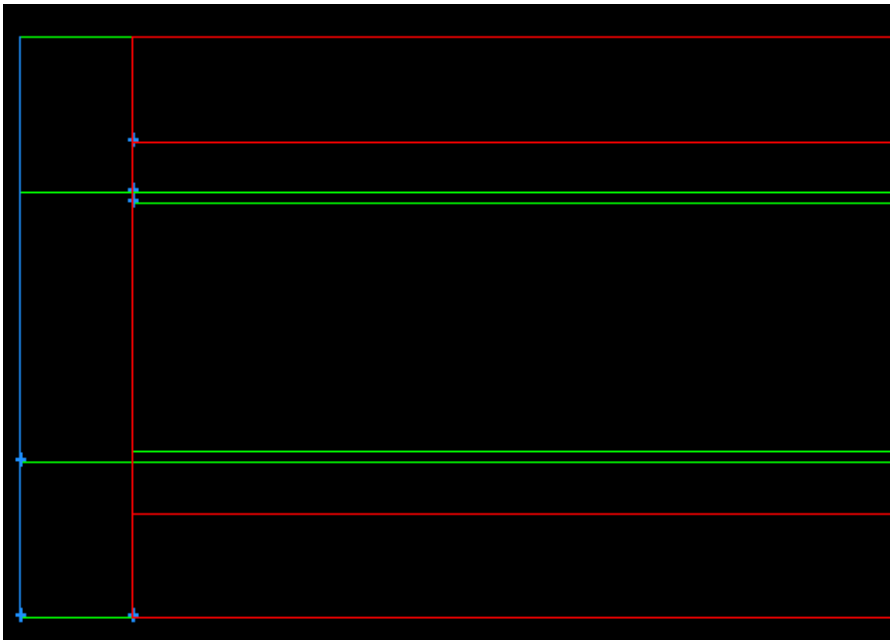

(B)

Figure A-13 Five separate Volumes that make Zone four (A) Volume 4 (B) Volume 7 (C) Volume 10 (E) Volume 11 and (E) Volume 13

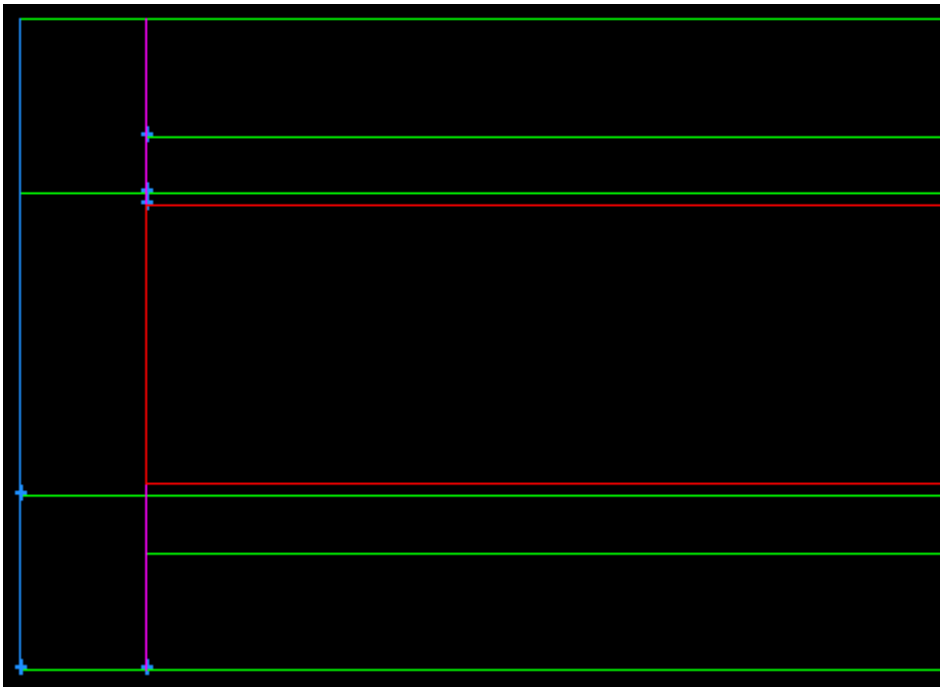

(C)

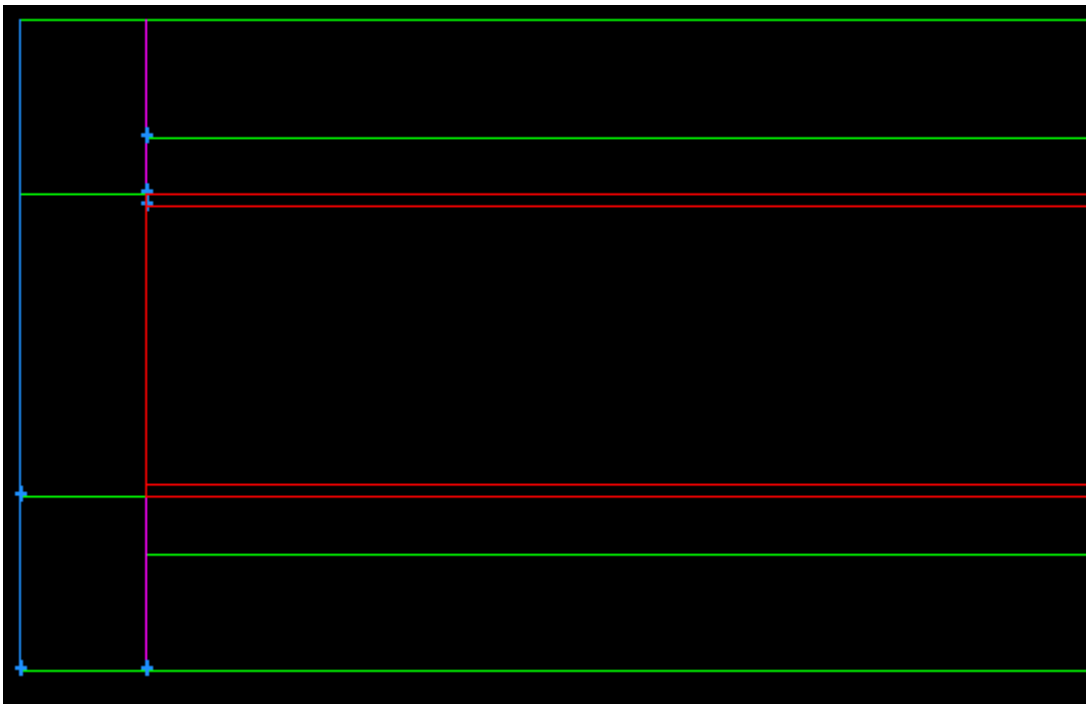

(D)

Figure A-13 Five separate Volumes that make Zone four (A) Volume 4 (B) Volume 7 (C) Volume 10 (E) Volume 11 and (E) Volume 13

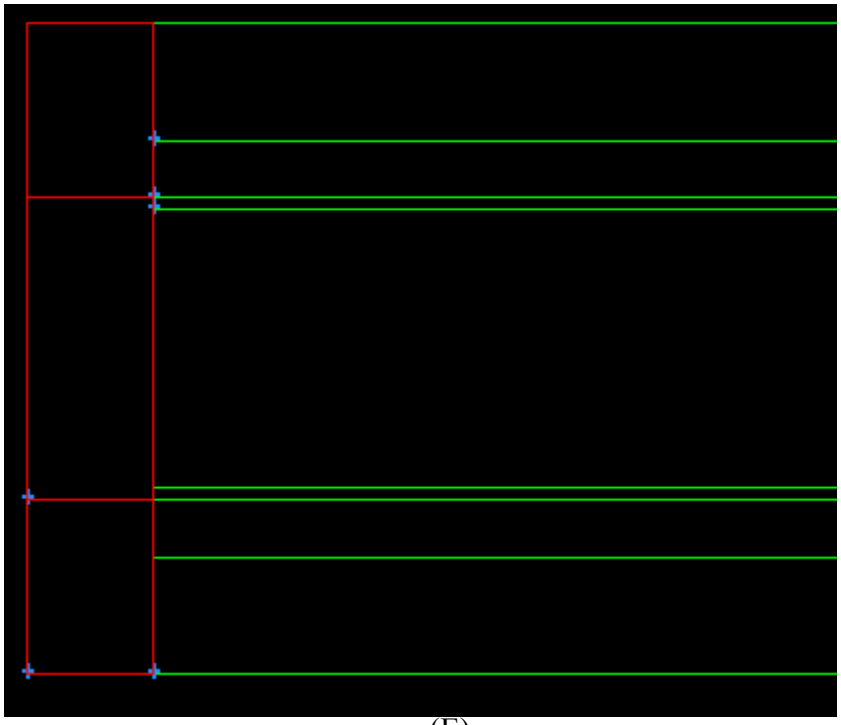

(E)

Figure A-13 Five separate Volumes that make Zone four (a) Volume 4 (b) Volume 7 (c) Volume 10 (d) Volume 11 and (e) Volume 13

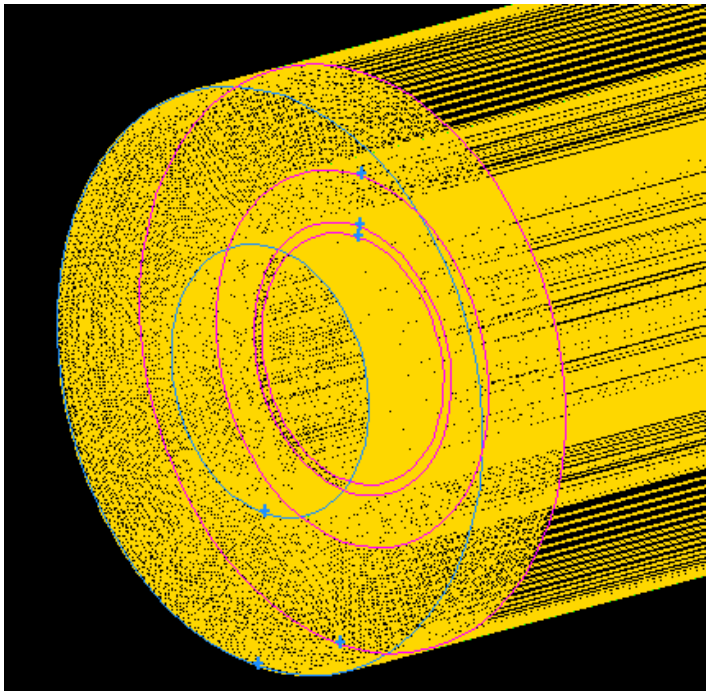

Figure A-14 Meshed Zone four

APPENDIX B
GAMBIT PROGRAM FOR DESIGN AND MESH GENERATION

```
/ Journal File for GAMBIT 2.2.30, Database 2.2.14, ntx86 BH04110220
/ Identifier "default_id636"
/ File opened for write Fri Jun 02 11:10:32 2006.
/ Journal File for GAMBIT 2.2.30, Database 2.2.14, ntx86 BH04110220
/ Identifier "default_id3260"
/ File opened for write Tue May 16 14:44:35 2006.
volume create height 255.6 radius1 3.302 radius3 3.302 offset 127.8 0 0 xaxis frustum
volume create height 255.6 radius1 2.3785 radius3 2.3785 offset 127.8 0 0 \
  xaxis frustum
volume split "volume.1" volumes "volume.2" connected bientity
volume create height 255.6 radius1 5.1435 radius3 5.1435 offset 127.8 0 0 \
  xaxis frustum
volume create height 255.6 radius1 2.1 radius3 2.1 offset 127.8 0 0 xaxis frustum
/ERROR occurred in the next command!
/ERROR occurred in the next command!
volume move "volume.2" "volume.3" "volume.4" offset -27 0 0
volume create height 255.6 radius1 3.302 radius3 3.302 offset 127.8 0 0 xaxis frustum
volume create height 255.6 radius1 2.3875 radius3 2.3875 offset 127.8 0 0 \
  xaxis frustum
volume split "volume.1" volumes "volume.2" connected bientity
volume create height 255.6 radius1 5.1435 radius3 5.1435 offset 127.8 0 0 \
  xaxis frustum
```

volume move "volume.3" offset -27 0 0

volume split "volume.3" volumes "volume.1" connected bientity

undo

/Undone to: volume split "volume.3" volumes "volume.1" connected bientity

/Undone to: volume delete "volume.1" lowertopology

undo

/Undone to: volume move "volume.3" offset -27 0 0

/Undone to: volume split "volume.3" volumes "volume.1" connected bientity

undo

/Undone to: volume create height 255.6 radius1 5.1435 radius3 5.1435 offset 127.8

/Undone to: volume delete "volume.2" lowertopology

volume split "volume.3" volumes "volume.1" connected bientity

/ERROR occurred in the next command!

/ERROR occurred in the next command!

volume move "volume.2" offset -27 0 0

volume create height 228.6 radius1 8 radius3 8 offset 114.3 0 0 xaxis frustum

volume split "volume.3" volumes "volume.5" connected bientity

default set "GRAPHICS.GENERAL.CONNECTIVITY_BASED_COLORING" numeric 1

save name \

"C:\\Documents and Settings\\saurav\\Desktop\\3Dtestsection\\without-cooling-air-16thmay.dbs"

/ File closed at Tue May 16 15:14:19 2006, 2.64 cpu second(s), 3009008 maximum memory.

```
/ Journal File for GAMBIT 2.2.30, Database 2.2.14, ntx86 BH04110220
/ Identifier "without-cooling-air-16thmay"
/ File opened for append Tue May 16 15:28:18 2006.
/ERROR occurred in the next command!
identifier name \
  "C:\\Documents and Settings\\saurav\\Desktop\\3Dtestsection\\without-cooling-air-
16thmay.dbs" \
  old savepreviously
volume split "volume.2" faces "face.11" connected
save
volume create height 23 radius1 3.683 radius3 3.683 offset -11.5 0 0 xaxis frustum
/ERROR occurred in the next command!
volume move "volume.9" offset -4 0 0
volume create height 27 radius1 2.3875 radius3 2.3875 offset -13.5 0 0 xaxis frustum
volume unite volumes "volume.9" "volume.10"
/ERROR occurred in the next command!
volume delete "volume.8" lowertopology
volume unite volumes "volume.2" "volume.9"
undo
/Undone to: volume unite volumes "volume.2" "volume.9"
/Undone to: volume unite volumes "volume.2" "volume.9"
undo
/Undone to: volume delete "volume.8" lowertopology
```

/Undone to: volume delete "volume.8" lowertopology

/ERROR occurred in the next command!

volume delete "volume.8" lowertopology

save

save name \

"C:\\Documents and Settings\\saurav\\Desktop\\3Dtestsection\\without-cooling-air-16thmay-copy.dbs"

LIST OF REFERENCES

[1] Deutschmann, O., Schmidt, R., Behrendt, F., and Warnatz, J., "Numerical Modeling of Catalytic Ignition," *Proceedings of the Combustion Institute*, Pittsburg, Vol. 26, 1996, pp.1747-1754.

[2] Mantzaras, Appel, C., and P. Benz, P., "Catalytic Combustion of Methane/Air Mixtures over Platinum: Homogeneous Ignition Distances in Channel Flow Configurations," *Proceedings of the Combustion Institute*, Edinburg, Vol. 28, 2000, pp. 1349-1358.

[3] Veser, G., and Schmidt, L.D., "Ignition and Extinction in the Catalytic Oxidation of Hydrocarbons over Platinum," *American Institute of Chemical Engineering Journal*, Vol. 42 (4), 1996, pp. 1077-1087.

[4] Krebs, W., Gruschka, U., Fielenbach, C., and Hoffman, S., "CFD-analysis of reacting flow in an annular combustor," *Progress in Computational Fluid Dynamics*, Vol 1, pp.104-116, 2001.

[5] Hua, J., Meng Wu, M., and Kumar, K., "Numerical Combustion of Hydrogen-air mixture in micro-scaled chambers Part II: CFD analysis for a micro-combustor," *Chemical Engineering Science*, Vol 60, pp. 3507-3515.

[6] Lefebvre, A. H., *Gas Turbine Combustion*, Hemisphere Publishing Corporation, 1983.

[7] "Control of Nitrogen Oxide emissions: Selective Catalytic Reduction (SCR)," *Report conducted jointly by The U.S Department of Energy and Southern Company Services, Inc*, Number 9, July 1997.

[8] Maxwell, J.D., and A.L. Baldwin, A. L., "Demonstration of Selective Catalytic Reduction (SCR) Technology for the Control of Nitrogen Oxide (NOx) Emissions from High-Sulfur, Coal-Fired Boilers," *First Annual Clean Coal Technology Conference*, Cleveland, OH, September 1992.

[9] Rao, S. N., McIlvried, H. G., and Mann, A. N., "Evaluation of NOx Removal Technologies", *Selective Catalytic Reduction*, Vol 1.

[10] Chorpening, B., Richards, A. G., Casleton, K. H., "Demonstration of a Reheat Combustor for Power Production with CO_2 Sequestration," *Journal of Engineering for Gas Turbines and Power*, Vol-127, Issue-4, October 2005, pp. 740-747.

[11] Woike, M., and Willis, B., "Performance of a dry low-NO_x Gas Turbine combustor design with a new fuel supply concept," *Journal of Engineering for Gas Turbines and Power*, Vol 124, Issue 4, October 2002, pp.771-775.

[12] *Institute for Interfacial Catalysis*, Pacific Northwest National Laboratory, (http://iic.pnl.gov)

[13] Melhado, E. M., *Jacob Berzelius, the emergence of his chemical systems.*

[14] *IUPAC Compendium of Chemical Terminology*, 2nd Edition, 1997.

[15] Bond, G. C., *Heterogeneous Catalysis: Principles and Applications*, Second Edition, Oxford University Press.

[16] Boreskov, G. K., *Heterogeneous Catalysis*, Nova Science Publishers, Inc., New York, 2003.

[17] Masel, R. I., *Chemical Kinetics and Catalysis*, John Wiley & Sons, Inc., Publication, 2001.

[18] James. C., *Chemical and Catalytic reaction engineering*, McGraw Hill 1976.

[19] Smith, J. M. Chemical engineering kinetics 3rd edition. New York; London: McGraw-Hill, 1981.

[20] Xu and Chuang, "Kinetics of acetic acid esterification over ion exchange catalysts," *Canadian journal of chemical engineering*, Vol. 74, 1996, pp. 493

[21] Deutschmann, O., Maier, L. I., and Riedel, U., "Hydrogen Assisted Catalytic Combustion of Methane on Platinum," *Catalysis Today*, Vol. 59, 2000, pp. 141-150.

[22] Nakra, S., Green J. R., and Anderson, L. S., "Thermal decomposition of JP-10 studied by micro-flowtube pyrolysis-mass spectrometry," *Combustion and Flame,* Vol. 144, Issue 4, March 2006, pp. 662-674.

[23] Seery, D. J., and Zabielski, M. F., "Comparisons between flame species measured by probe sampling and optical spectrometry techniques," *Combustion and Flame*, Vol. 78, Issue 1, October 1989, pp. 169-177.

[24] Korobeinichev, O. P., Kuibida, L. V., Volkov E. N., and Shmakov, G., "Mass spectrometric study of combustion and thermal decomposition of GAP," *Combustion and Flame,* Vol. 129, Issues 1-2, April 2002, pp. 136-150.

[25] *American Society for Mass Spectroscopy*, (http://www.asms.org)

[26] *American Society for Chromatography,* (www.chromatography-online.org

[27] Ancia, R., Tiggelen, P. J. V., and Vandooren, J., "Gas Chromatography as a complementary Analytic Technique to Molecular Beam Mass Spectrometry for Studying Flame Temperature," *Combustion and Flame*, Vol. 116, pp. 307-309 (1999).

[28] Eckbreth, A. C., *Laser Diagnostics for Combustion Temperature and Species*, 2nd Edition, Gordon and Breach Publications.

[29] EML 6934 Course Study material, Dr. D. Hahn, spring 2006, University of Florida, Gainesville, FL.

[30] Barlow, R. S., and Carter, C. D., "Raman/Rayleigh/LIF Measurements of Nitric Oxide Formation in Turbulent Hydrogen Jet Flames," *Combustion and Flame*, Vol. 97, 1994, pp. 261-280.

[31] Barlow, R. S., and Frank, J. H., "Simultaneous Rayleigh, Raman, and LIF Measurements in Turbulent Premixed Methane-Air Flames," 27th *International Symposium on Combustion, the Combustion Institute*, Pittsburg, PA, pp. 759-766.

[32] Steffen, C. J. Jr., and Yungster, S., "Computational Analysis of the Combustion Process in an Axisymmetric, RBCC Flow path," *NASA/TM-2001-210679 Paper.*

[33] Cline, M. C., Deur, J. M., Micklow, G. J., Harper, M. R., and Kundu, P. K., "Computation of the Flow Field in an Annular Gas Turbine Combustor," *29th Joint Propulsion and Exhibit, AIAA 93-2074*., June 28-30, 1993.

[34] *GAMBIT user's guide documentation*, Version 2.3.32

[35] *FLUENT users guide*, Version 6.2.16

[36] Patankar, S. V., *Numerical Heat Transfer and Fluid Flow*, Taylor and Francis Publications.

[37] Dalla Betta, R.A., Schlatter, J.C., Nickolas, S.G., Yee, D.K. and Shoji, T., *ASME Paper*, No. 94-GT-260 (1994).

[38] Schlegel, A., Buser, S., Benz P., Bockhorn, H., and Mauss, F., *Proceedings, 25th Symposium (International) on Combustion, the Combustion Institute*, Pittsburgh, PA, 1994, pp. 1019-1026.

[39] Kraft, M., Fey, H., Bockhorn, H., Schlegel, A., and Chen, J. Y., "A Numerical Study on the Influence of Mixing Intensity on NO_x formation," *International: Proceedings of the 3rd Workshop on Modeling of Chemical Reaction Systems*, 1997.

[40] Deutschmann, O., Behrendt, F., and Warnatz, J., "Modeling and Simulation of Heterogeneous Oxidation of Methane on a Platinum foil", *Catalysis Today*, Vol. 21, pp. 461-470, 1994.

[41] Otto Beeck, "Catalysis- A Challenge to the Physicist," *Reviews of Modern Physics*, Vol. 17, No. 1, January, 1945.

[42] Song, X., Williams, W. R., Schmidt, L. D., and Aris, R., "Bifurcation behavior in homogeneous-heterogeneous combustion: II. Computations for stagnation-point flow," *Combustion and Flame*, Vol. 84, Issues 3-4, April 1991, pp. 292-311.

[43] Williams, W. R., Stenzel, M. Song T. X., and Schmidt, L. D., "Bifurcation behavior in homogeneous-heterogeneous combustion: I. Experimental results over platinum," *Combustion and Flame*, Vol. 84, Issues 3-4, pp. 277-291, 1991.

[44] Pfefferle, L. D., Griffin, T. A., Winter, M. D. R., and Dyer, M. J., "The influence of catalytic activity on the ignition of boundary layer flows Part I: Hydroxyl radical measurements," *Combustion and flame*, Vol. 76, 1989, pp. 325-338.

[45] Markatou, P., Pfefferle L. D., and Smooke, M. D., "A computational study of methane-air combustion over heated catalytic and non-catalytic surfaces," *Combustion and Flame*, Vol. 93, 1993, pp.185-201.

[46] Hickman, D.A. and Schmidt, L.D., *AIChE Journal*, Vol. 39, 1993, pp. 1164-1177.

[47] Griffin, T. A., and Pfefferle, L.D., "Gas Phase and Catalytic Ignition of Methane and Ethane in Air over Platinum," *AIChE Journal*, Vol. 36, 1990, 861-870.

[48] Veser, G. and Schmidt, L. D., "Ignition and Extinction in the Catalytic Oxidation of Hydrocarbons over Platinum," *AIChE Journal*, Vol. 42 (4), 1996, pp. 1077-1087.

[49] F. Behrendt, F., "Ignition and Extinction of Hydrogen-Air and Methane-Air Mixtures over Platinum and Palladium," *ACS Symposium Series*, 1996, pp. 48-57.

[50] Schwiedernoch, R. "Experimental and numerical investigation of the ignition of methane combustion in a platinum-coated honeycomb monolith," *Proceedings of Combustion Institute*, Saporo, Japan, Vol. 29, 2002, pp. 1005-1011.

[51] Baulch, D. L., "Evaluated Kinetic Data for Combustion Modeling," *Journal of Physical Chemistry*, Vol. 21 (3), 1992, pp. 411-734.

[52] Yong, S. S., Sung J. C., Sung, K. K., and Hyun, D. S., "Numerical Studies of Catalytic Combustion in a Catalytically Stabilized Combustor," *International Journal of Energy Research*, Vol. 24, 2000, pp. 1049-1064.

[53] Reinke, M., Mantzaras, J., Schaeren, R., Bombach, R., Kreutner W., and Inauen, A., "Homogeneous Combustion in High Pressure Combustion of Methane/Air over Platinum: Comparison of Measurements and detailed Numerical Predictions," *Proceedings of the combustion Institute*, Vol. 29, 2002, pp. 1021-1029.

[54] Nedunchezian, N., and Dhandapani, S., "Study of Flame quenching and near-wall combustion of lean burn fuel-air mixture in a catalytically activated spark-ignited lean burn engine," *Combustion and Flame*, Vol. 144, 2006, pp. 407-409.

[55] Heywood, J. B., *Internal Combustion Engine Fundamentals*, McGraw-Hill, New York, 1989.

[56] Aghalayam, P., "A C1 mechanism for methane oxidation on platinum," *Journal of Catalysis*, Vol. 213 (1), 2003, pp. 23-38.

[57] Ihmann, K., Ihmann, Jentoft, F. C., Geske, M., Taha, Pelzer A. K., and Schlogl R., "Molecular beam mass spectrometer equipped with a catalytic wall reactor for *insitu* studies in high temperature catalysis research," *Review of Scientific Instruments -- May 2006. Review of Scientific Instruments*, Vol. 77, 2006

[58] Grunwaldt1, J. D., Hannemann, S., Schroer, C. G., Baiker, A., "2D-mapping of the structure of a heterogeneous catalyst inside a catalytic micro reactor during the partial oxidation of methane," *Journal of Physical Chemistry B*, Vol. 110, 2006.

[59] Yeh, T., Lee, H., Chu, K., and Wang C., "Charecterization and catalytic combustion of methane over hexaaluminate," *Materials Science and Engineering A*, Vol. 384, Issue 1-2, pp. 324-330.

[60] Dogwiler, U., Mantzaras, J., Benz, P., "Homogeneous Ignition of Methane/Air Mixtures over Platinum: Comparison of Measurements and Detailed Numerical Predictions," *27th International Symposium on Combustion*, Boulder, CO, August 1998.

BIOGRAPHICAL SKETCH

Saurav Pathak was born in Bettiah, India, on December 17th, 1976, and raised in Kolkata, India. Saurav attended the Birla Institute of Technology, located in Mesra India, where he received a Bachelor of Engineering degree in mechanical engineering in 2000. Thereafter Saurav joined the Department of Mechanical Engineering at the Ohio University in August 2001 and got a M. S. in Mechanical Engineering in May 2003. After 2003, he has attended the College of Engineering at the Louisiana State University, Baton Rouge, LA to pursue his Ph.D. in Mechanical Engineering. After staying there for two semesters, Saurav transferred to the University of Florida, Gainesville and started working as Ph.D. from December 2005.During this time he worked as a research assistant in the Mechanical and Aerospace Engineering Department on a full-time basis. His research interests include experimentation and computational catalytic combustion.